LOW TEMPERATURE DEFORMATION OF COPPER SINGLE CRYSTALS ORIENTED FOR MULTIPLE SLIP

by

SHIGEO SAIMOTO

B.A.Sc. (1958), M.A.Sc. (1960)

University of British Columbia

Submitted in partial fulfillment of the

Requirements for the degree of

DOCTOR OF PHILOSOPHY

at the

Massachusetts Institute of Technology

January 1964

Signature of Author Signature redacted
Department of Metallurgy

Certified by Signature redacted
Thesis Advisor

Accepted by Signature redacted
Chairman, Departmental Committee
on Graduate Students

LOW TEMPERATURE DEFORMATION OF COPPER SINGLE CRYSTALS ORIENTED FOR MULTIPLE SLIP

by

SHIGEO SAIMOTO

Submitted to the Department of Metallurgy on January 17, 1964
in partial fulfillment of the requirements for the
Degree of Doctor of Philosophy

ABSTRACT

Tensile tests on copper single crystals of $[\bar{1}11]$ and $[001]$ orientations and on coarse-grained polycrystalline copper were performed at 4.2°, 78°, 162°, and 273°K. Certain broad correlations were found between linear (Stage II) hardening in $[\bar{1}11]$ and prominent slip-cluster formation, and between non-linear hardening in $[001]$ with much less evident clustering. The temperature insensitivity of initial hardening rates in $[001]$ suggested that a non-linear Stage II was being displayed; this possibility was supported by the fact that whenever clustering did occur the initial hardening rate decreased towards the Stage II value of $[\bar{1}11]$ as a lower limit.

The Cottrell-Stokes law was found to be valid for both orientations upon cycling between 162° and 78°K, with $\frac{\Delta\tau}{\tau_{78}}$ being lower for [001]. Between 273° and 78°K, $\frac{\Delta\tau}{\tau_{78}}$ was independent of stress over only a limited range, up to about 8000 psi.

Differences between [001] and $[\bar{1}11]$ in both isothermal hardening and thermal-cycling behavior have been rationalized on the basis of the character of jogs produced by the intersection of primary and critical systems that is unique to [001].

Identical experiments on the coarsely polycrystalline copper led to the conclusion that its hardening behavior represents a transition from [001] - type deformation at small strains to $[\bar{1}11]$ - type as straining is continued.

$[\bar{1}11]$ crystals twinned in tension at 4.2°, 20°, and 78°K, at stresses that increased with temperature. [001] could only be twinned in compression; the stress at 4.2°K agreed favorably with that for $[\bar{1}11]$ crystals in tension at this temperature. The active systems were consistent with those predicted by the usual hard-ball model of deformation twinning in face-centered cubic crystals.

Thesis Supervisor: Walter A. Backofen

Title: Professor of Metallurgy

TABLE OF CONTENTS

Page

Page

LIST OF ILLUSTRATIONS

LIST OF TABLES

ACKNOWLEDGEMENTS

It is a pleasure to acknowledge Professor W. A. Backofen for his help and encouragement throughout the progress of this work. The experimental aid and inspiring guidance of Professor W. F. Hosford, Jr. made the analyses presented in this work possible. Professor Hosford has recently departed to assume an Associate Professorship at the University of Michigan. The author gratefully acknowledges Professor A. S. Argon for making available his Berg-Barrett X-ray apparatus and for many profitable discussions. The author is indebted to Dr. L. A. Shepard and Professor G. Pearsall for their enthusiastic participation in many fruitful discussions. The author owes thanks to Mr. Henry Piehler for supplying the diagram shown in Fig. 1-II and for many hours of discussion with him and other members of the Metal Processing Laboratory. Thanks are extended to Mr. R. Foss for preparation of the machined blanks and Mr. R. L Jones for technical advice and assistance. The program was generously supported by the Atomic Energy Commission.

INTRODUCTION

The present understanding of the deformation of face-centered cubic metals has been derived mostly from the results of experiments on crystals oriented for single slip.[1] The hardening pattern has been characterized by three "stages" with reference to the shear stress-strain curve: Stage I, easy glide; Stage II, rapid linear hardening; and Stage III, dynamic recovery, characterized by a diminishing hardening rate. More recently, the pattern has been elaborated with findings of two linear regions of slightly different slope in Stage II,[2,3,4] and, in some cases, of a linear region in Stage III.[5,6]

It is generally agreed that the flow stress, τ, of face-centered cubic metals is comprised of a temperature-dependent part, τ_s, and another part, τ_g, which is dependent upon temperature only through the shear modulus. Three major theories associate τ_g with the stress required (1) to drive dislocations through the relatively long-range elastic stress fields around dislocation pile-ups,[7,8] (2) to drive dislocations through the elastic fields around other (forest) dislocations penetrating the glide plane,[9,10] (3) to accomplish the non-conservative motion of sessile jogs.[11,12,13] In both the "long-range" and "forest" theories, τ_s is the stress for the mutual cutting of dislocations in a forest relationship that leads to jog formation, while in the "jog" theory τ_s is the stress required to constrict interstitial-forming jogs.

From experimental observations, Stage II has been identified with an increasing dislocation density, unchecked by annihilation based on cross slip.[14] Quantitative derivation of hardening rate is least complex for Stage II, and all theories have been shown to predict the observed linear hardening in Stage II. Also basic to the theories is a requirement for slip on other systems than the most highly stressed as the pre-requisite for production of dislocation barriers or forests. Accordingly, it has long been felt that study of the hardening behavior of crystals oriented for multiple slip in which the several active systems are known should reveal additional information with which the mechanisms of hardening can be better understood.

Lange and Lücke,[15] and Staubwasser[16] working with aluminum crystals, and Rosi[17] and Diehl[18] with copper crystals, have shown that as the tensile axis approaches the symmetrical orientations of $[001]$ and $[\bar{1}11]$, the extent of easy glide decreases and the slope of Stage II rises. Systematic study of these orientations was made by Hosford, Fleischer, and Backofen[19] on aluminum and, more recently, by Ramaswami[20] on silver and silver-gold alloys. Sawkill and Honeycombe[21] found that for orientations near $[001]$, deformation at room temperature involves non-uniform thinning along the gauge length of both aluminum and gold crystals. Hosford et al. confirmed this behavior in aluminum for the $[001]$ orientation at 273°K, but at 200°K and below, a uniform, symmetrical shape change with stability of orientation was observed; in addition, it was learned that $[\bar{1}11]$ was stable at all temperatures

and that stability of [001] was associated with an initially higher rate of hardening for this orientation than for $[\bar{1}11]$. In follow-up experiments by Fleischer[22] on polycrystalline aluminum wires, a double $\langle 111 \rangle + \langle 100 \rangle$ fiber texture was found after drawing at 78°K, whereas only a single $\langle 111 \rangle$ texture could be developed by room-temperature drawing. Thus there is a strong implication that the hardening mechanisms operative in [001] and $[\bar{1}11]$ crystals are different whether comparison is made at a fixed temperature or as a function of temperature.

It has been suggested by Kocks[23] from experiments on aluminum at room temperature that multiple-slip hardening, even as it occurs in polycrystalline material, is well represented in the behavior of $[\bar{1}11]$ single crystals. Still others have investigated multiple-slip deformation in polycrystalline material by focussing on the strain-rate[24] and temperature dependence of hardening,[25] and by observations of dislocation structure with transmission electron microscopy.[26,27] However, considering the aforementioned evidence that multiple-slip hardening is in fact both orientation and temperature dependent, any extensive interpretation of such results is difficult. Essentially for these reasons the present work on strain hardening in [001] and $[\bar{1}11]$ single crystals of copper and in polycrystalline copper was undertaken.

EXPERIMENTAL PROCEDURES

The copper single crystals were grown under helium by the directional solidification of premachined blanks embedded in graphite powder (as described in Appendix I). The gauge length was 2.5-in, and the cross section was square, about 0.120-in on a side (Fig. 1). The variation of cross-sectional area was less than $\pm$ 2 percent. A standard 1/4 - 20 thread was machined initially at the ends of each blank and grown into the crystal to minimize the gripping difficulties which can arise with soft crystals. Axial orientations of $[\bar{1}11]$ and $[001]$ were obtained by seeding. The starting material, obtained from the American Smelting and Refining Company, was 99.999 percent pure, according to spectroscopic specification. However, a chemical analysis of one crystal revealed that impurities were picked up during growth leading to a final distribution in weight percent of: Si, 0.017; Fe, 0.005; Al, 0.013; Ni, 0.0015; Pb, < 0.001; Zn and Na < 0.0002.

Growth occurred at a rate of 0.6 to 0.8 in/hr, after which the crystals were annealed under helium for 36 hours at 1000°C, cooled at about 50°C/hr down to 600°C, and then furnace cooled. Orientations determined by the Laue back-reflection method were within 2° of those indicated in the standard triangle (Fig. 2). Each of the $[001]$ and $[\bar{1}11]$ crystals was prepared with one face approximately parallel to (110). Berg-Barrett[28,29] photographs of a few

Fig. 1. As-grown single crystal of copper with grown-in standard 1/4 - 20 threads for gripping.

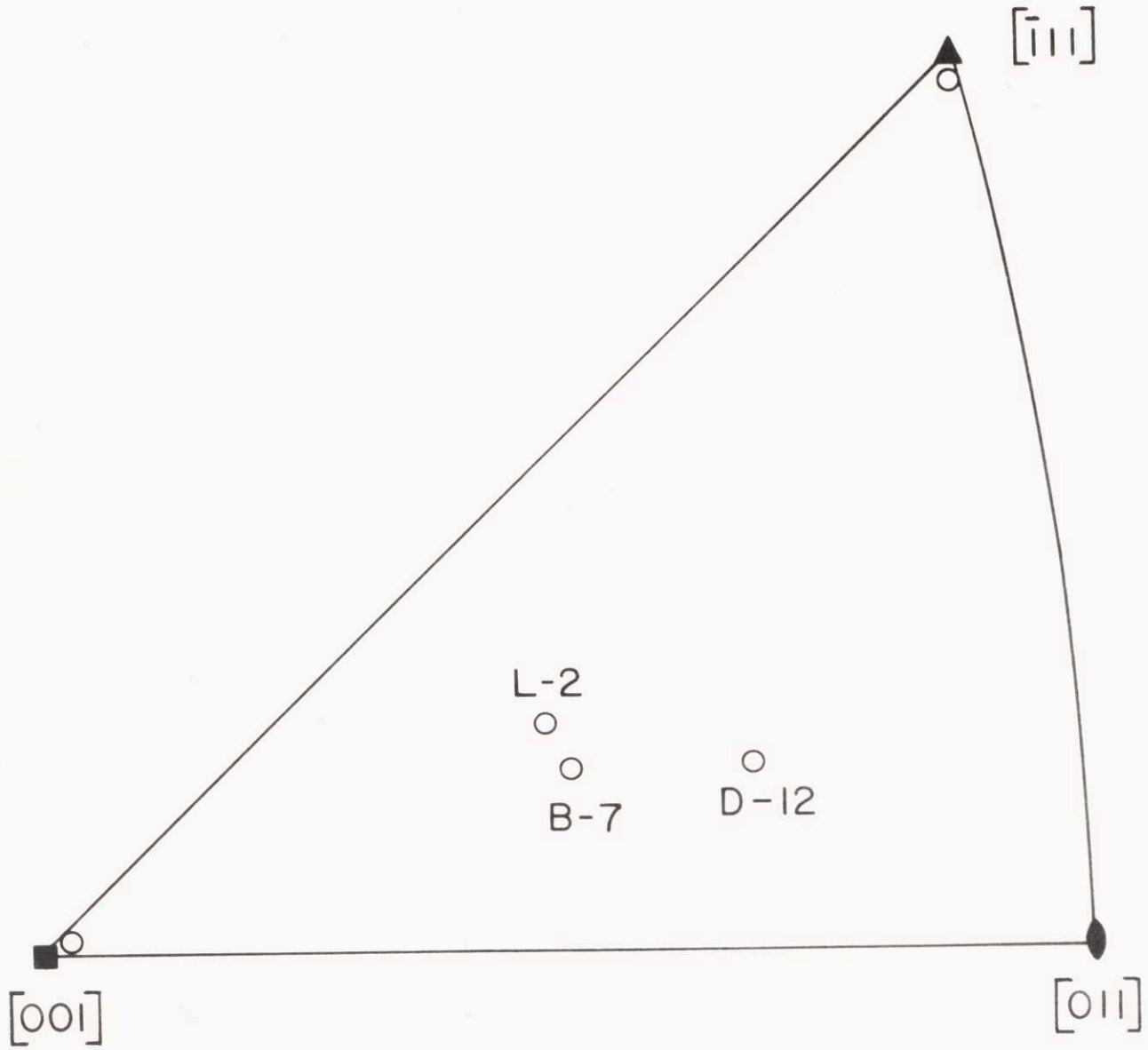

Fig. 2. Axial orientations of crystals tested (open circles).

electropolished crystal surfaces showed at most only one low angle grown-in boundary which was parallel to the specimen axis.

Polycrystalline samples were prepared from the as-received rods of 99.999 percent copper by first cold swaging to give a 55 percent reduction in area. Cylindrical specimens with a 2.5-in long gauge section of 0.150-in diameter were then machined and recrystallized in a single batch in an evacuated pyrex tube at 360°C. The final grain size was rated by Heyn's intercept method[30] as 10 grains per square millimeter; annealing-twin boundaries were not counted in this measurement.

The testing was carried out in an elastically "hard" screw-driven machine described elsewhere.[31] The basic design involved a moving rod suspended vertically inside a stationary tube. The crystal was threaded into a universal joint at the lower end of the rod (upper grip) and into a hemispherical nut surrounded by a mating collar that was fastened at the bottom of the tube (lower grip). From the difference in extension measured by crosshead motion and with reference to fiducial marks on the sample, it is estimated that the "pulling out" at the grips under maximum load reached in any of the tests represented less than 1 percent strain over the gauge length. A voltage-suppression circuit was incorporated in the load recording system to obtain the smallest scale used of about 100 lbs across the full width of the

9-1/2 in wide chart paper. A constant strain rate of about 0.8×10^{-4} sec^{-1} was used throughout.

Isothermal tensile tests were performed with the crystals completely immersed in a constant-temperature bath of liquid helium ($4.2^{o}K$), liquid nitrogen ($78^{o}K$), ethyl alcohol at its freezing point ($162^{o}K \pm 2^{o}$), or ice water ($273^{o}K$). One test was performed in helium vapor at $20^{o}K \pm 5^{o}$. Temperature was measured in the ethyl-alochol tests with a copper-constantan thermocouple and in the helium-vapor test with a calibrated graphite-resistance thermometer placed beside the crystal.

For the $[\bar{1}11]$ and $[001]$ crystals, shear stress-strain curves were derived from the true tensile stress-strain values with a constant Schmid resolving factor, $m = \cos \lambda \cos \phi$, where ϕ and λ are angles between the tensile axis and the slip-plane normal (ϕ) and the slip direction (λ). In this procedure, the assumption is made that slip occurs on octahedral planes in close-packed directions without lattice rotation. For inside-triangle crystals, shear stress and strain were computed from the loads and extensions by the single-slip formulae of Schmid and Boas.[32]

RESULTS

Tensile Stress-strain Curves (σ vs ϵ)

It is clear from the true tensile stress-strain curves of Fig. 3 that at all four temperatures the over-all strain-hardening rate is greatest for the $[\bar{1}11]$ and least for the $[001]$ crystals. The general behavior of both the $[001]$ and polycrystalline samples was to harden at monotonically decreasing rates, starting from yield; therefore, the initial portions of the curves could be represented, if only approximately, by the relation[33] $\sigma = \sigma_o + K\epsilon^n$ where σ is the flow stress, σ_o is the yield stress, and K and n are constants. Values of n determined from the slopes of the initial linear regions of log $(\sigma - \sigma_o)$ vs. log ϵ plots (a typical plot is shown in Fig. 4) and the strain, ϵ_p, at which this linearity terminated are recorded in Table I. The n values are similar for $[001]$ and polycrystalline samples and are almost temperature independent.

At 78°K and 4.2°K the slope of the log $(\sigma - \sigma_o)$ vs log ϵ plot for polycrystalline samples was observed to increase beyond ϵ_p instead of decrease as observed at higher temperatures; this reflects linear regions in the hardening curves and such regions are indicated (beginning and end) by arrows in Fig. 3, although they are only apparent upon plotting on much expanded coordinates. The linear region has been attributed by Kocks[23] to a hardening comparable to that in Stage II of single crystals. In more detail,

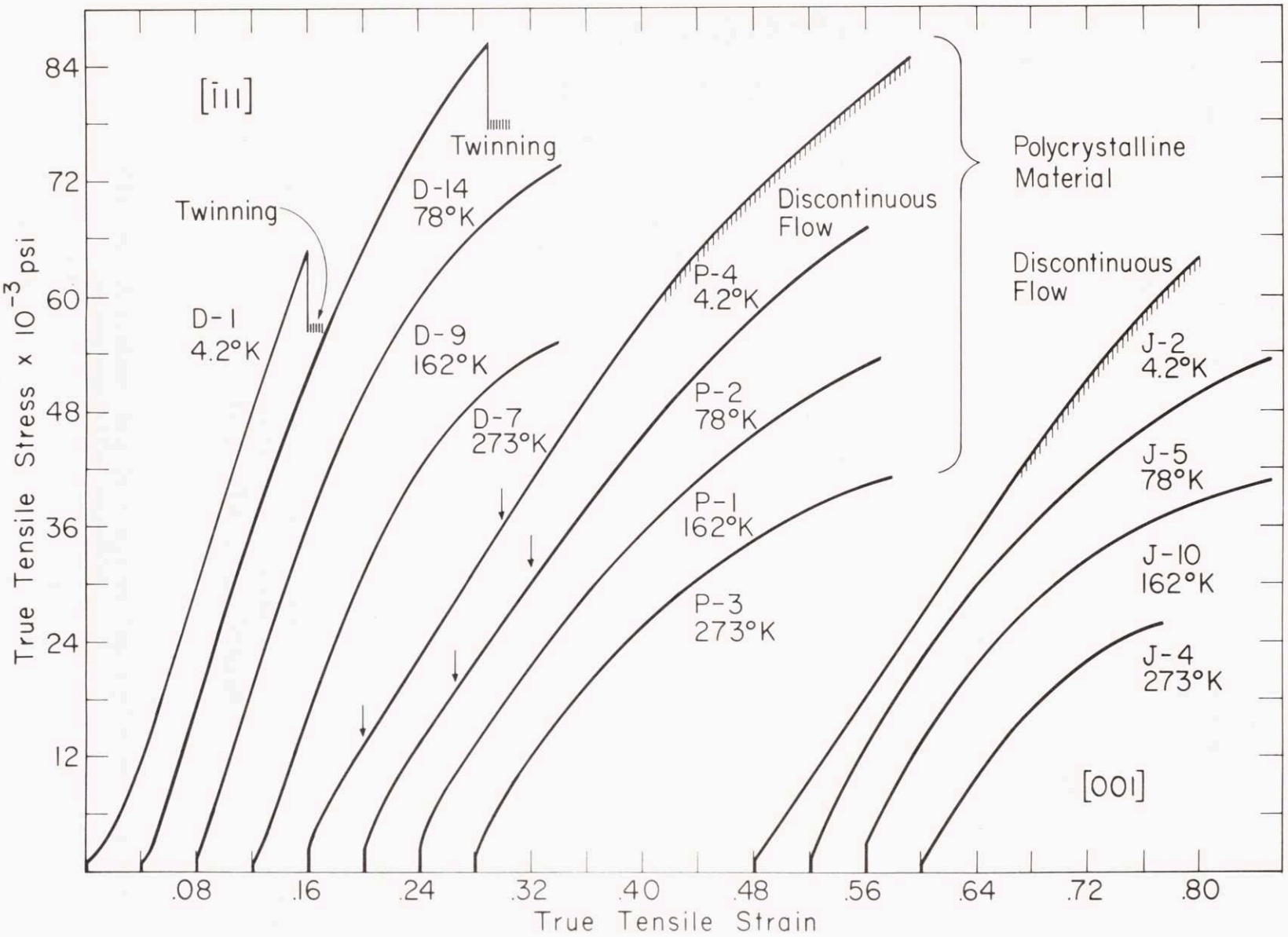

Fig. 3. True tensile stress-strain curves at 4.2°, 78°, 162° and 273°K. All crystals were pulled to fracture unless otherwise indicated. The vertical arrows indicate beginning and end of linear portion in polycrystalline material.

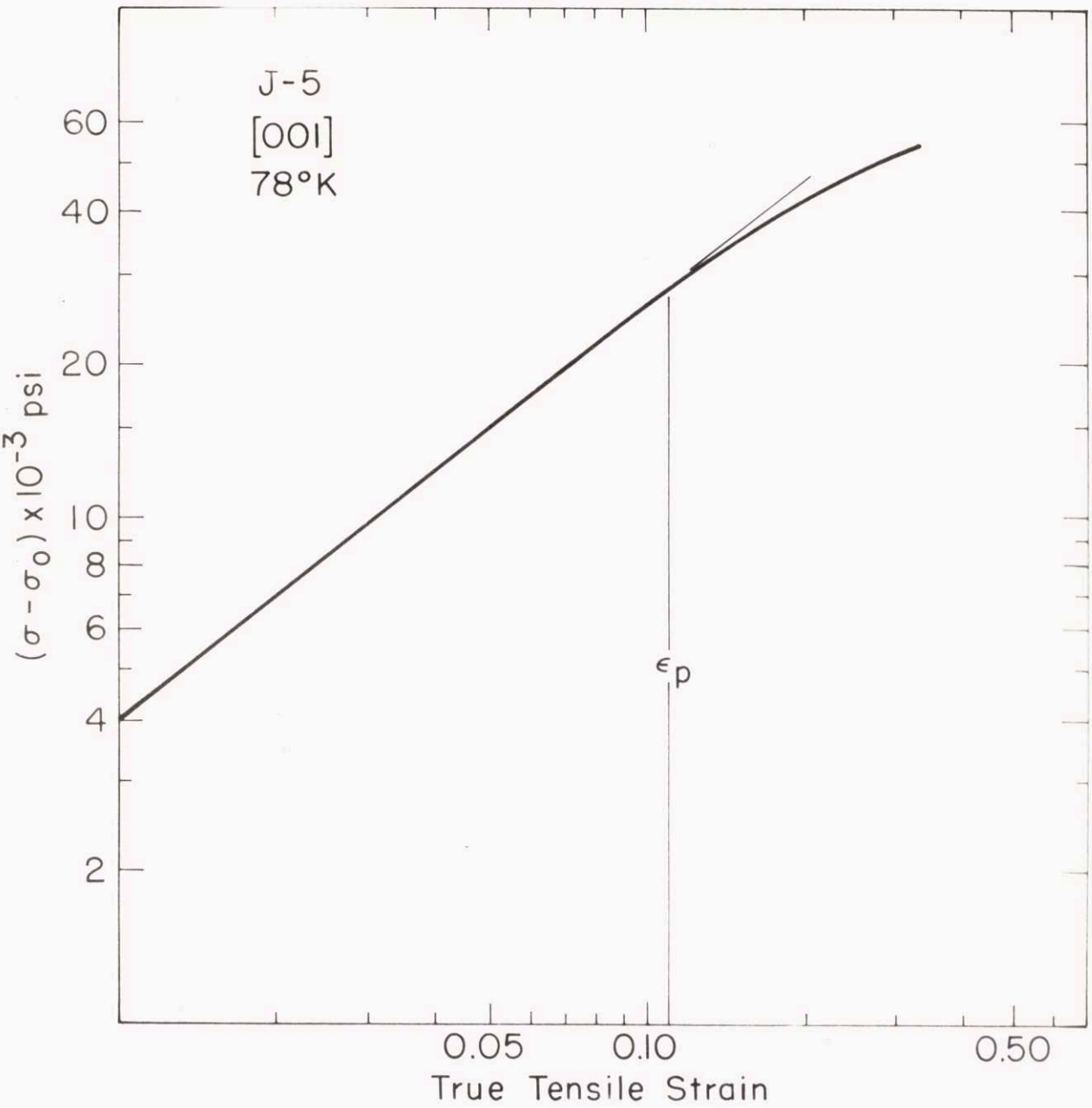

Fig. 4. A typical log $(\sigma - \sigma_o)$ vs log ϵ plot for 001 and polycrystalline material.

TABLE I. Work hardening parameters for [001] crystals and polycrystalline material.

Code Number	Test Temp. ^{o}K	σ_o x 10^{-3} psi	τ_o x 10^{-3} psi	n	ϵ_p	τ_p x 10^{-3} psi	$(\frac{d\tau}{d\gamma})_{\gamma=.016}$ x 10^{-4} psi	$\frac{(\frac{d\tau}{d\gamma})_{\gamma=.016}}{\mu}$ x 10^{3}	Number of Clusters
Polycrystalline Material									
P-3	273	2.00	----	.82	.087	----	----	----	----
P-6+	273	1.80	----	----	----	----	----	----	----
P-1	162	3.00	----	.85	.125	----	----	----	----
P-5+	162	2.00	----	----	----	----	----	----	----
P-2	78	2.20	----	.83	.052	----	----	----	----
P-4	4.2	2.12	----	.86	.068	----	----	----	----
[001] Crystal									
J-4	273	.478	.194	.88	.062	5.9	3.96	6.65	>20
J-8+	273	.408	.166	----	----	----	4.70	7.90	<5
J-10*	162	2.5	----	.82	.068	7.3	4.87	7.90	<5
J-6+	162	.820	.334	----	----	----	4.23	6.81	>20
J-5	78	.696	.284	.80	.115	11.7	5.57	8.74	<5
J-2	4.2	.852	.348	~1.0	----	----	3.58	5.60	>30
J-9	4.2	1.050	.429	~1.0	----	----	3.41	5.33	>30
J-11	4.2	.473	.193	.92	----	----	4.56	7.14	>10

* Prestrained about 0.007

\+ Thermal cycling tests

Kocks has suggested that the hardening curves of all polycrystalline face-centered cubic metals are initially linear. Here, however, the linearity did not appear until after some hardening at decreasing rate; a similar observation has been made by Jaoul[33] with aluminum at 78°K. Shear stress-strain curves (Figs. 5-8) were computed for the polycrystalline material from the tensile quantities and the formulae $\tau = 0.375\sigma$ and $\gamma = \frac{\epsilon}{0.375}$. The 0.375 was chosen arbitrarily to show a parallelism between hardening in polycrystalline material and $[\bar{1}11]$ crystals at large strains. By the analyses of Taylor,[34] and Bishop and Hill[35] the appropriate factor would be 0.326 for a randomly oriented aggregate. But since there could have been a broad $[001]$ texture in the as-received copper rods,[36] in which case a larger factor could be expected on the basis of the above mentioned analyses, there is some justification for the choice of 0.375. The appearance of a linear hardening region in the polycrystalline case, larger in extent at 4.2°K than 78°K, also supports the effort to show a similarity to $[\bar{1}11]$ at large strains. However, at small strains, just beyond yielding, the resolved shear hardening curve for the coarse-grained polycrystalline copper of this work does resemble that for $[001]$ crystals. The implication is that the hardening characteristics change with strain from those of an $[001]$ orientation to a $[\bar{1}11]$. The clearest indication of the point being made is found in Fig. 7.

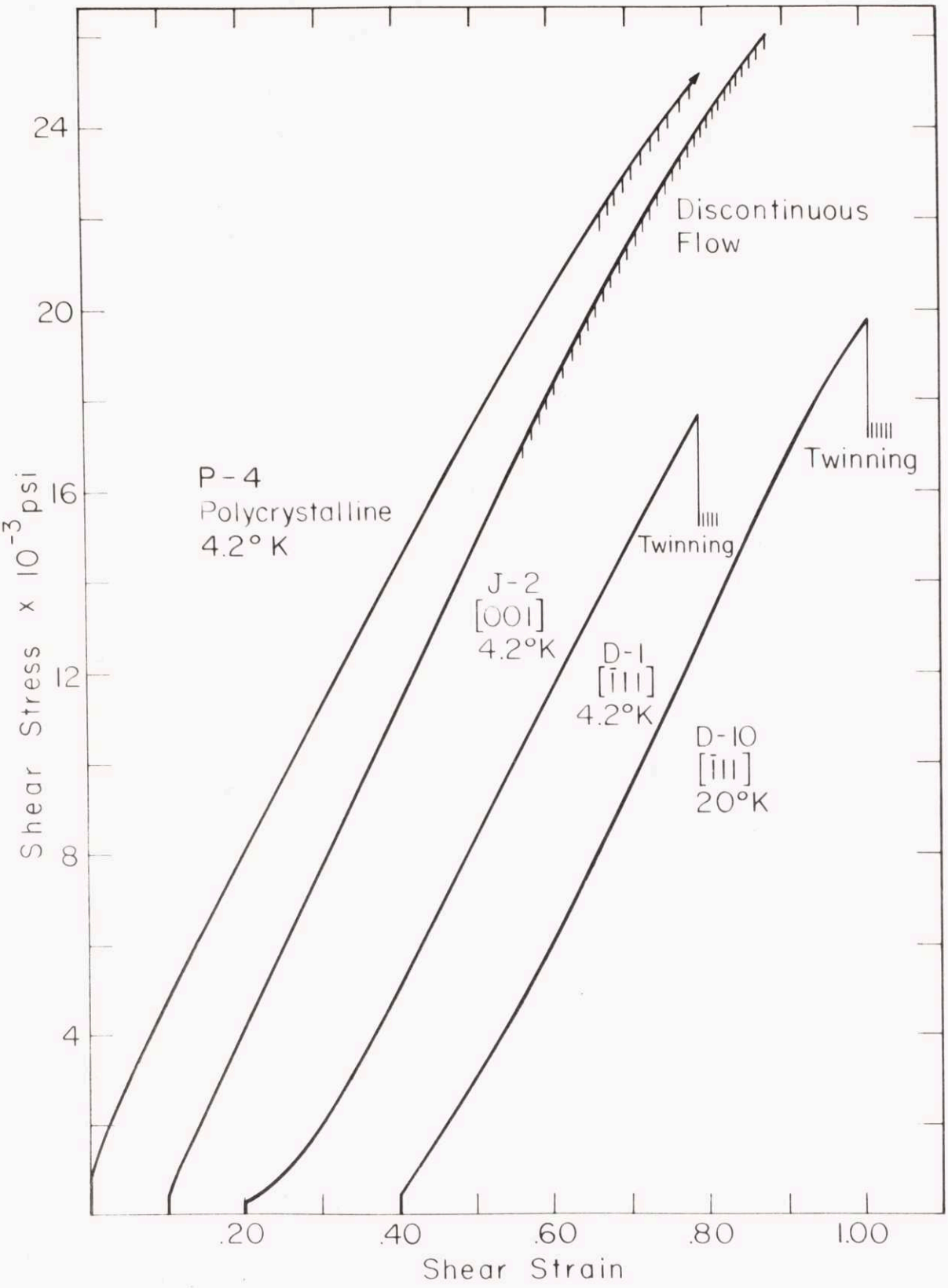

Fig. 5. Shear stress-strain curves at 4.2° and 20°K. Discontinuous flow and twinning load drops are schematically indicated.

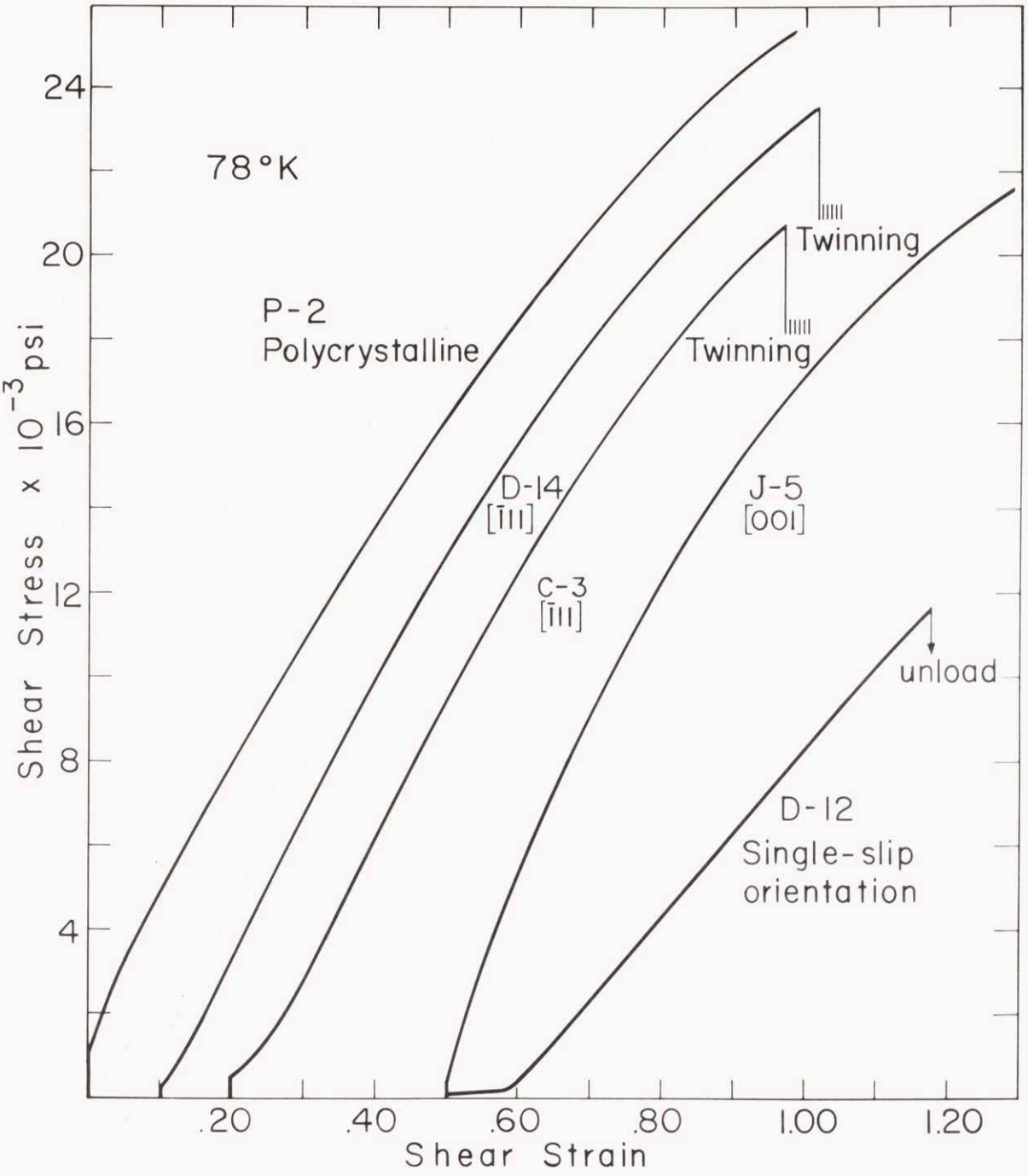

Fig. 6. Shear stress-strain curves at 78°K.

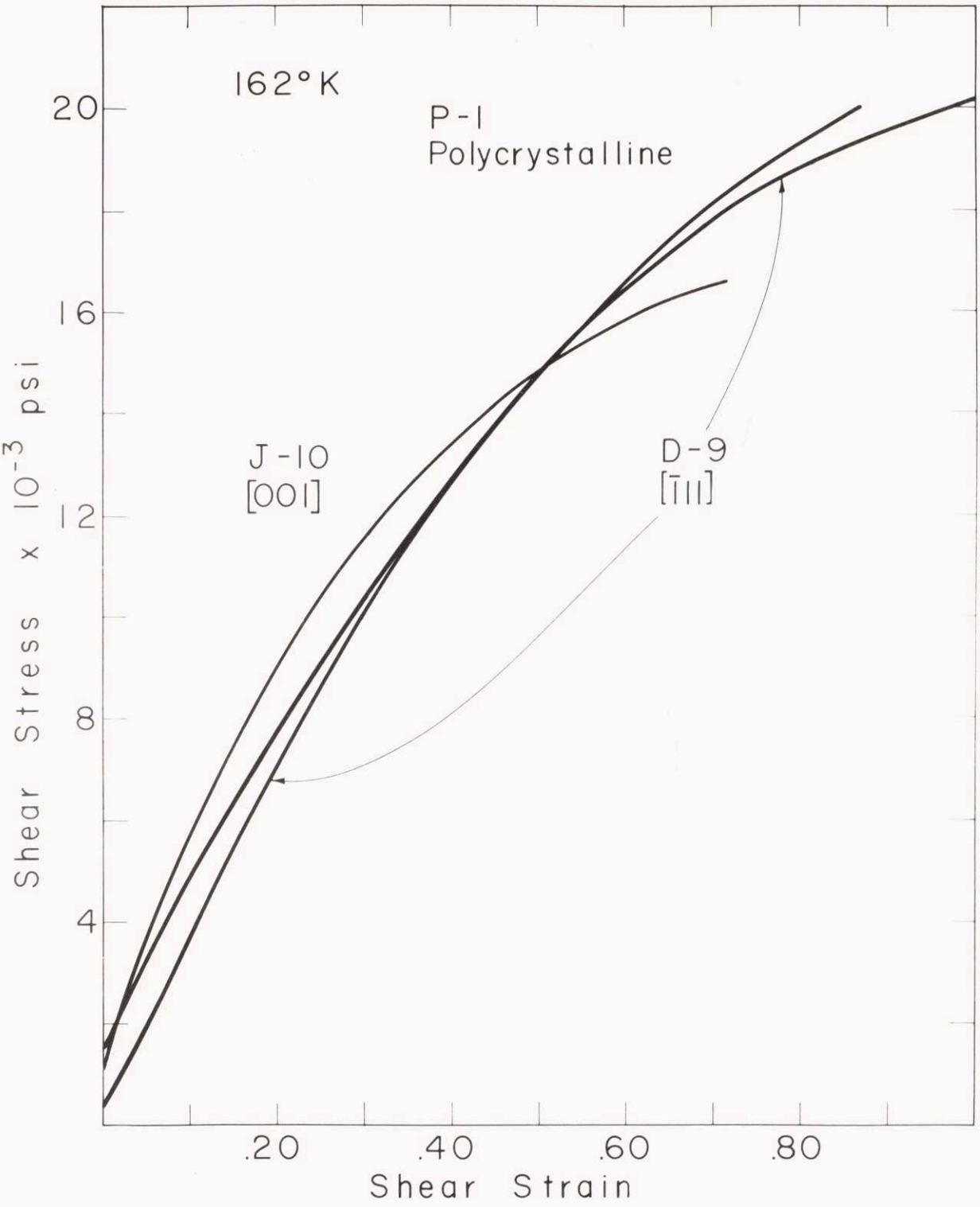

Fig. 7. Shear stress-strain curves at 162°K.

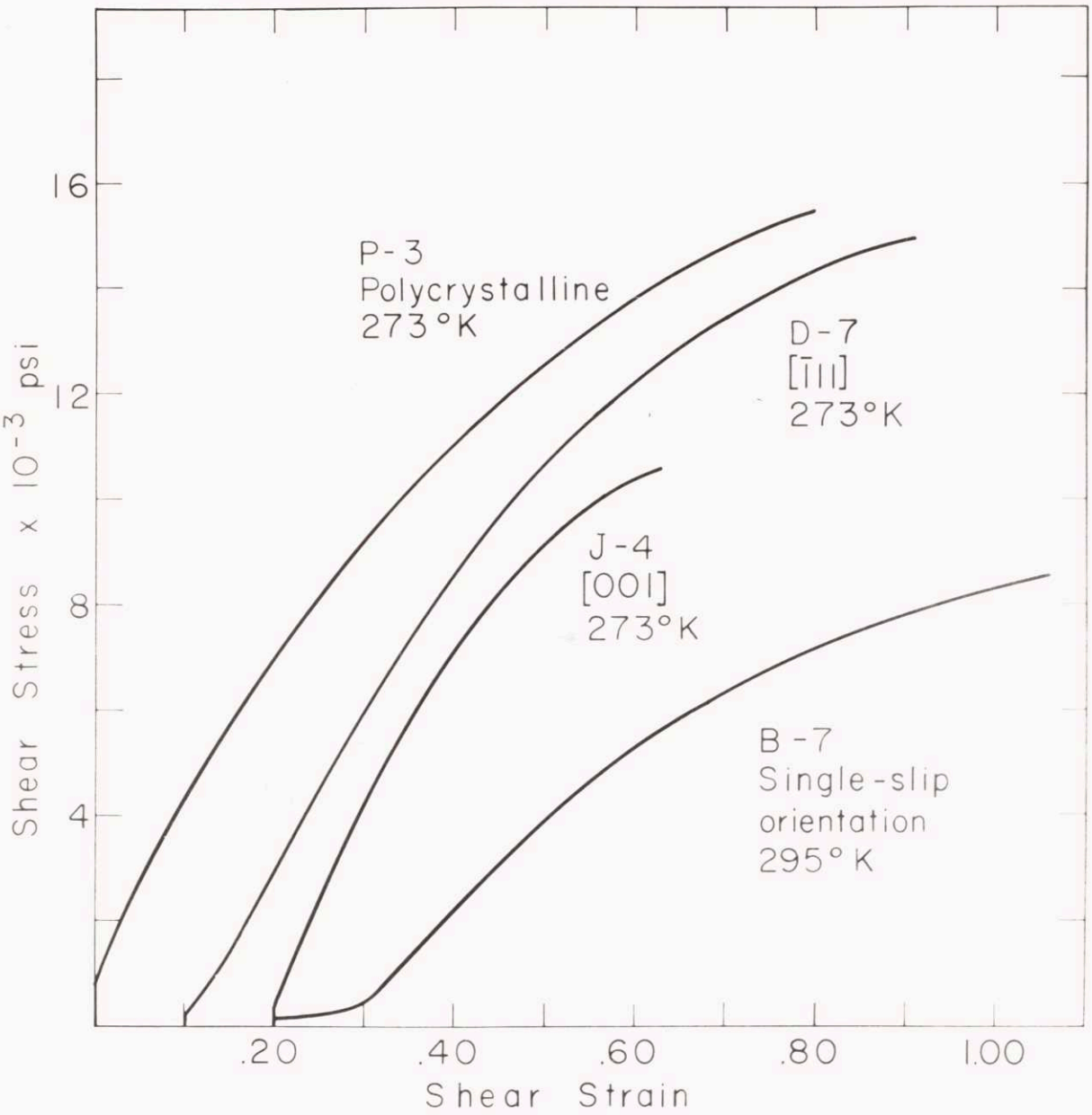

Fig. 8. Shear stress-strain curves at 273° and 295°K.

Shear Stress-strain Curves (τ vs γ)

$[\bar{1}11]$ and Inside-triangle (Single-slip) Orientations: Two linear regions were found in Stage II, although they are not obvious in Figs. 5-8 owing to a reduction in scale. The slopes,* θ_{II_1} and θ_{II_2}, and the corresponding shear stresses at the end of the first and second, τ_K and τ_{III}, respectively, were determined from expanded curves and are recorded in Table II. A comparison of θ_{II_1} at 273°K with the room-temperature values from Diehl[18] and from Rosi[17] for similar orientations near $[\bar{1}11]$ indicates fair agreement, while θ_{II_1} at 4.2°K compares favorably with a value estimated from a curve of Blewitt, Coltman, and Redman.[39] The waviness of the $[\bar{1}11]$ curve at 20°K, caused by measurable temperature fluctuations during the test, made the determination of θ_{II_2} and τ_{III} impossible. In the present results, for the $[\bar{1}11]$ orientation θ_{II_1}/μ was temperature independent** (Fig. 9). As shown in Fig. 9, the θ_{II_1}/μ values for single-slip orientations, which agree favorably with the mean value from Diehl and Berner,[37] are lower than those for $[\bar{1}11]$ crystals by a factor of about 2.

---

* Notation after Mader, Seeger, and Leitz.[4]

** The shear modulus, $\mu = (1/3)(C_{11} - C_{12} + C_{44})$ where the elastic constants are those of Overton and Gaffney.[40]

TABLE II. Work hardening parameters for multiple and single-slip orientations.

Code Number	Test Temp. ^{o}K	σ_o x 10^{-3} psi	τ_o x 10^{-3} psi	θ_{II_1} x 10^{-4} psi	τ_K x 10^{-3} psi	θ_{II_2} x 10^{-4} psi	τ_{III} x 10^{-3} psi	θ_{II_1}/μ x 10^{3}
$[\bar{1}11]$ Crystals								
D-7	273	.558	.152	3.12	6.5	2.51	8.7	5.25
B-12+	273	.710	.193	----	----	----	----	----
D-9	162	1.242	.338	3.52	6.4	2.93	10.8	5.66
B-9+	162	.749	.204	----	----	----	----	----
D-14	78	.494	.134	3.48	7.1	3.20	11.6	5.45
C-3++	78	1.65	.450	3.44	7.6	3.24	11.8	5.40
D-10*	20±5	1.81	.492	~3.50	----	----	----	5.47
D-1	4.2	.764	.208	3.39	13.5	3.10	>17.6	5.30
Diehl[18]	295	----	----	3.55	----	----	----	----
Rosi[17]	295	----	----	2.70	----	----	----	----
Blewitt et al.[39]	4.2	----	----	~3.36	----	----	----	----
[001] Crystals								
J-2	4.2	.852	.348	3.55	----	----	----	5.55
J-9	4.2	1.050	.428	3.64	----	----	----	5.70
Single-slip Crystals								
B-7	295	----	.135	1.89	2.3	1.67	4.2	3.18
D-12	78	----	.075	2.03	9.5	1.77	12.3	3.18

+ Thermal cycling test
++ Cylindrical specimen
* Slightly prestrained

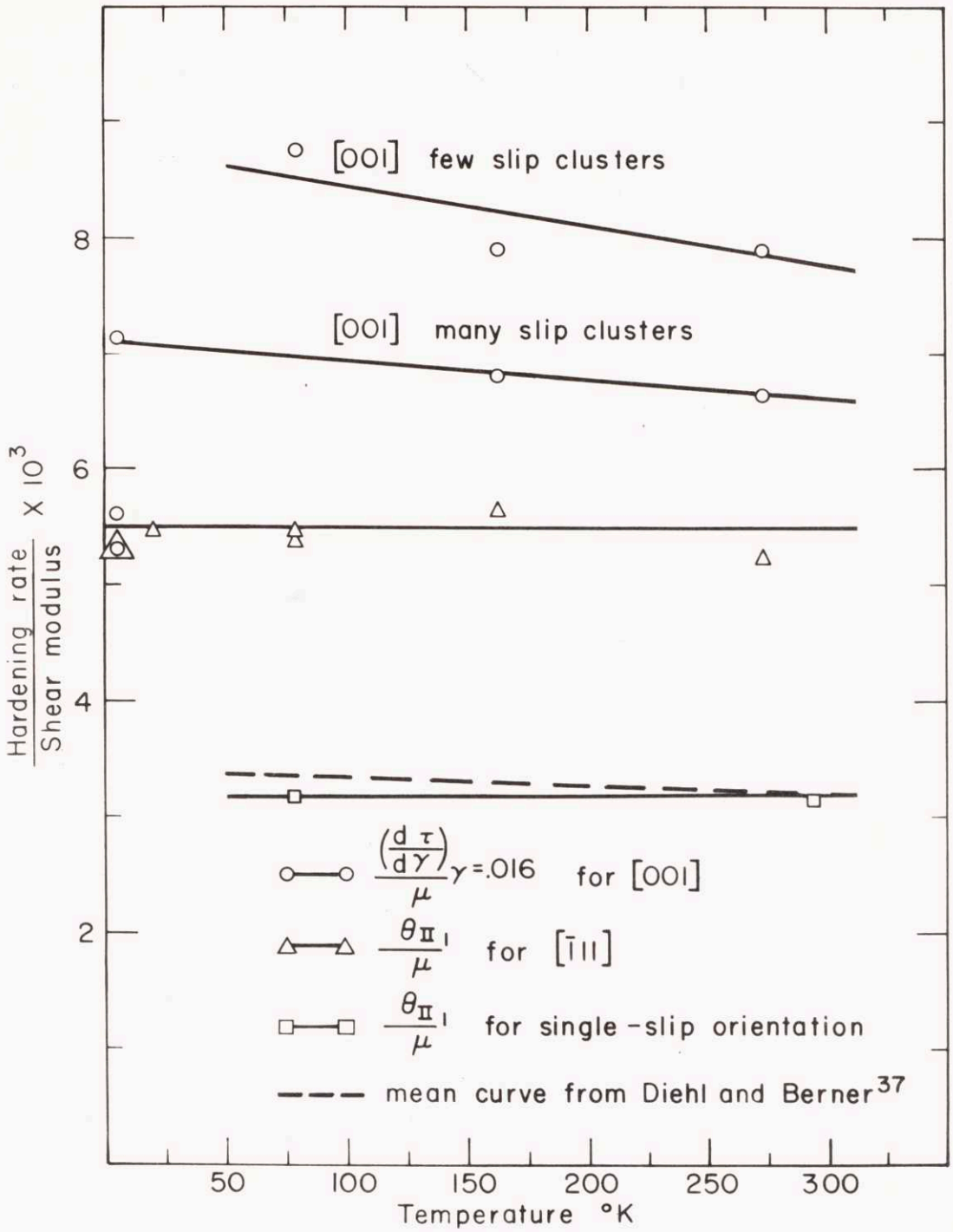

Fig. 9. Dependence of the slope of shear stress-strain curves (in linear region for $[\bar{1}11]$ and single-slip crystals; at $\gamma = 0.016$ for [001]), normalized by the shear modulus, on the testing temperature.

An initially concave-upward trend in the $[\bar{1}11]$ curves (Fig. 10) can be termed "easy glide" and is probably the result of slight deviation from true $[\bar{1}11]$, as demonstrated by Kocks[23] with aluminum of this orientation. The larger extent at 4.2°K might be attributed to the use of a different type of lower grip in the test, one with the nut bearing on a flat collar instead of the ball-and-socket arrangement, and this could have aggravated the tendency towards a deviation from true $[\bar{1}11]$. However, a similar observation of increase in the extent of easy glide with decrease of temperature has also been found in aluminum.[19]

A plot of log τ_{III} vs T (used by Haasen[5] in determining stacking-fault energy) is generally linear, although a discontinuity appears for $[\bar{1}11]$ at 78°K (Fig. 11). The $[\bar{1}11]$ value for 4.2°K is not entirely appropriate for this plot since it is identified with the onset of twinning (Fig. 5); Stage III was never reached at 4.2°K so that the true τ_{III} must be larger still. The single-slip results are in reasonable agreement with a mean curve from Seeger, Berner, and Wolf;[38] the slope is about three times that for $[\bar{1}11]$.

[001] Orientation: The only indication of linear hardening is found at 4.2°K (Fig. 5). At all temperatures, the initial rate of hardening is greater than the maximum rate, θ_{II_1} of $[\bar{1}11]$ crystals. However, the rate decreases more rapidly in [001] than $[\bar{1}11]$ and the τ vs γ curves cross at large strains. Such behavior has been observed

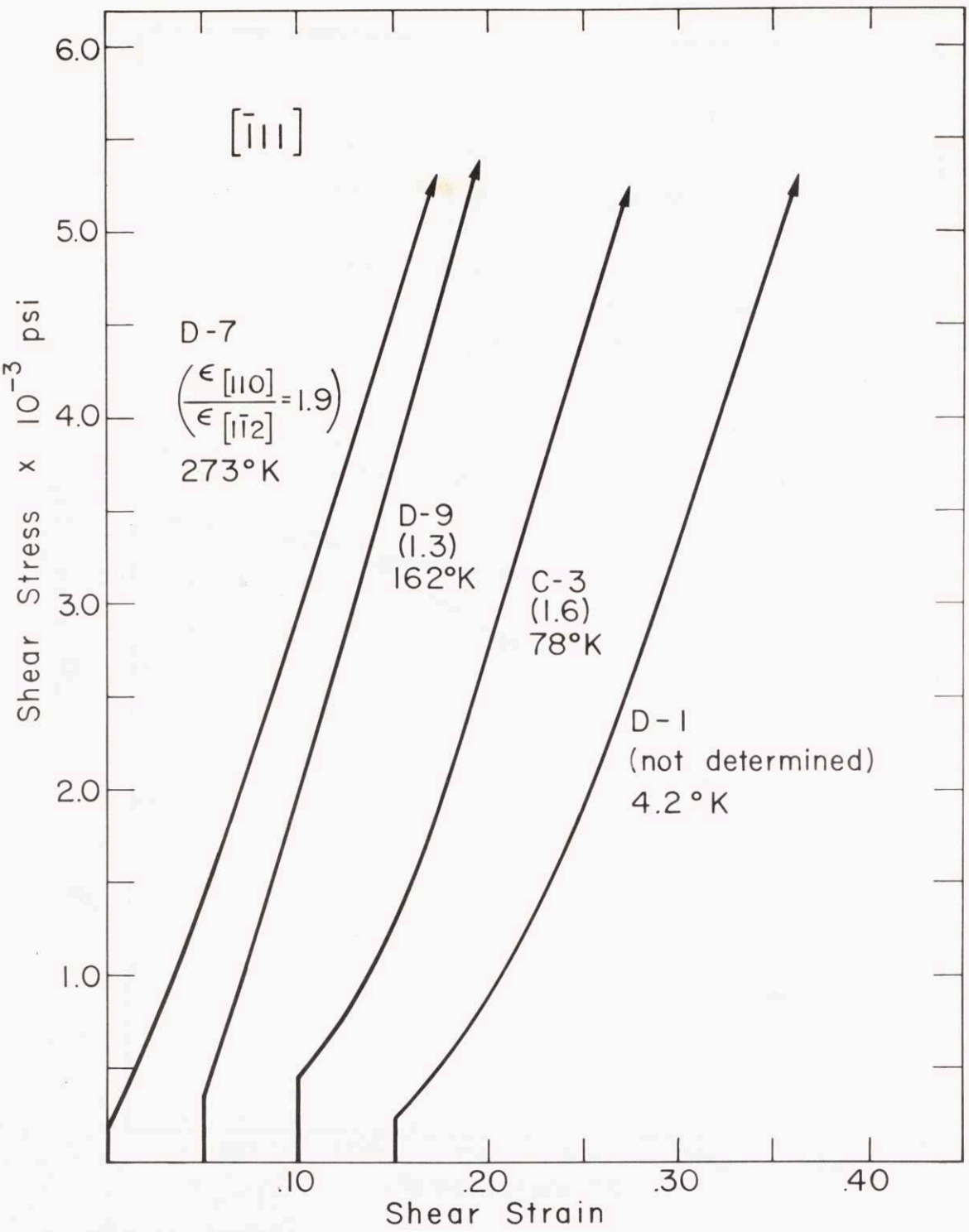

Fig. 10. "Easy glide" portion of the shear stress-strain curves of [$\bar{1}$11] crystals, with the $\epsilon_{[110]}/\epsilon_{[112]}$ ratio as marked. Crystal C-3 was cylindrical and the ratio given is the $\epsilon_{max}/\epsilon_{min}$ value.

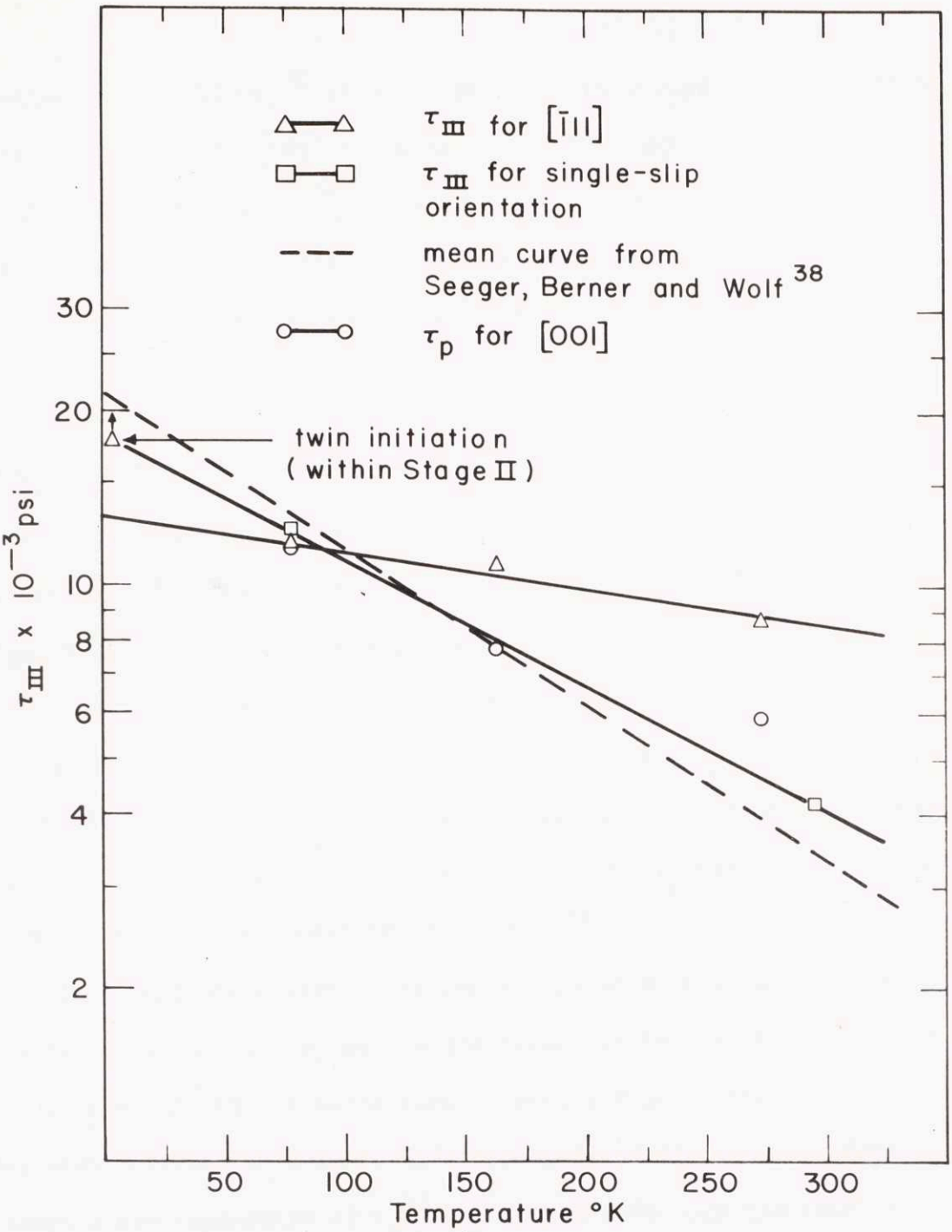

Fig. 11. The dependence of τ_{III} on temperature for crystals oriented for multiple and single slip. τ_p for [001] is considered to be equivalent to τ_{III}.

in aluminum[19] and silver,[20] although in the latter case Ramaswami found a linear region in the [001] curve at low strains over a range of temperatures. The slopes $\left(\frac{d\tau}{d\gamma}\right)_{\mu}$ at an arbitrary strain of $\gamma = 0.016$ are listed in Table I and plotted against temperature in Fig. 9 where it may be seen that the general level is higher than that of θ_{II_1} for $[\bar{1}11]$.

Critical Resolved Shear Stress, τ_o

The basic load value for the calculation was taken from the strip chart where the initial loading path was observed to deviate from a straight line. The corresponding plastic strain was about 5×10^{-4}. The yield stress of polycrystalline samples σ_o was similarly defined, and all values are recorded in Tables I and II. The τ_o for [001] and $[\bar{1}11]$ at 273°K are somewhat lower than those estimated from Livingston's curves.[41] However, the room-temperature value of τ_o for the single-slip orientation is in accord with those of Diehl[18] and Rosi[17] for similar purity. The noticeable scatter at various temperatures, which obscures any temperature dependence, may be due either to the pre-test handling of the crystals or to the variations of purity from crystal to crystal. It has been observed that small differences in purity greatly affect the temperature dependence of τ_o[42] but do not influence the rate of hardening in Stage II.[17] For example, the Stage II parameters in Table II for crystals D-14 and C-3 agree quite well, even though τ_o differs by a factor of 3. As found by previous workers,[43] the yield stress of coarse polycrystalline copper is quite temperature

independent. Furthermore, it is considerably higher than that of single crystals oriented for multiple slip.

Surface Observations and Lateral Strain Measurements

$[\bar{1}11]$ Crystals: Slip clusters were observed at all temperatures. Others have reported such markings after room temperature deformation of copper,[17,18] aluminum[15,21] and gold[21] crystals oriented near $[\bar{1}11]$ and $[001]$. Unlike aluminum crystals of this orientation, however, copper crystals did not develop the ridges found by Hosford et al.[19] In any one region, no more than two sets of clusters were observed. Shown in Fig. 12 are typical markings with a fine structure between them which has been described by Diehl[18] as "cloth-like structure with marked graininess". Clusters, as viewed in the various photomicrographs, are not coincident with $\{111\}$ traces because of elongation of the crystal subsequent to their formation.

Although Laue spots were diffuse,* the zone taken through the center of the spots indicated no lattice rotation. However, width and thickness-strain measurements made with a micrometer on the crystals after extension revealed more thinning in the $[110]$ than $[\bar{1}\bar{1}2]$, the cross section remaining rectangular. The differential

---

* For annealed crystals, Laue spots were about $1/2^{o}$ in diameter, measured with the Greninger net, whereas after deformation the spots were about 4^{o} in diameter.

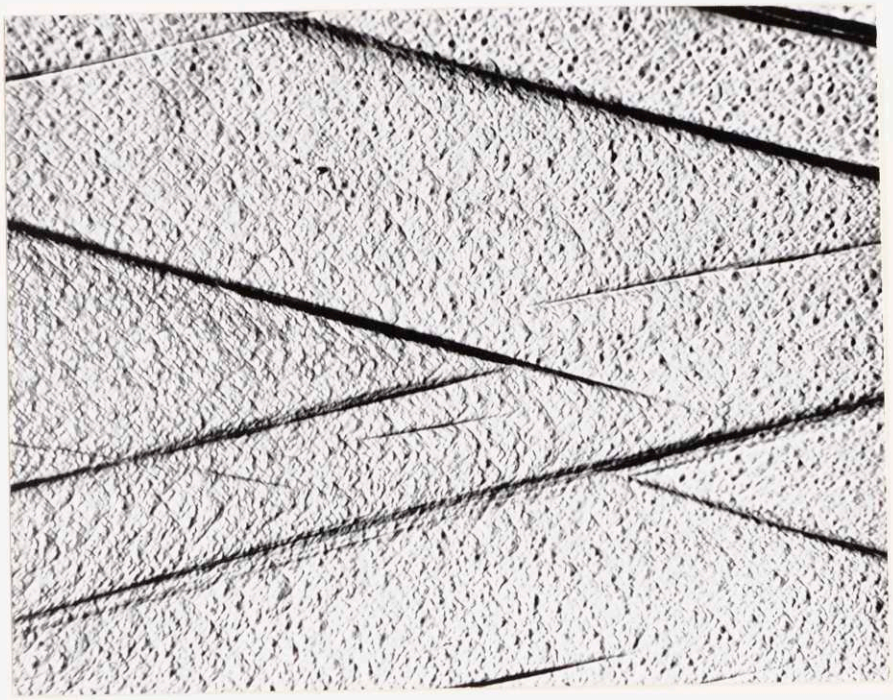

Fig. 12. Clusters and "cloth-like structure" on (112) surface of $[\bar{1}11]$ crystal extended to fracture at 162°K; tensile axis horizontal, X250.

straining cannot be explained in terms of single slip and easy glide since, as shown in Fig. 10, crystal D-9 gave no indication of easy glide yet was characterized by a $\epsilon_{[110]}/\epsilon_{[1\bar{1}2]}$ ratio of 1.3. Therefore, the observed asymmetric deformation must result from different amounts of slip on the 6 initially equally stressed systems. A computation (Appendix II) shows that for $\epsilon_{[110]}/\epsilon_{[1\bar{1}2]} = 2$ and for likely values of shear strains on the different slip systems, a lattice rotation of no more than 4° (for a tensile strain of 0.40) can be expected. Owing to diffuseness of the Laue spots, such small rotations could not be detected. If unequal amounts of slip on different systems should occur, a Schmid-factor consideration shows that the tensile axis will tend to rotate away from the $[\bar{1}11]$ along one of the $\{110\}$ planes. This means that a primary-conjugate* pair of systems would undergo the most slip.

[001] Orientation -- Cluster-free Crystals: Crystals which did not exhibit linear hardening ($78^{\circ}K$, $162^{\circ}K$, $273^{\circ}K$) were also almost devoid of clustered slip. Usually the clusters that were present were associated with geometrical irregularities such as depressions formed during growth on crystal edges. However, a few clusters were found where geometrical stress concentrators were not apparent, as seen in Fig. 13a. The cluster-free regions also had the "cloth-like structure"

---

* Notation of slip systems after that adopted by Rosi and Mathewson[44] and by Clarebrough and Hargreaves.[1]

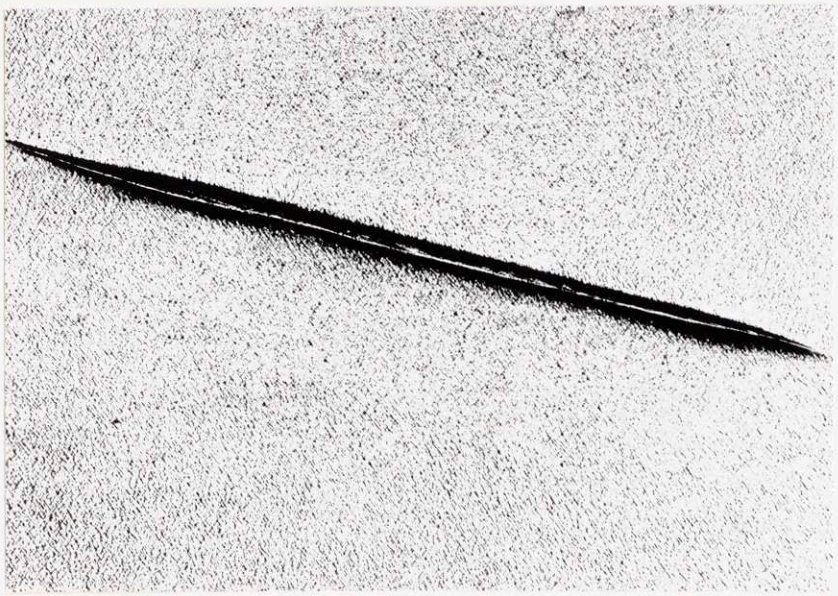

(a)

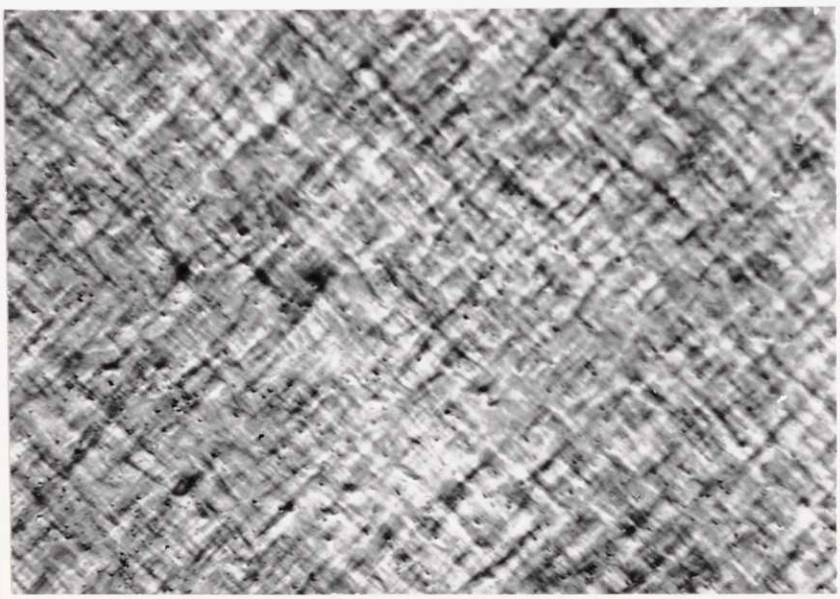

(b)

Fig. 13. (a) Large area of "cloth-like structure" with a rarely occurring cluster on a (110) surface of [001] crystal extended to fracture at 78°K; tensile axis horizontal, X50. (b) Enlarged view of "cloth-like structure" found in (a); tensile axis horizontal, X1000.

as shown in Fig. 13b, the appearance of which did not change much with temperature of deformation. In a few clusters penetrating from the crystal edges, traces of several slip planes were clearly evident within the cluster (Fig. 14a). Cross slip was abundant both in the clusters and near the necked region in extended crystals (Fig. 14b).

No lattice rotation in cluster-free regions could be detected in X-ray photographs. Laue spots were slightly less diffuse than those from $[\bar{1}11]$ crystals, and were elliptical with axes of 3° and 1°. No significant temperature dependence of the diffuseness was detectable with either orientation. Staubwasser[16] has reported that asterism is small for [001] and $[\bar{1}11]$ crystals of aluminum. Micrometer measurements of width and thickness strains in the [001] case revealed axially symmetric deformation, which indicates that four $\langle 110 \rangle$ directions and probably all eight slip systems had operated in equal amounts. Since asterism is attributed to kink-band formation,[45] its near absence is not surprising for orientations associated with such intimate mixing of slip.

Similar observations of very limited slip clustering (except in the vicinity of a neck), non-detectable lattice rotation, and axially symmetric extension have been made on [001] crystals of aluminum at low temperatures.[19]

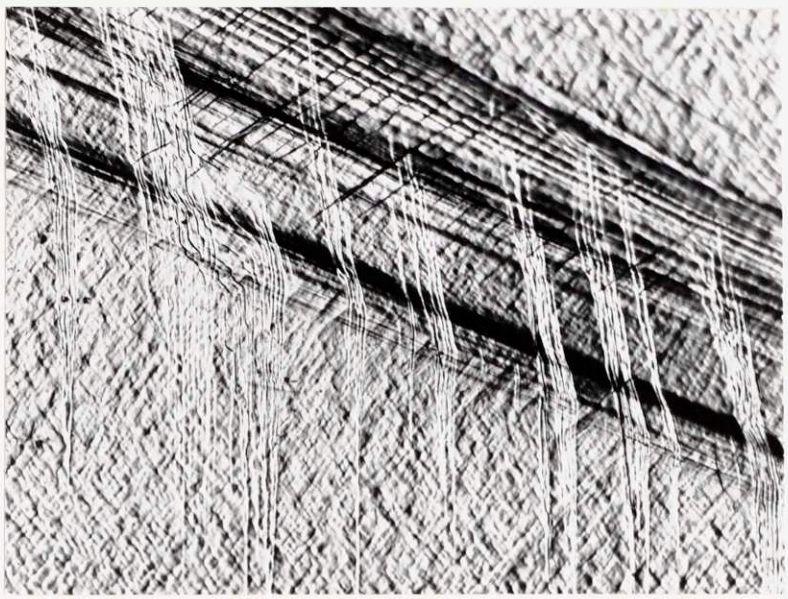

(a)

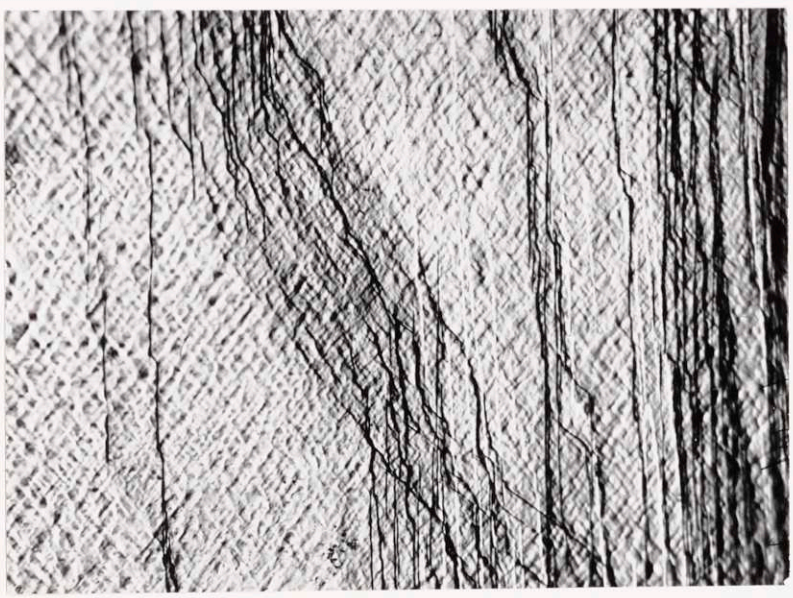

(b)

Fig. 14. (a) Large cluster which seemed to have been initiated from the edge of [001] crystal tested to fracture at 162°K; tensile axis horizontal, (110) surface, X250. (b) Cross slip in [001] crystal near the fracture end tested at 273°K; tensile axis horizontal, (110) surface, X250.

[001] Orientation -- Crystals with Clusters: At 4.2°K, slip clusters were observed on all crystals. However, clusters were not consistently narrow as they were at higher temperatures, but many were broad with a feathery appearance and did not span the width of the crystal (Fig. 15a). Crystals J-2 and J-9 (Table I), on which large numbers of clusters appeared, were also characterized by linear shear stress-strain curves, the slopes of which were similar in value to that of $[\bar{1}11]$ crystal at this temperature (Table II). Crystal J-11, also tested at 4.2°K, showed less clustering than J-2 or J-9 together with non-linear hardening; at the same time, its flow curve was initially lower than that of J-5 tested at 78°K (Fig. 16).

To relate cluster formation to the rate of hardening, clusters of the type shown in Fig. 14a, which seemed to be initiated at the edge of the crystal, were counted and entered in Table I. It seems clear that $(\frac{d\tau}{d\gamma})_{\gamma=.016}$ values are higher for those crystals with 4 or less clusters than for those with 10 or more. Owing to the sensitivity of $(\frac{d\tau}{d\gamma})_{\gamma=.016}$ to the occurrence of clusters, it is difficult to determine whether the temperature dependence of $\frac{(\frac{d\tau}{d\gamma})_{\gamma=.016}}{\mu}$ in Fig. 9 is significant.

From examination of a crystal after four percent extention at 4.2°K, it was found that the regions of predominantly single-slip traces, which give rise to the feathery appearance, are surrounded by traces of other slip planes. The suggestion is that at this temperature slip has a greater tendency to be confined to parallel planes and intermixing of slip systems is avoided if possible. Where the regions of different

Fig. 15a. Broad feathery cluster with bounding "deformation boundaries" on [001] crystal extended four percent at 4.2°K; tensile axis vertical, (110) surface, X100.

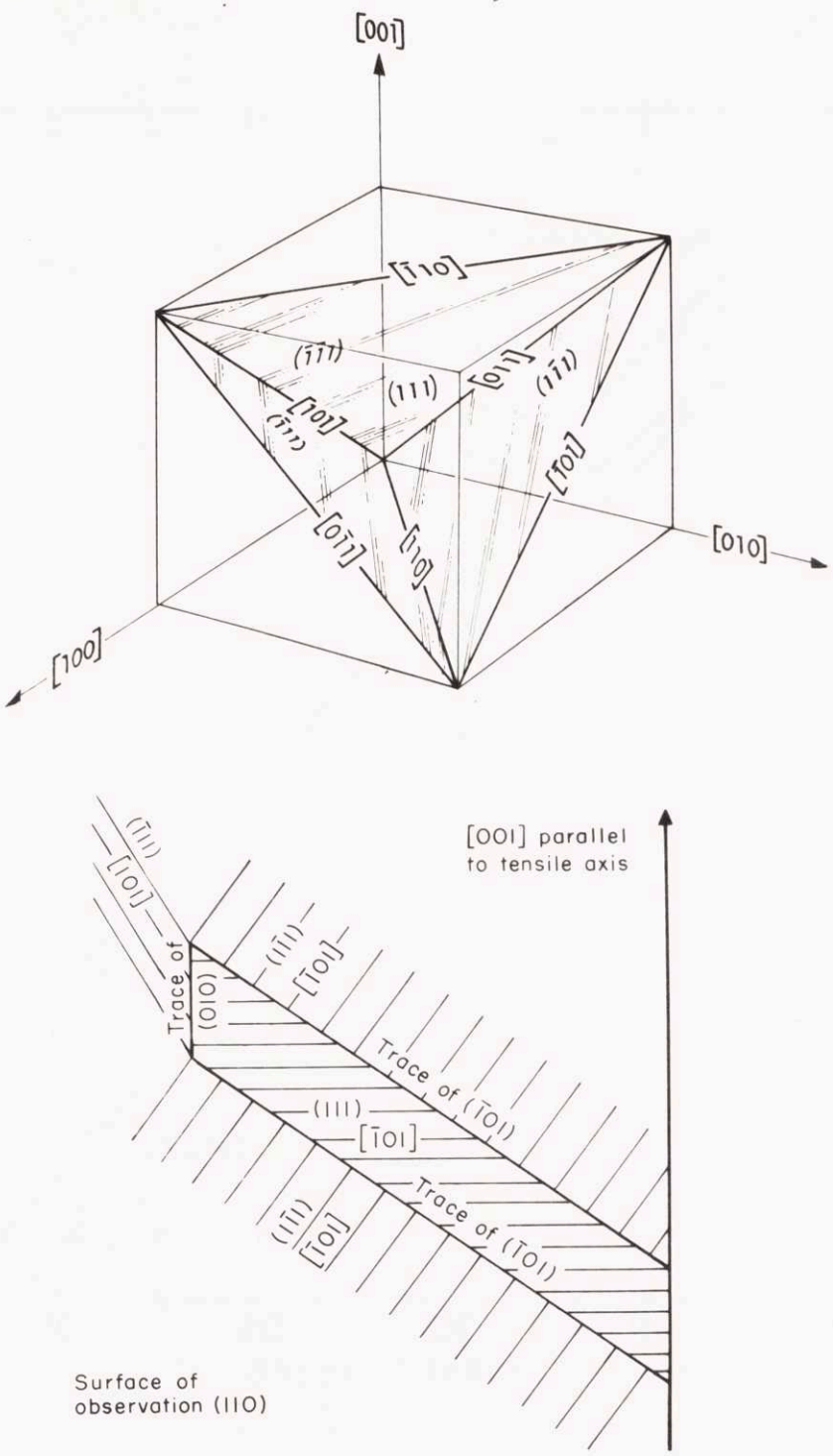

Fig. 15b. Schematic drawing of (a) designating the "deformation-boundary" traces and the slip systems which formed them.

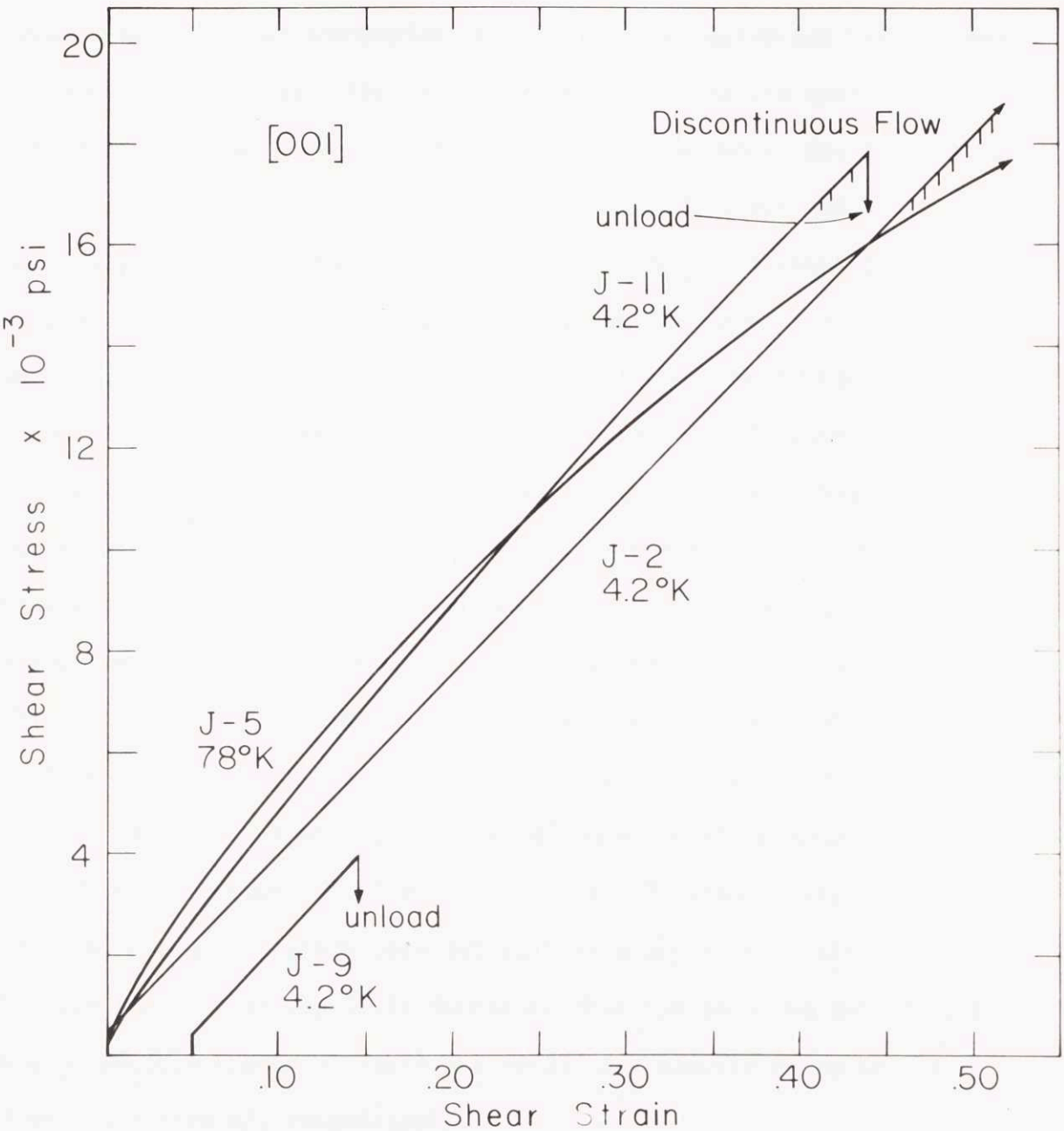

Fig. 16. Shear stress-strain curve for [001] crystals tested at 4.2°K and 78°K.

traces meet, diffuse boundaries or "deformation boundaries" are formed. Although at low strains the sharpness of the boundaries varies from cluster to cluster, when a distinct boundary does form, its trace on a (110) face is parallel to either a $(\bar{1}01)$ or (010) trace and becomes more distinct with increasing deformation. The predominant slip systems operative on each side of the boundaries were determined with reasonable certainty from the lattice rotations found in Laue pictures taken with the X-ray beam straddling the observed deformation boundary. The active slip systems in the region of Fig. 15a are schematically represented in Fig. 15b. Since a two-surface analysis was not possible, the planes of the deformation boundaries could not be determined uniquely. However, it can be shown that strains due to $(111)\ [\bar{1}01]$ and $(1\bar{1}1)\ [\bar{1}01]$ slip are compatible across $(\bar{1}01)$ and, similarly, $(111)\ [\bar{1}01]$ and $(\bar{1}11)\ [101]$ slip are compatible across (010). Kear[46] has recently considered "two-dislocation boundaries" formed by these types of slip interactions. It seems reasonable that two slipping regions interact in such a way as to minimize the lattice strain. Hence, it is concluded that the observed deformation boundaries are traces of $(\bar{1}01)$ and (010), and correspond to Kear's case i and case vi, respectively.

At low strains, very intimate mixing of slip lines from at least three planes was observed (the fourth trace is parallel to that of the third on the (110) surface). Examination of the "cloth-like structure" revealed that it should not be attributed to slip steps but rather to

general topographical upheavals caused by the intermixing of slip systems.

Temperature Dependence of Flow Stress

Thermal cycling experiments similar to those of Adams and Cottrell[47] were performed between 162° and 78°K, and between 273° and 78°K. The difference in flow stress, $\Delta\tau$, was determined by changing the testing temperature from high to low, to avoid work softening effects, and by extrapolating through the yield point as suggested by Makin[48] to eliminate unloading effects. The results are presented as $\Delta\tau$ vs τ_{78} plots in Fig. 17. The Cottrell-Stokes Law[49] seems to be obeyed in both orientations for cycling between 162° and 78°K, with the $\frac{\Delta\tau}{\tau_{78}}$ ratio being lower for the $[001]$. However, in cycling tests between 273° and 78°K, $\frac{\Delta\tau}{\tau_{78}}$ is not constant (Fig. 17) beyond a τ_{78} of about 8000 psi. Moreover, the difference between $[001]$ and $[\bar{1}11]$ orientations disappears. In the linear regions the temperature dependence of flow stress compares favorably with the values estimated from Basinski's[10] results on single-slip orientations (insert in Fig. 17).

The results of similar tests on polycrystalline copper are included in Fig. 17; again, 0.375 was used as the resolving factor. Initially, at low stresses, the $\frac{\Delta\tau}{\tau_{78}}$ points for 162°K fall along those for $[001]$ crystals before shifting at higher stresses towards those for $[\bar{1}11]$ crystals. In cycling between 273° and 78°K the $\frac{\Delta\tau}{\tau_{78}}$ trend is essentially identical with that of $[001]$ and $[\bar{1}11]$.

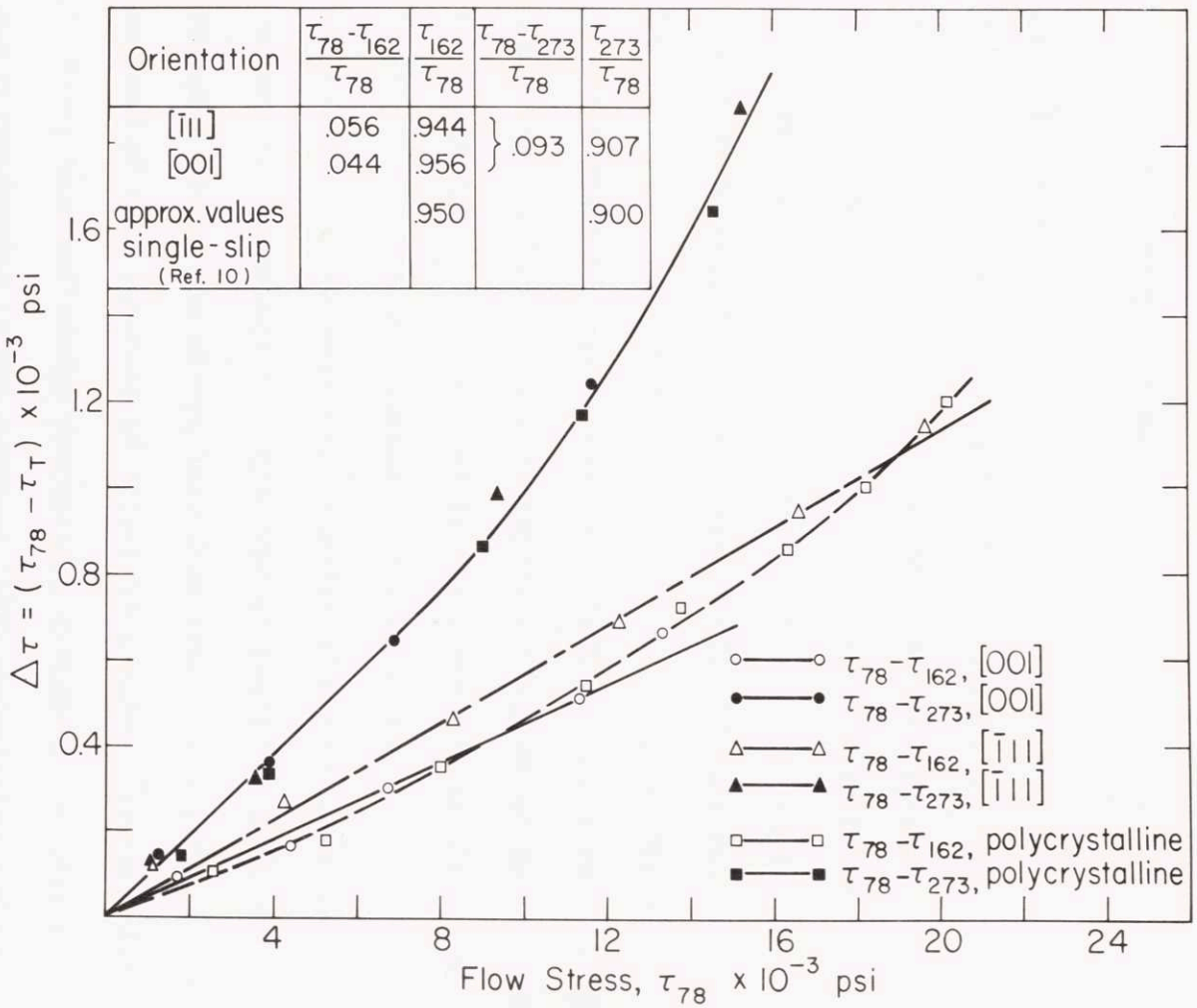

Fig. 17. Curves of $\Delta\tau$ vs τ_{78} for cycling temperatures 162° and 273°K. Inserted table gives the slopes of the linear regions.

For the lower temperature, the trend suggested by the stress dependence of $\frac{\Delta\tau}{\tau_{78}}$ is consistent with that observed earlier in the hardening curves (Figs. 5-8), suggesting a transition from [001] - type to $[\bar{1}11]$ - type hardening with increasing strain.

Deformation Twinning

$[\bar{1}11]$ Crystals: During tests of $[\bar{1}11]$ crystals at 4.2°, 20° and 78°K, the load was observed to drop abruptly and to register in an irregular fashion at some lower level, as previously reported by Blewitt, Coltman, and Redman.[50] Stress-strain curves (engineering basis) are given in Fig. 18. Comparison of Fig. 18 with Figs. 5 and 6 shows that twinning occurred in Stage II at 4.2°K and in Stage III at 78°K. In which stage twinning occurred at 20°K could not be determined owing to the previously mentioned temperature fluctuation during the test. The variation of load evident in the three curves after the initial drop is most probably caused by slight variations in cross-sectional area preventing smooth propagation of Lüders-type band of twinned material. Examination of one crystal tested at 78°K and pulled somewhat beyond the abrupt load drop revealed that the Lüders band consisted of thin lamellae of alternating twinned and untwinned material; X-ray back-reflection photographs contained two sets of spots, one corresponding to the original $[\bar{1}11]$ orientation and the other to a twinned orientation, (111) $[\bar{2}11]$, as reported by Blewitt et al.

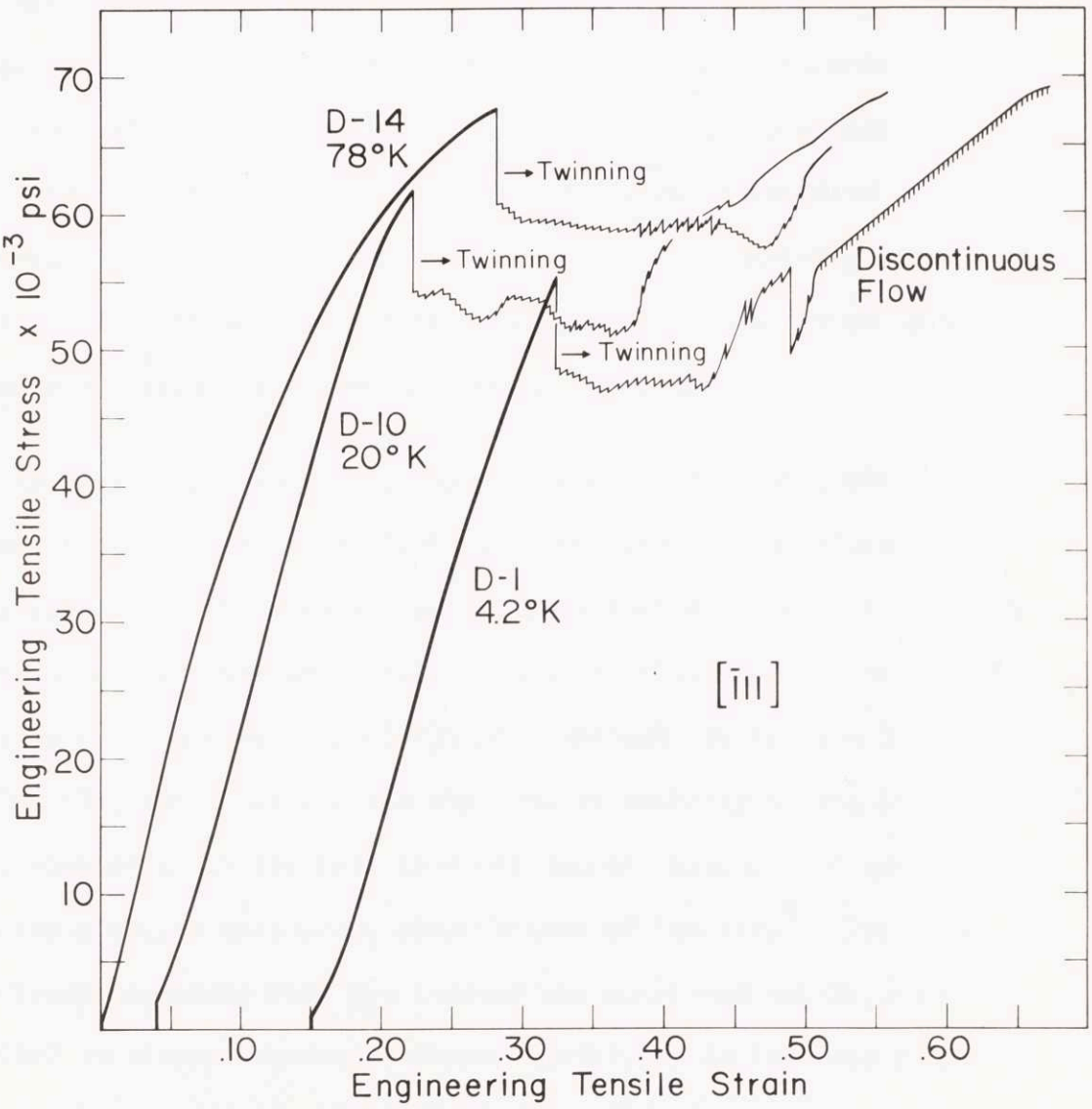

Fig. 18. Engineering tensile stress-strain curves of [$\bar{1}$11] crystals tested at 4.2°, 20° and 78°K.

The geometry of the specimen was found to affect Lüders-band formation as it is being reported here. Preliminary tests on crystals with slightly tapered gauge sections showed that, when twins are nucleated near the grip, where the diagonal spreading of a twinned region is inhibited by the grip, the stress concentration produced near the head of the first set of twins initiated the operation of a second twin system. Twinning on the two systems propagated with a V-shaped front, apparently without intersecting. However, with crystals of uniform cross-section, twins of only one system were formed and propagated throughout the gauge length.

In Fig. 19a, twinned regions appearing as dark wavy bands can be seen together with slip clusters which formed both before and after twinning. The clusters in the untwinned material which formed prior to twinning are not parallel to $\{111\}$ slip traces since these markings have rotated with elongation, whereas the lattice has not. In Fig. 19b, twin lamellae are observed as white-appearing bands at least some of which are less than one micron thickness in accord with the electron microscopy observations of Venables.[51] The wavy slip traces crossing both the twinned and untwinned matrix are parallel to planes sharing a common $\langle 110 \rangle^*$, as in the case of deformation by "pencil glide" (Appendix III).

The shear stresses for twin initiation, τ_t, and for Lüders-band propagation of the twinned material, τ_{tp}, are listed in Table III.

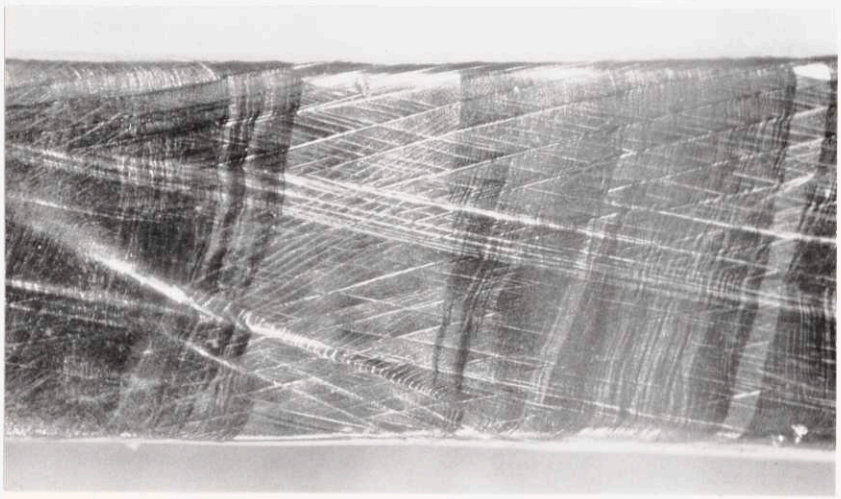

(a)

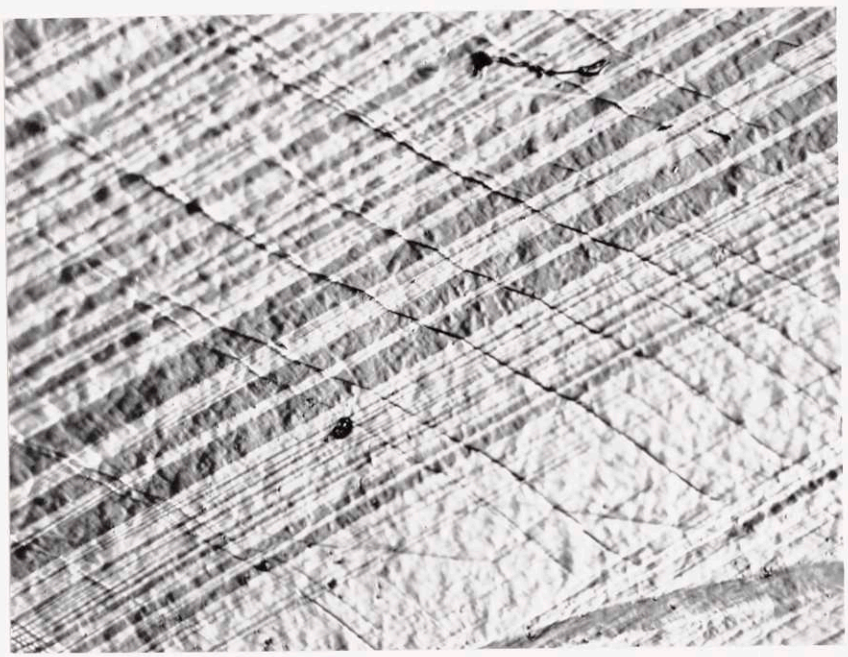

(b)

Fig. 19. (a) Twin lamellae (wavy dark traces) in $[\bar{1}11]$ crystal tested at 78°K. The long clusters at low angles to the tensile axis were formed before twin initiation, whereas the fine white traces in the untwinned (center) section were formed after twinning, $(1\bar{1}2)$ surface, X18. (b) Twin lamellae (white traces) in $[\bar{1}11]$ crystal tested at 4.2°K; tensile axis horizontal, (110) surface, X500.

TABLE III. Twinning stresses at various temperatures.

Code Number	Test Temp. ^{o}K	Initiation stress $\tau_t \times 10^{-3}$ psi	Propagation stress $\tau_{tp} \times 10^{-3}$ psi
$[\bar{1}11]$ in tension			
C-3	78	24.4	21.4
D-5	78	24.4	21.4
D-14	78	27.2	24.6
B-9*	78	24.9	22.2
D-10	20±5	22.7	20.1
D-1	4.2	20.3	17.9
D-2+	4.2	19.7	17.5
[001] in compression			
J-1	4.2	< 21.2	----

* Thermal cycling test

\+ Tested in soft machine

Crystal D-2 was tested in another machine (described elsewhere[52]) having a spring constant two orders of magnitude smaller than that of the standard machine employed for crystal D-1; apparently, τ_t and τ_{tp} are not influenced by machine stiffness. Prior thermal cycling of crystal B-9 between 162° and 78°K had little effect on the twinning stresses at 78°K. Thus τ_t and τ_{tp} also seem to be independent of prior strain. $[\bar{1}11]$ crystals were compressed at 4.2°K, but this orientation was not stable; the compression axis rotated away from $[\bar{1}11]$ and a banded structure was developed without twinning.

In previous reports[53-55] of the twinning stress, large scatter has obscured any temperature dependence. However, the present findings clearly show that τ_t rises with increase in temperature (Table III).

[001] Crystals: These did not twin in tension, although twins were formed in compression at 4.2°K. A crystal with square cross section and height-to-width ratio of about 1.3 was compressed in a special cage adapted to the already-described tensile machine. The loading plates and surfaces of the crystal were coated with Aqua Dag for lubrication. At a load which corresponded to a shear stress of 21.2×10^3 psi on a preferred twin system, the crystal was unloaded, metallographically polished, and etched with Young's $\{011\}$ etch.[56] In Fig. 20a a few twins with traces parallel to three (and possibly four) $\{111\}$ planes are evident. By examining etch pits* (Fig. 20b)

---

* The formation of crystallographic etch pits is attributed to the presence of impurities in the copper.

(a)

(b)

Fig. 20. (a) Twins in [001] crystal compressed at 4.2°K and sectioned parallel to (110). The dark rectangular spots are etch pits; tensile axis horizontal, X250. (b) Enlarged view of twins in (a) showing distortion of crystallographic pits at the twin boundary, X1000.

in the twinned and untwinned matrix, the lattice rotation was found to be $70^{\circ} \pm 5^{\circ}$, which is in good agreement with the predicted $70^{\circ}32'$. Another [001] crystal was compressed to a shear stress for twinning of 25.9×10^3 psi; no irregular loading behavior was recorded, but after metallographic polishing profuse twinning was observed throughout the section. As a result of these observations, it was concluded that the shear stress for twinning in compression at $4.2^{\circ}K$ must be slightly lower than 21.2×10^3 psi. This corresponds favorably with observed values for $[\bar{1}11]$ crystals in tension.

Discontinuous Flow

Discontinuous flow similar to that observed by Blewitt et al.[50] occurred in [001] crystals at $4.2^{\circ}K$ at a tensile stress of about 41×10^3 psi ($\tau = 16.2 \times 10^3$ psi); a difference in machine stiffness by a factor of about 100 had no effect on this value of τ. In $[\bar{1}11]$ crystals, discontinuous flow was not observed until after twinning, although twinning did not begin until a tensile stress of about 64×10^3 psi ($\tau = 17.4 \times 10^3$ psi) was reached. The load drops were of the order of one percent of the applied load and did not vary significantly between the hard and soft machines. However, the extension per load drop was larger for the softer machine. The adiabatic heating which has been demonstrated to be responsible for the load drops[57] was reflected in the fracture appearance of the crystals at $4.2^{\circ}K$; the crystal tested in the hard machine failed by shear, whereas that tested in the softer machine failed by necking to rupture, which was the mode normally observed at $78^{\circ}K$.

Warming the crystal up to room temperature after straining at 4.2°K produced a yield point and heterogeneous flow upon retesting at 4.2°K (Fig. 21). This yield phenomenon is attributed to unloading and strain-aging effects.[58,59] Examination of the crystal after electropolishing (at room temperature) and further extension at 4.2°K, part way into the heterogeneous region, showed a Lüders band consisting of the "fine cloth-like structure" and slip bands (Fig. 22b). Comparison of the same region before electropolishing (Fig. 22a) and after electropolishing and retesting (Fig. 22b) makes it clear that the slip bands appear only in areas where clusters were formerly present. Furthermore, slip traces of an additional plane are evident. Blewitt et al.[50] also observed intersecting slip bands in copper crystals oriented for single slip after electropolishing and retesting, but did not report any yield point. Recently Buck[60] has performed a similar test, also with a copper crystal. However, it was his finding that upon reloading discontinuous flow did not occur before fracture intervened. These observations suggest that the process by which adiabatic flow is nucleated[57] is structure sensitive.

During the deformation of a polycrystalline sample at 4.2°K, load drops similar in size and frequency to the load drops observed with [001] crystals were initiated at a tensile stress of 58.5×10^3 psi. Although metallographic examination after fracture revealed profuse deformation twinning, these load drops are attributed to adiabatic heating. One indication that twinning is not responsible in this

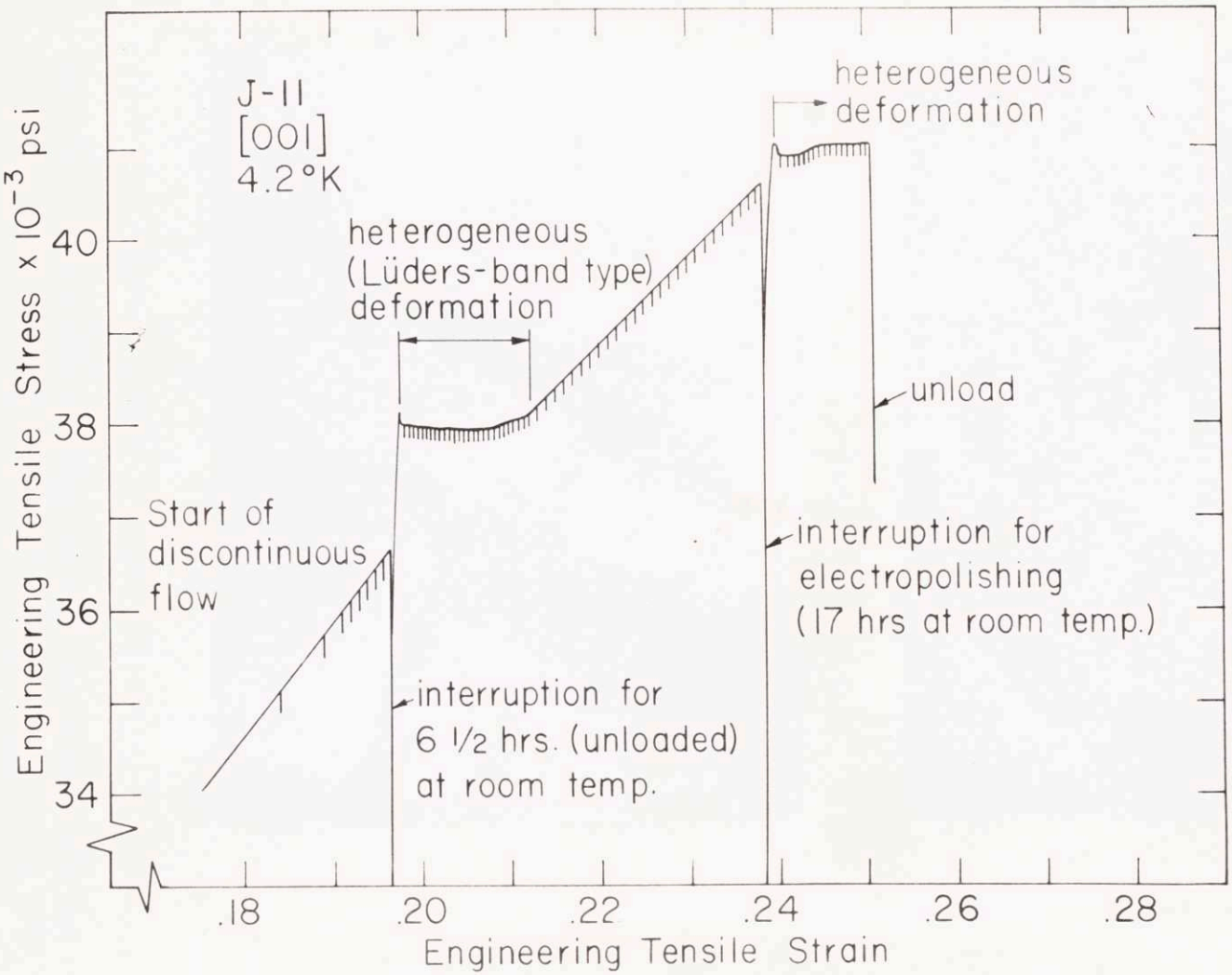

Fig. 21. Engineering tensile stress-strain curve of [001] crystal at 4.2°K, the loading was interrupted for metallographic examination at room temperature.

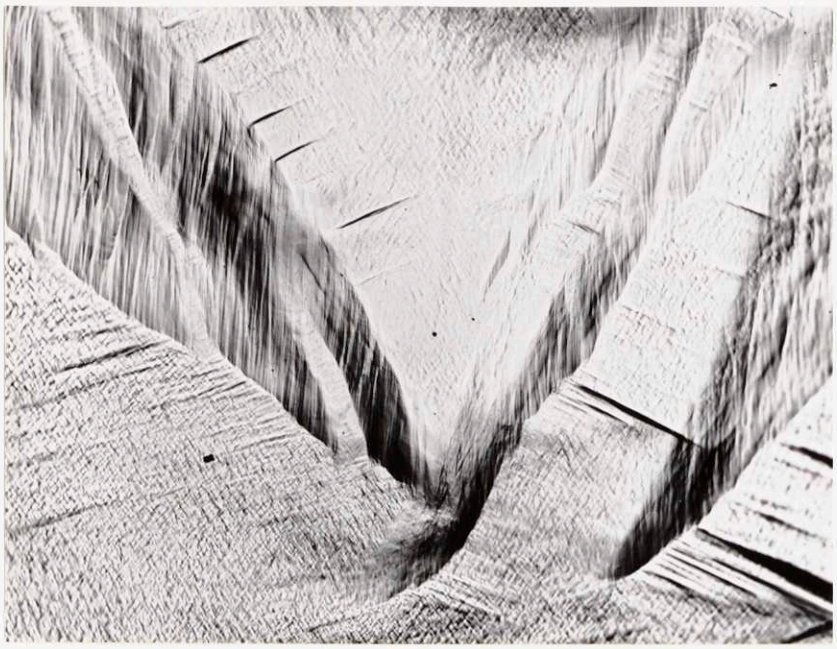

(a)

(b)

Fig. 22. (a) Feathery clusters in [001] crystal tested at 4.2°K and unloaded at start of discontinuous load drops, tensile axis horizontal, (110) surface, X150. (b) Same region as (a) showing intersecting slip bands in former regions of clusters and "cloth-like structure" after electropolishing and retesting at 4.2°K, X150.

case is that many twins were found in the vicinity of the neck in a polycrystalline sample tested at 78°K, yet no load drops were observed. On the other hand, even if the actual load drop should not be associated directly with twinning, the formation of a twin lamella may provide the necessary local heating to initiate adiabatic flow at 4.2°K.

DISCUSSION

Strain Hardening of Crystals Oriented for Multiple Slip

The processes underlying the linear hardening region in the shear stress-strain curve of single crystals (Stage II) involve dislocation generation on more than one $\{111\}$ plane and some kind of interaction which prevents extensive dislocation motion. All dislocations are imagined to be confined to the planes on which they originate and/or travel; there is no cross slip in Stage II.

The observation of non-linear hardening in $[001]$ crystals contrasted with the linear hardening of $[\bar{1}11]$ crystals (Figs. 6-8), might be interpreted as showing either that Stage III is initiated at yield or that a non-linear Stage II exists. Assuming that the cross-slip model of Schoeck and Seeger[61] applies for both $[001]$ and $[\bar{1}11]$ crystals, it can be argued that the monotonic decrease of $\frac{d\tau}{d\gamma}$ in the case of $[001]$ (Figs. 6-8) is not caused by "dynamic recovery" setting in with yielding. For one reason, dislocation pile-ups behind Lomer-Cottrell[62,63] (L-C) barriers in $[001]$ crystals would be of mixed character, in contrast

to the pure screw to be expected in $[\bar{1}11]$; accordingly, cross slip should occur with more difficulty in $[001]$, the orientation that exhibits non-linear hardening. Secondly, if "dynamic recovery" were initiated at yield, the initial rate of hardening in $[001]$ ought to be smaller than that in $[\bar{1}11]$ in Stage II, contrary to observation, and the temperature dependence of $\left(\frac{d\tau}{d\gamma}\right)_{\gamma=.016}$ should be larger than observed (Fig. 9). Therefore, it is concluded that a non-linear Stage II exists for $[001]$ crystals. An obvious difficulty arises in finding the strain at which Stage II passes into Stage III; a reasonable approach is to choose a value near ϵ_p where the log $(\sigma - \sigma_o)$ vs log ϵ plot (Fig. 4) deviates from linearity. Such a choice results in a stress τ_p which is about the τ_{III} value for single-slip orientations (Fig. 11).

The question to be considered is whether current hardening mechanisms which are used to predict linear Stage II are sufficiently flexible to explain a non-linear Stage II as well; in view of the nature of the theories, an answer in the affirmative might well be expected.

The long range stress-field theories require L-C dislocations to act as barriers to dislocation motion. Although it is conceivable that different arrangements of such barriers may give rise to linear and non-linear hardening, the abundant clustering and the tendency for easy glide in $[\bar{1}11]$ crystals but not in $[001]$ cannot easily be explained by changing the array of sessile dislocations. As discussed by Kocks,[65] and by Hosford, Fleischer and Backofen,[19] there are

four ways to produce L-C dislocations lying parallel to the two unstressed $\langle 110 \rangle$ directions in crystals of $[001]$ orientation, while there are three ways of producing them in $[\bar{1}11]$ crystals, all lying parallel to potentially active $\langle 110 \rangle$ directions. Now, since the sessile dislocations in $[\bar{1}11]$ orientation lie along the intersection of two potentially active planes, the hardening rate in this orientation would be expected to be larger than that in $[001]$, again contrary to observation (Fig. 8). Kocks[65] also could not explain, in terms of the formation of L-C barriers, the work hardening behavior of aluminum crystals oriented for various types of multiple slip.

A specific disagreement with Seeger's theory of hardening arises for $[\bar{1}11]$ crystals. According to the theory[38] the stacking-fault energy can be derived from the expression $B = \frac{k}{A} \log \frac{\dot{\epsilon}_o}{\dot{\epsilon}}$, where B is the slope of the log τ_{III} vs T plot, k is the Boltzmann constant, A is a parameter which is principally sensitive only to the stacking-fault energy, $\dot{\epsilon}$ and $\dot{\epsilon}_o$ are the strain rates at any given temperature (at which τ_{III} is evaluated) and at 0^oK, respectively. $\dot{\epsilon}_o$, which is determined from the strain rate sensitivity of τ_{III}, is not expected to be highly orientation sensitive. Thus the plots in Fig. 11 for $[\bar{1}11]$ and single-slip orientations should be nearly parallel, which they are not. Such a finding rules against long-range stresses from pile-ups at L-C barriers as the dominant source of hardening.

Other mechanisms of hardening are based on forest dislocations[9,10] and jogs.[13] To investigate implications from these mechanisms, all possible interactions among slip systems are classified into five types[66] (Appendix IV), and the number of ways in which each type can occur for the two orientations of interest are listed in Table IV. According to Cottrell,[67] slip systems activated by the same applied stress undergo screw-screw intersections which produce interstitial-forming jogs, except for type-d intersection which produces equal numbers of interstitial-forming and vacancy-forming jogs. Those pairs of slip systems which are capable of producing jogs are indicated in Table IV together with the relative numbers of interstitial-forming jogs, N_I, and of vacancy-forming jogs, N_v, assuming equal amounts of slip on all systems. Although the numbers of interstitial and vacancy-forming jogs actually produced are impossible to determine, the ratio might reasonably be assumed to be proportional to $\frac{\sum N_I}{\sum N_v}$.

According to the jog theory of hardening, the temperature independent part of the flow stress, τ_g, is the result of the drag on dislocations caused by vacancy-forming jogs; the temperature dependent part, τ_s, arises from the stress-aided constriction of extended interstitial-forming jogs which permits conservative glide along the screw dislocations. Hence, it would seem that $\frac{\tau_s}{\tau_g}$ ought to be dependent on the ratio $\frac{\sum N_I}{\sum N_v}$. However, the temperature dependence of the flow stress (Fig. 17) is smaller for the [001] orientation which has the larger $\frac{\sum N_I}{\sum N_v}$, contrary to this prediction. Thus the

TABLE IV. Interacting combinations of slip systems and the types of jogs formed.

Orientation	Type of interaction	Number of possible ways of interaction	Product of interaction	N_I, relative number of interstitial jogs	N_V, relative number of vacancy jogs	$\frac{\sum N_I}{\sum N_V}$
$[\bar{1}11]$	a	3	none	----	----	$\frac{9}{3}=3$
	b	3	"	----	----	
	c	3	2 jogs	6	0	
	d	6	1 kink, 1 jog	3	3	
$[001]$	a	4	none	----	----	$\frac{28}{4}=7$
	b	4	"	----	----	
	c	4	2 jogs	8	0	
	d	8	1 kink, 1 jog	4	4	
	e	8	2 jogs	16	0	

Interacting combinations of slip systems

(a) Primary - different Burgers vector with common glide plane.

(b) Primary - cross

(c) Primary - conjugate

(d) Primary - intersecting system with Burgers vector parallel to the primary plane; other than combinations a and b.

(e) Primary - critical

extension of jogs in the manner envisaged by Hirsch[13] to account for temperature dependence is not likely.

From a forest-hardening viewpoint, differences between [001] and $[\bar{1}11]$ hardening must follow from differences in the character of the forest dislocations. Table IV shows that only the primary-critical intersection is not shared by both [001] and $[\bar{1}11]$. This attaches a basic importance to the intersection of dislocations, unique in [001], with Burgers vectors at 90° to each other (90° intersection). The absence of any trace of easy glide, the initial high rate of hardening, and the axially symmetric straining without cluster formation of [001] crystals (Table I) suggest that the 90° intersections give more hindrance to slip than 60° (or 120°) intersections alone. Also, the observed difference in $\frac{\Delta\tau}{\tau_{78}}$ for [001] and $[\bar{1}11]$ crystals (Fig. 17) could be interpreted to mean that the thermally activated process may be different in the two cases of intersection. On the other hand the $\frac{\Delta\tau}{\tau_{78}}$ difference can equally well be rationalized by pointing out that jogs resulting from 90° intersections may be less mobile than those from 60° intersections; the point made by Stroh[68] that the plane defined by the jog-line and the Burgers vector of the jog formed from 90° intersection is a {100} plane, not {111} as in the case of 60° intersection, supports this argument about the character of 90°-intersection jogs. The less mobile jogs can act as pinning points contributing to τ_g but not to τ_s; the result should be a reduction $\frac{\Delta\tau}{\tau_{78}}$ for [001], but not for $[\bar{1}11]$ in which such pinning is absent,

and an increase in hardening rate for [001]. Certainly when long jogs are formed by 90° intersections, they may dissociate and produce sessile dislocation as discussed by Hosford and Fleischer.[69]

If jogs from 90° intersection can pin so much more effectively than those from 60° intersections, their formation should also interfere, more than that of the other type, with long-distance dislocation motion and discourage the localization of slip leading to clusters. Ordinarily, the predominant slip system would be that with the largest density of dislocations, for this could operate with the least amount of forest cutting. However, from the symmetry of [001] it can easily be imagined that the forest dislocations interacting at 90° with each equally stressed slip system are of nearly the same density for all. Therefore, with the high pinning capacity of the 90°-intersection jogs, the amount of slip on all systems ought to remain about the same. From yielding onward, this situation should prevail for the [001] orientation and thus account for its stability.

Since 90°-intersection jogs are not produced in $[\bar{1}11]$ crystals, only forest dislocations can act as breaking agents to control long-range dislocation motion. Accordingly, the stability of this orientation should be very sensitive to slight variations in forest-dislocation density. The observed tendency for easy glide and cluster formation could be interpreted as reflecting such a condition. If it were not for the grip effect, these tendencies would be expected to be even more apparent. However, as discussed by Huaser and Jackson,[70]

all six slip systems are made operative. Equal slip on the six systems is predicted as a consequence of the gripping; that it is not observed (asymmetric straining being found) indicates an inequality of flow stress among the systems. This finding is also consistent with the notion that without the presence of 90°-intersection jogs the system which is first to operate will operate the most.

Strain Hardening in Polycrystalline Copper

It has already been argued from comparisons of isothermal hardening behavior (Figs. 5-8) and the stress dependence of the $\frac{\Delta\tau}{\tau_{78}}$ ratio (Fig. 17) that coarse-grained polycrystalline copper hardens similarly to [001] crystals at low strains and $[\bar{1}11]$ crystals at high strains. In the previous section, an attempt was made to attribute the [001] hardening behavior to the presence of 90° dislocation intersections, in among 60° intersections, and the $[\bar{1}11]$ behavior to the presence of 60° intersections only. Therefore, along such lines, it is further suggested that as plastic straining begins in polycrystalline material, slip on systems with 90° intersections is significant, but that with increasing strain the amount of 90° intersection and its importance decrease.

Some reasons can in fact be found for anticipating that slip systems with 90° intersections will be most active at yield and become increasingly inactive with strain. Lin[71,72] has considered the possible sequence in which slip systems in a grain of an aggregate become operative under rising load; he investigated a range of strain that might well be identified with the pre-yield region of microstraining.

The sequence calculated by Lin seems to require slip on systems leading to both 90° and 60° intersections. However, as the aggregate becomes fully plastic, it is only necessary that at least five independent slip systems in each grain be operative to ensure compatibility of strain at grain boundaries; there are many possible combinations for this purpose. Unlike the $[001]$ case, slip in a grain of an aggregate undergoes differential amounts of slip in the microstrain region. Therefore, the density of 90°-intersection forest dislocations confronting any one slip system would vary at full plasticity. Those systems which have to cut through a higher 90°-intersection forest would harden more rapidly than others, and their operation would gradually cease. With the decrease in operation of one system, the imposed strain would be accommodated by operation of other systems with lower active hardening. In this way it is possible to eliminate slip systems with 90° intersections.

Deformation Twinning

Geometry: The process of mechanical twinning can be modeled with a close-packed array of hard balls. Within the twin, each $\{111\}$ plane of a particular family must slide, relative to its neighboring planes, by the same distance along one of the three $\langle\bar{2}11\rangle$ directions, passing through the "saddle" lying along these directions. The upper half of an octahedron bounded by four $\{111\}$ planes (shaded atoms) is shown in Fig. 23a. The possible movements of an atom (white ball in Fig. 23a) in the next $\{111\}$ plane, through the saddle-regions in the planes of

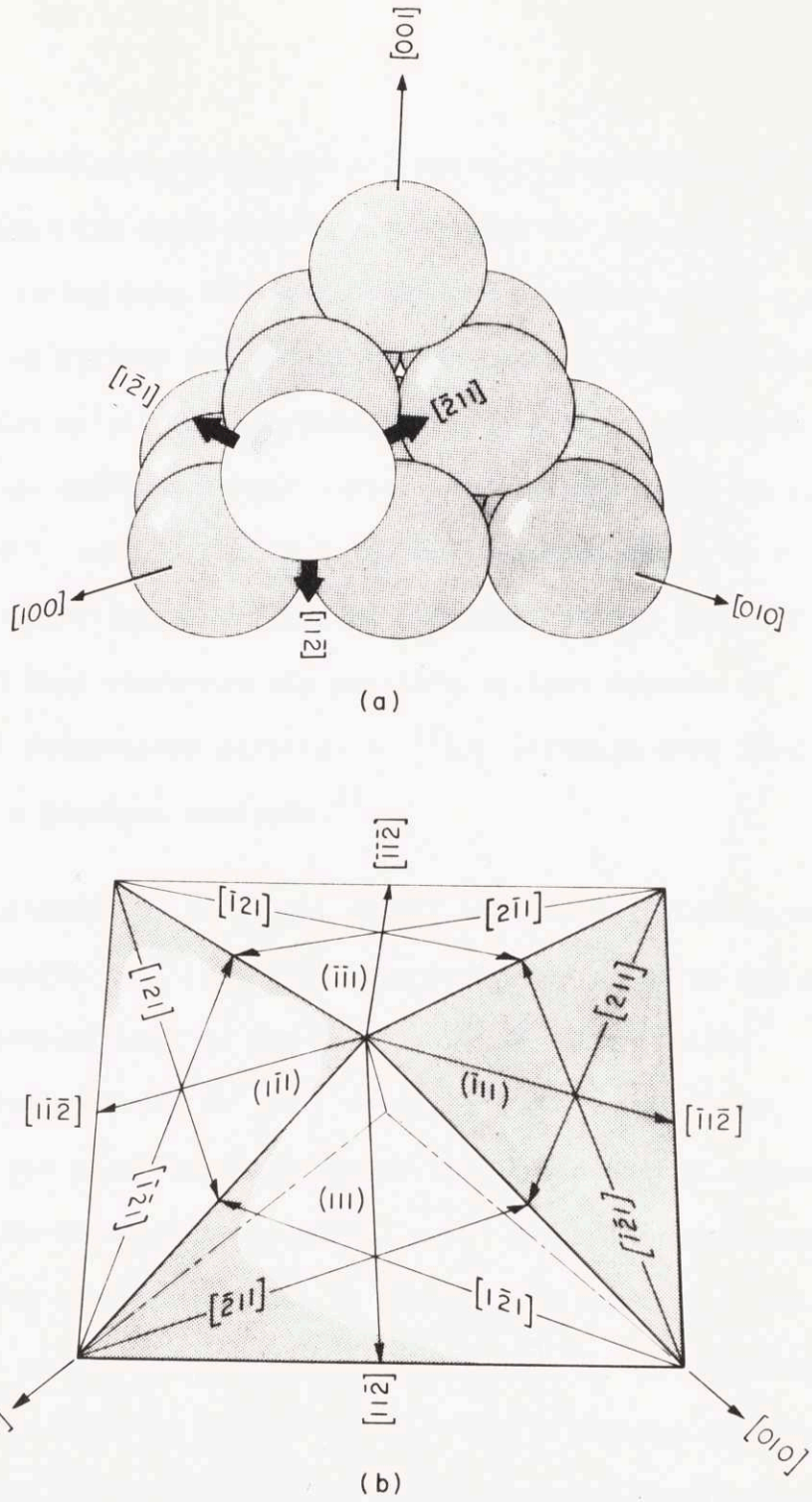

Fig. 23. (a) Hard-ball model of top half of octahedron bounded by $\{111\}$ planes showing twinning directions on (111); mirror plane is the shaded layer. (b) Projection of octahedron on (001) plane showing all the twinning systems.

shaded atoms, immediately determine all possible twinning systems (Fig. 23b). Since the saddle path is available for only one direction of shearing, twinning must be a unidirectional process: with a given stress axis, some systems can operate under tension only, the others under compression only. All possible twinning systems are listed in Table V, together with the Schmid factors for twinning, m_t, in crystals loaded along $[001]$ and $[\bar{1}11]$. Positive and negative signs on m_t indicate systems operating under tension and compression, respectively. It may be noted that there are six possible systems capable of operating under compression parallel to $[\bar{1}11]$ although only three were listed in a previous analysis.[73]

In this conventional hard-ball model, a possible twinning system for $[\bar{1}11]$ in tension is $(111)[\bar{2}11]$, the operation of which was confirmed in the present work by the Laue back-reflection method. Twinning was also observed in $[001]$ crystals under compression (Fig. 20), and the resolved shear stress for the predicted system was calculated to be approximately 21.2×10^3 psi. The agreement with the twinning stress for $[\bar{1}11]$ in tension, of about 20×10^3 psi (Table III), is good. Under tension along $[001]$, m_t for twinning is only 0.236, while that for slip is 0.408. Thus a necking down and fracture could be expected before the twinning stress was reached, and this proved to be the case in crystal J-2 (Fig. 3). If the stress at fracture is resolved onto the predicted twin system in J-2, the result, 14.9×10^3 psi, is much below those noted above

TABLE V. Twinning systems with the resolving factors for the given orientations.

Twin system	[001] parallel to load axis	[$\bar{1}$11] parallel to load axis
(111) [11$\bar{2}$]	- .472	- .157
[1$\bar{2}$1]	+ .236	- .157
[$\bar{2}$11]	+ .236	+ .315
($\bar{1}$11) [$\bar{1}$1$\bar{2}$]	- .472	0
[211]	+ .236	0
[$\bar{1}$2$\bar{1}$]	+ .236	0
($\bar{1}\bar{1}\bar{1}$) [$\bar{1}\bar{1}\bar{2}$]	- .472	- .157
[$\bar{1}$21]	+ .236	+ .315
[2$\bar{1}$1]	+ .236	- .157
($\bar{1}$1$\bar{1}$) [1$\bar{1}\bar{2}$]	- .472	+ .315
[121]	+ .236	- .157
[$\bar{2}$11]	+ .236	- .157

(+) tension

(-) compression

(20-21.2 x 10^3 psi) and the 17.5 - 23.5 x 10^3 psi range reported for copper single crystals at 4.2°K by Thornton and Mitchell.[54] Any possible operation of twinning systems in the direction reverse to that deduced from the hard-ball model must require a substantially higher stress, since no twinning was observed in crystal J-2 although the shear stress for reverse operation of twinning systems reached 29.8 x 10^3 psi.

Mechanism: A corrollary to the above results is that twins are formed by a sequence of abc/bcabc type stacking faults, classed as intrinsic, rather than by faults of an extrinsic type, abcbabc.[74] Hence any dislocation model for twin formation must involve a partial dislocation which trails an intrinsic fault. This view is in accord with Venables'[75] proposal, supported by electron microscopy observations,[76] that intrinsic faulting is responsible for twinning, not extrinsic faulting. A number of proposed mechanisms[53,77,78] may be ruled out on this basis since their operation would most probably result in partial dislocations trailing extrinsic rather than intrinsic faults.[75] The most recent suggestion of Cohen and Weertman[79] requires that dislocations of the conjugate systems near the head of pile-up become constricted and dissociate on the primary plane sending out twinning dislocations. Since the constriction process is thermally activated,[61] such a mechanism ought to require a twinning stress that increases as temperature is lowered, which is contrary to observation (Table III). The only other possibility is the "double-pole" mechanism

of Venables,[80] which does seem to be in accord with the present observations.

In the mechanism of Venables, the twinning stress τ_t which is required for the nucleation of a twin lamella is expressed as[75,80]

$$n\tau_t = \frac{\gamma}{b_l} + \frac{\alpha \mu b_l}{\ell}$$

when n is the local shear-stress concentration factor, γ the stacking fault energy, b_l the Burgers vector of the twinning dislocation, μ the shear modulus, ℓ the length of the twinning source, and α a value of order unity. In relation to this formula, a temperature dependence of τ_t must grow out of n and ℓ. In particular, to account for τ_t increasing with temperature, n and ℓ ought to be shown to decrease. A basis for doing this is found in dynamic recovery. At 4.2°K, the temperature is sufficiently low that twinning begins before dynamic recovery (Fig. 5). However, at 78°K twinning occurs in Stage III (Fig. 6) presumably after dynamic recovery has started to relieve stress concentrations and thus acted to lower n. With the reduced value of n in the latter case, the higher τ_t can be understood, at least partially, from the Venables equation. With reference to ℓ, the twinning source is a long jog formed by the successive cutting of a dislocation of the conjugate system by others of the primary system. The jog length, ℓ, will increase the longer it remains in the primary plane. However, it can glide on the cross-slip plane

and would be expected to with dynamic recovery. As a result, increase in ℓ would be limited so that the appropriate ℓ at 78°K could well be less than that at 4.2°K. In that event, the formula again leads to the prediction of higher τ_t at the higher temperature.

CONCLUSIONS

The tensile deformation of the multiple-slip orientation $[\bar{1}11]$ differed from that of $[001]$ in certain characteristic details. Over a range of temperatures (4.2° - 273°K) there was a well-defined Stage II in the $[\bar{1}11]$ hardening (with some evidence for a subdivision into Stages of only slightly different slope); the over-all slope was about twice that for single-slip orientations. Beyond this, prominent slip clusters were formed and the transverse strains were unequal. A tendency towards easy glide was apparent. In the $[001]$ crystals, hardening was non-linear throughout; cluster formation was less evident; the cross section was reduced uniformly; and there was no indication of easy glide. The shear-hardening rates in $[001]$ were initially higher and finally lower than the maximum Stage II slope of $[\bar{1}11]$, and this has been associated with non-linear Stage II in $[001]$ largely on the basis of insensitivity to temperature of the early hardening in $[001]$. With these observations, linearity of hardening (or its absence) could be correlated with the presence (or absence) of slip clusters.

From temperature-cycling experiments, the Cottrell-Stokes Law was found to apply between 162° and 78°K for both orientations, with $\frac{\Delta\tau}{\tau_{78}}$ being less for [001]. Between 273° and 78°K and beyond τ of about 8000 psi $\frac{\Delta\tau}{\tau_{78}}$ increased with stress.

Of all possible slip interactions, that involving primary and critical systems is unique to [001]. It has been suggested that the jogs so formed would be less mobile than those formed from other intersections since the former lie on a cube plane rather than a plane of close packing. Differences between $[\bar{1}11]$ and [001], both in isothermal hardening and in temperature-cycling results, have been rationalized on this basis.

The hardening of coarse-grained polycrystalline copper was evaluated from isothermal tension as well as thermal-cycling tests as representing a transition from [001] to $[\bar{1}11]$ behavior during the deformation process.

Deformation twinning occurred in $[\bar{1}11]$ under tension at 4.2°, 20°, and 78°K. The twinning stress, τ_t, increased with temperature. Twinning was also found in [001] under compression at 4.2°K; τ_t was approximately that for twinning of $[\bar{1}11]$ in tension. All results are consistent with the usual hard-ball model that operates with a layer-by-layer shear along $\langle 112 \rangle$ to generate a twin from intrinsic stacking faults.

REFERENCES

1. L. M. Clarebrough and M.E. Hargreaves, Prog. in Met. Phys. 8, 1 (1959).

2. R. Berner, Z. Naturforshg. 15a, 689 (1960).

3. G. F. Bolling, L. E. Hays, and H. W. Wiedersich, Acta Met. 10, 185 (1962).

4. S. Mader, A. Seeger, and C. Leitz, J. Appl. Phys. 34, 3368 (1963).

5. P. Haasen, Phil. Mag. 3, 384 (1958).

6. T. E. Mitchell and P. R. Thornton, Phil. Mag. 8, 1127 (1963).

7. J. Friedel, Phil. Mag. 46, 1169 (1955).

8. A. Seeger, J. Diehl, S. Mader, and H. Rebstock, Phil. Mag. 2, 323 (1957).

9. P. B. Hirsch, Internal Stresses and Fatigue of Metals, p. 139, Eds. G. M. Rassweiler and W. L. Grube, Elsevier Pub. Co., New York (1959).

10. Z. S. Basinski, Phil. Mag. 4, 393 (1959).

11. N. F. Mott, Trans. Amer. Inst. Min. (Metall.) Engrs. 218, 962 (1960).

12. P. B. Hirsch and D. H. Warrington, Phil. Mag. 6, 735 (1961).

13. P. B. Hirsch, Phil. Mag. 7 67 (1962).

14. A. Seeger, Dislocations and Mechanical Properties of Crystals, p. 243, Eds. J. C. Fisher, W. G. Johnston, R. Thomson, and T. Vreeland, Wiley, New York (1957).

15. H. Lange and K. Lücke, Z. Metallk. 44, 183 (1953); Ibid. 43, 55 (1952).

16. W. Staubwasser, Acta Met. 7, 43 (1959).

17. F. D. Rosi, Trans. Amer. Inst. Min. (Metall.) Engrs. 200, 1009 (1954).

18. J. Diehl, Z. Metallk. 47, 331 (1956).

19. W. F. Hosford, Jr., R. L. Fleischer, and W. A. Backofen, Acta Met. 8, 187 (1960).

20. B. Ramaswami, Ph. D. Thesis, Harvard Univ. (1963).

21. J. Sawkill and R. W. K. Honeycombe, Acta Met. 2, 854 (1954).

22. R. L. Fleischer, Trans. Amer. Inst. Min. (Metall.) Engrs. 224, 194 (1962).

23. U. F. Kocks, Acta Met. 6 (1958).

24. P. R. Thornton, T. E. Mitchell, and P. B. Hirsch, Phil Mag. 7, 337 (1962).

25. F. P. Bullen and M. M. Hutchinson, Phil. Mag. 7, 557 (1962); Ibid. 8, 461 (1963).

26. J. E. Bailey and P. B. Hirsch, Phil. Mag. 5, 485 (1960).

27. J. E. Bailey, Phil. Mag. 8, 223 (1963).

28. W. Berg, Naturwissenschaften 19, 391 (1931); Z. Kristallographie 89, 286 (1934).

29. C. S. Barrett, Trans. Amer. Inst. Min. (Metall.) Engrs. 161, 15 (1945).

30. G. L. Kehl, Principles of Metall. Lab. Practice, p. 300, McGraw-Hill Book Co., New York (1949).

31. Z. S. Basinski, Proc. Roy. Soc. A240, 229 (1957).

32. E. Schmid and W. Boas, Plasticity of Crystals, F. A. Hughes and Co., London (1950).

33. B. Jaoul, J. Mech. Phys. Solids 5, 95 (1957).

34. G. I. Taylor, J. Inst. Metals 62, 307 (1938); Proc. Colloq. in Deformation and Flow of Solids (Madrid, 1955), p. 3, Springer, Berlin (1956).

35. J. F. W. Bishop and R. Hill, Phil. Mag. 42, 1298 (1951).

36. A. Freda and B. D. Cullity, Trans. Amer. Inst. Min. (Metall.) Engrs. 215, 538 (1959).

37. J. Diehl and R. Berner, Z. Metallk. 51, 522 (1960).

38. A. Seeger, R. Berner, and H. Wolf, Z. Physik 155, 247 (1959).

39. T. H. Blewitt, R. R. Coltman and J. K. Redman, Defects in Crystalline Solids, p. 369, The Phys. Soc., London (1955).

40. W. C. Overton and J. Gaffney, Phys. Rev. 98, 969 (1955).

41. J. D. Livingston, Acta Met. 10, 229 (1962); by private communication.

42. W. Schüle, O. Buck and E. Köster, Z. Metallk. 53, 172 (1962).

43. R. P. Carreker, Jr., and W. R Hibbard, Jr., Acta Met. 1, 654 (1953).

44. F. D. Rosi and C. H. Mathewson, Trans. Amer. Inst. Min. (Metall.) Engrs. 188, 1950).

45. P. Gay and R. W. Honeycombe, Proc. Phys. Soc. A64, 844 (1951).

46. B. H. Kear, Trans. Amer. Inst. Min. (Metall.) Engrs. 224, 675 (1962).

47. M. A. Adams and A. H. Cottrell, Phil. Mag. 46, 1187 (1955).

48. M. J. Makin, Phil. Mag. 3, 309 (1958).

49. A. H. Cottrell and R. J. Stokes, Proc. Roy. Soc. A233, 17 (1955).

50. T. H. Blewitt, R. R. Coltman, and J. K. Redman, J. Appl. Phys. 28, 651 (1957); Dislocations and Mechanical Properties of Crystals, p. 179, Eds. J. C. Fisher, W. G. Johnston, R. Thomson, and T. Vreeland, Wiley, New York (1957).

51. J. A. Venables, Proc. 5th International Congress on Electron Microscopy 1, J8 (1962).

52. G. Y. Chin, W. F. Hosford, Jr., and W. A. Backofen, Trans. Amer. Inst. Min. (Metall.) Engrs., to be published.

53. H. Suzuki and C. S. Barrett, Acta Met. 6, 156 (1958).

54. P. R. Thornton and T. E. Mitchell, Phil. Mag. 7, 361 (1962).

55. T. H. Blewitt, quoted in Ref. 75.

56. F. W. Young, Jr., J. Appl. Phys. 32, 192 (1961).

57. Z. S. Basinski, Aust. J. Phys. 13, 354 (1960).

58. P. Haasen and A. Kelly, Acta Met. 5, 192 (1957).

59. T. H. Blewitt, Phys. Rev. 91, 1115 (1953).

60. O. Buck, Phys. Stat. Sol. 2, 535 (1962).

61. G. Schoeck and A. Seeger, Defects in Crystalline Solids, p. 340, The Phys. Soc., London (1955).

62. M. M. Lomer, Phil. Mag. 42, 1327 (1951).

63. A. H. Cottrell, Phil. Mag. 43, 645 (1952).

64. N. F. Mott, Phil. Mag. 43, 1151 (1952); Ibid. 44, 742 (1953).

65. U. F. Kocks, Acta Met. 8, 345 (1960).

66. U. F. Kocks, Ph. D. Thesis, Harvard Univ. (1959).

67. A. H. Cottrell, Dislocations and Mechanical Properties of Crystals, p. 509, Eds. J. C. Fisher, W. G. Johnston, R. Thomson, and T. Vreeland, Wiley, New York (1957).

68. A. N. Stroh, Proc. Phys. Soc. B67, 427 (1954).

69. W. F. Hosford, Jr. and R. L. Fleischer, Acta Met. 7, 816 (1959).

70. J. J. Hauser and K. A. Jackson, Acta Met. 9, 1 (1961).

71. T. H. Lin, J. Mech. Phys. Solids 5, 148 (1957).

72. T. H. Lin and B. Lieb, J. Mech. Phys. Solids 10, 65 (1962).

73. R. J. DeAngelis and J. B. Cohen, Conference on Deformation Twinning, Gainesville, Florida, to be published.

74. F. C. Frank, Phil. Mag. 42, 809 (1951).

75. J. A. Venables, Conference on Deformation Twinning, Gainesville, Florida, to be published.

76. A. Howie, Direct Observations of Imperfections in Crystals, p. 283, Eds. J. B. Newkirk and J. H. Wernick, Interscience Pub. (1962).

77. A. Ookawa, J. Phys. Soc. Japan 12, 825 (1957).

78. A. Haasen and A. King, Z. Metallk. 51, 722 (1960).

79. J. B. Cohen and J. Weertman, Acta Met. 11, 996 (1963).

80. J. A. Venables, Phil. Mag. 6, 379 (1961).

APPENDIX I

Description of Crystal-growing Furnace and Procedure for Crystal Growth

Furnace: Basically the furnace consisted of a graphite heater (to be discussed below) shielded with concentric nickel sheets, all of which were enclosed in a three-foot vycor tube which was surrounded in turn by fire bricks. Two water-cooled bus bars were held in place with a rubber stopper which sealed one end of the tube. The graphite boat (to be described below) was placed in the furnace through the other end of the tube, which was also sealed with a rubber stopper during crystal growth. The sealed furnace could be evacuated and an atmosphere of helium under which the crystals were grown could be introduced through appropriate valve arrangement. The boat was drawn out of the heater by winding up the wire attached to the boat with a clock motor at about 1.5 cm/hr. The power was supplied by a step-down transformer. During crystal growth the furnace operated at about 20 volts and 100 amperes. The temperature gradient at the solid-liquid interface was estimated by thermocouple measurements to be larger than $1000^{o}C/in$.

Graphite Heater: The heater shown in Fig. 1-I was made from a graphite* tube of 0.040-in wall thickness which had been slit with a jeweller's saw such that two heating elements were in parallel circuit.

---

* The graphite used was CS grade obtained from the National Carbon Co.

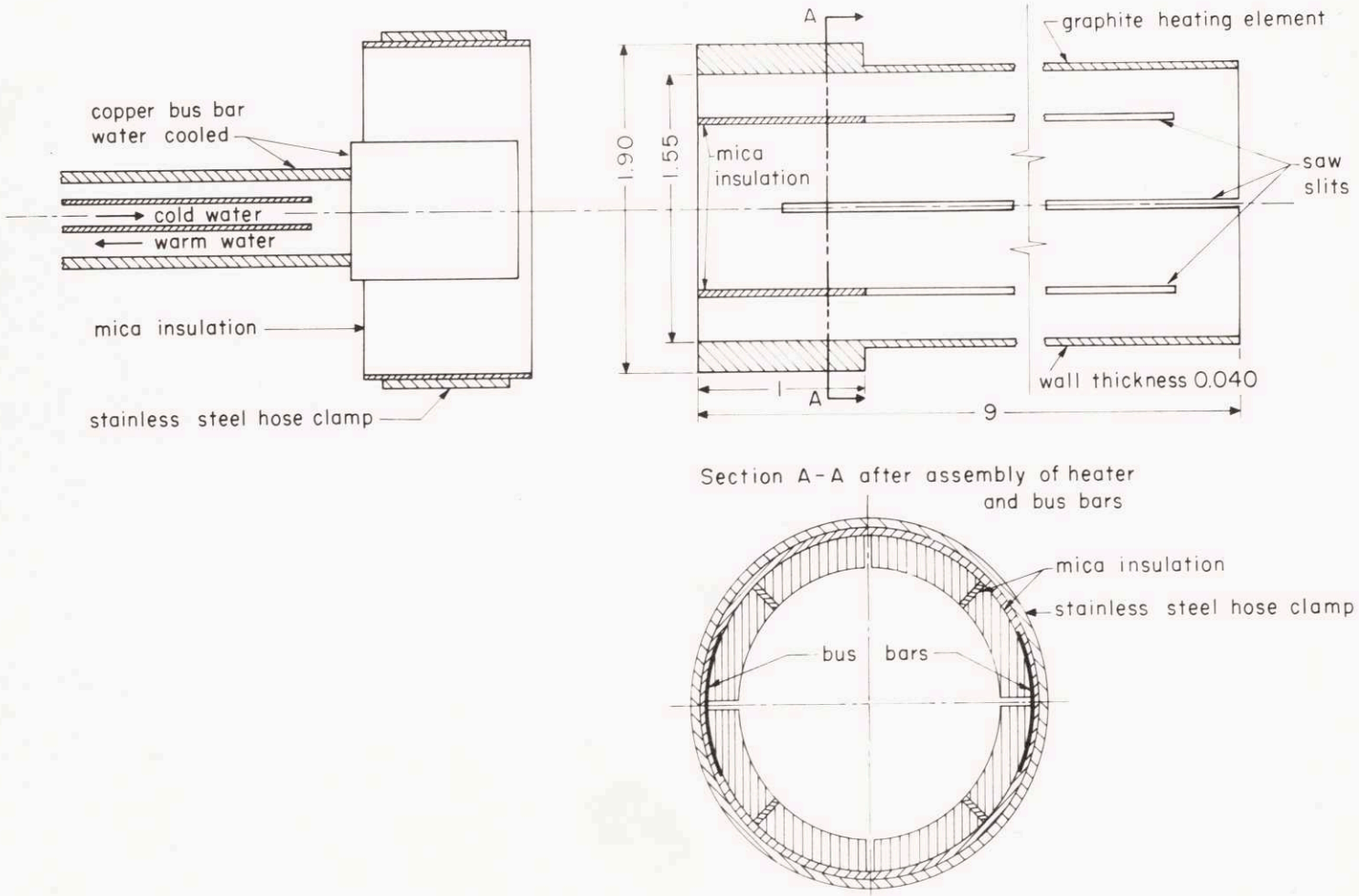

Fig. I-I. Longitudinal section through graphite heater showing its construction. The heater is displaced from the bus bars for clarity. All dimensions are given in inches.

The insulation used as indicated in Fig. 1-I was mica sheets and the water-cooled bus bars were clamped onto the heater with a stainless steel hose clamp, thus holding the cylindrical heater rigid.

Graphite Boat: A cantilevered boat (Fig. 2-I) was built so that it could slide inside the vycor tube and the protruding end could be located inside the graphite heater. The seed was placed on the sill indicated in Fig. 2-I and butted against the specimen blank which was held in a soft mould as described below. The open spaces were then filled with graphite powder and the cover placed over the slot. The boat was then ready to be placed in the furnace.

Positioning of Charge in the Mould: The premachined blank which is shown in Fig. 3-I was first lightly polished with 1 and 1/0 emery polishing paper to remove machining marks. Then the charge was chemically polished in 1/3 acetic, 1/3 orthophosphoric and 1/3 nitric acid (full bottle strength) solution and it was completely immersed with a slurry of Aqua Dag except for the end which came in contact with the seed. After the graphite coating was completely dry, the blank was centrally positioned in a cylindrical mould using the jig shown in Fig. 3-I. 200 mesh 99.9 percent pure graphite powder which had been fired in vacuum at 1500^{o}C for 24 hrs to drive off contaminants was tamped around the blank (Fig. 3-I). The bus bar end of the furnace was slightly raised and a copper rod attached to the end of the blank; thus a small hydrostatic head sufficient to retain the edges and the threads of the sample was created.

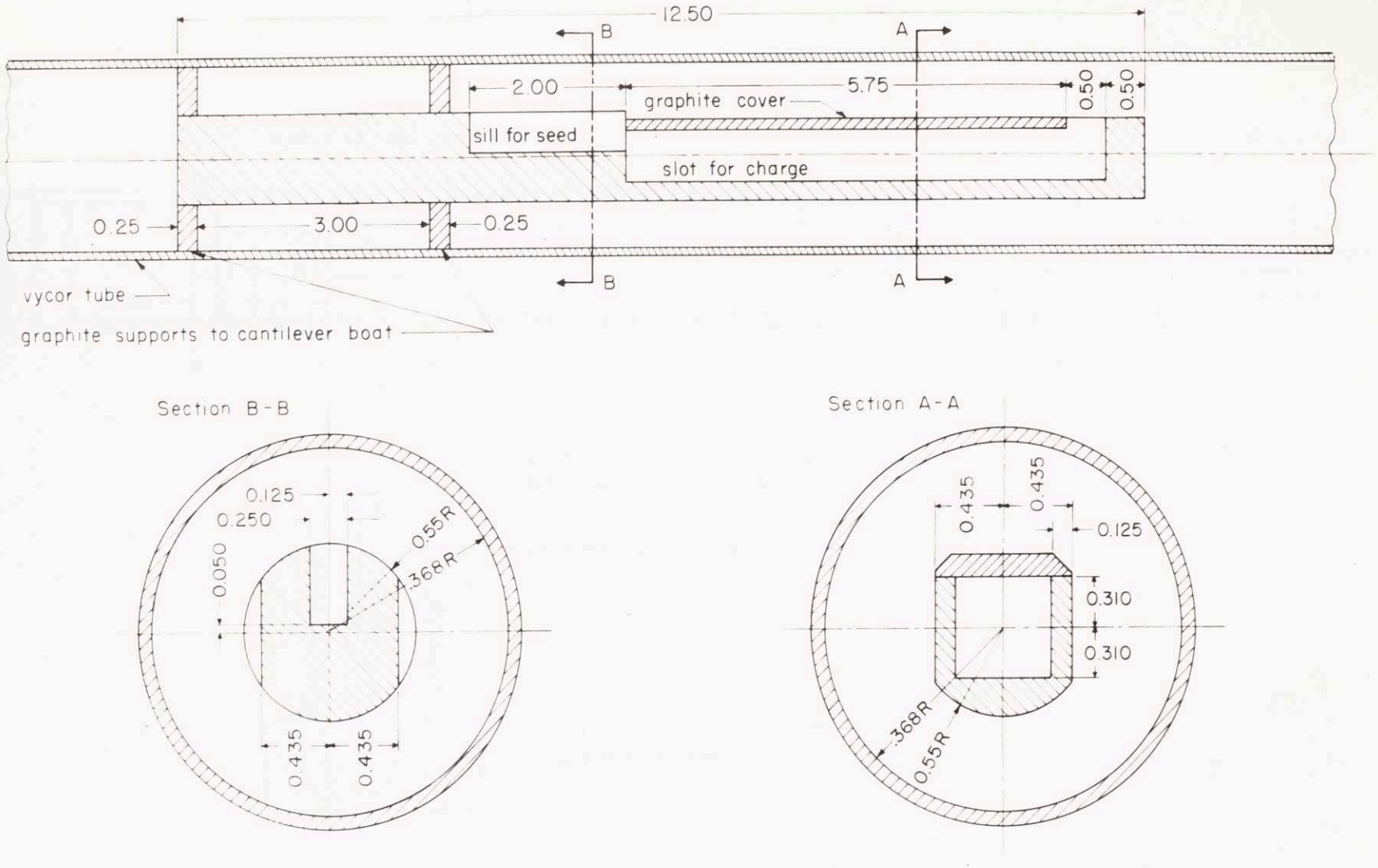

Fig. 2-I. Longitudinal section of graphite boat made from a 1.10 in diameter rod.

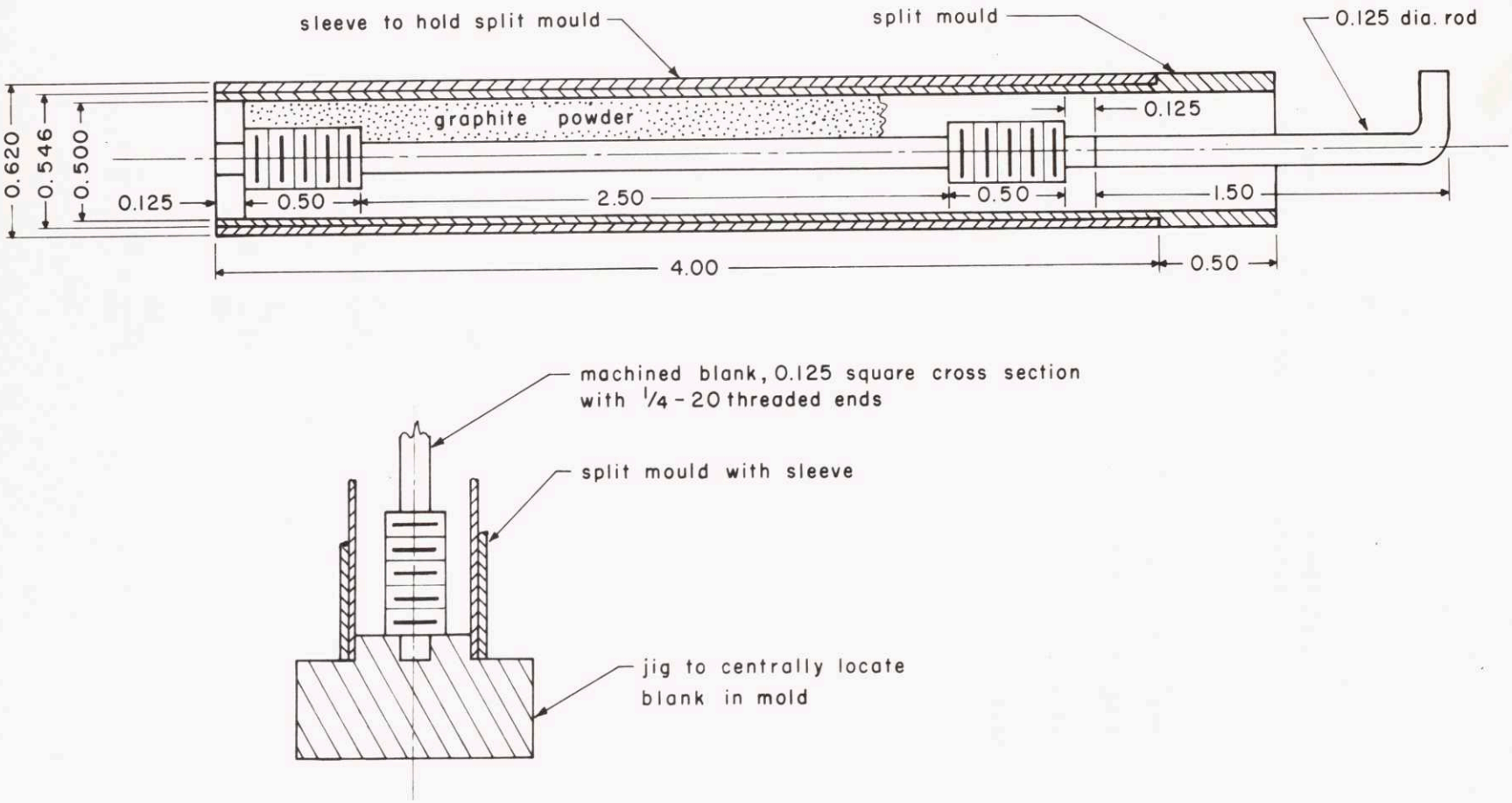

Fig. 3-I. Longitudinal section through cylindrical split mould with machined blank in place.

APPENDIX II

Estimation of the Amount of Lattice Rotation During Extension of $[\bar{1}11]$ Crystals

The six components of strains, ϵ_{xx}, ϵ_{yy}, ϵ_{zz}, ϵ_{xy}, ϵ_{xz}, ϵ_{yz}, and the three components of rotation, w_x, w_y, w_z, can be computed from the displacement vector, $\bar{u}$. For small strains, in which case the higher order differentials are disregarded, the strains and rotations are given by

$$\epsilon_{xx} = \frac{du_x}{dx}, \quad \epsilon_{yy} = \frac{du_y}{dy}, \quad \epsilon_{zz} = \frac{du_z}{dz}$$

$$\epsilon_{xy} = \frac{1}{2}\left(\frac{du_x}{dy} + \frac{du_y}{dx}\right)$$

$$\epsilon_{xz} = \frac{1}{2}\left(\frac{du_x}{dz} + \frac{du_z}{dx}\right)$$

$$\epsilon_{yz} = \frac{1}{2}\left(\frac{du_y}{dz} + \frac{du_z}{dy}\right) \qquad (1)$$

$$w_x = \frac{1}{2}\left(\frac{du_y}{dz} - \frac{du_z}{dy}\right)$$

$$w_y = \frac{1}{2}\left(\frac{du_x}{dz} - \frac{du_z}{dx}\right)$$

$$w_z = \frac{1}{2}\left(\frac{du_x}{dy} - \frac{du_y}{dx}\right)$$

The displacement vector at any point can be found from the equation

$$\bar{u} = \gamma_{d_l} \, (\bar{r} \cdot \hat{n}_d) \, \hat{s}_{d_l}$$

where γ_{d_l} is the amount of slip in plane d in the l direction, $\bar{r}$ is the radius vector from the origin of the original coordinates to any point (x, y, z), $\hat{n}_d$ is the unit vector normal of the plane d, and $\hat{s}_{d_l}$ is the unit vector along the shear direction. The displacement equation is geometrically illustrated in Fig. 1-II. Taylor[1] was the first to use this form of the displacement vector as applied to small plastic strains arising from slipping on crystallographic planes.

For the face centered cubic lattice, the slip systems are $\{111\}\langle\bar{1}01\rangle$ where the Miller index notation signifies that the coordinates referred to are Cartesian with $[100]$, $[010]$ and $[001]$ as axes. To calculate the strains and notations for extension along the $[\bar{1}11]$, it is convenient to use $[1\bar{1}2]$, $[110]$, and $[\bar{1}11]$ as coordinates as shown in Fig. 2-II. The matrix for the transformation of axes is given by[2]

		old		
		x'	y'	z'
new	x	$\frac{1}{\sqrt{6}}$	$-\frac{1}{\sqrt{6}}$	$\frac{2}{\sqrt{6}}$
	y	$\frac{1}{\sqrt{2}}$	$\frac{1}{\sqrt{2}}$	0
	z	$-\frac{1}{\sqrt{3}}$	$\frac{1}{\sqrt{3}}$	$\frac{1}{\sqrt{3}}$

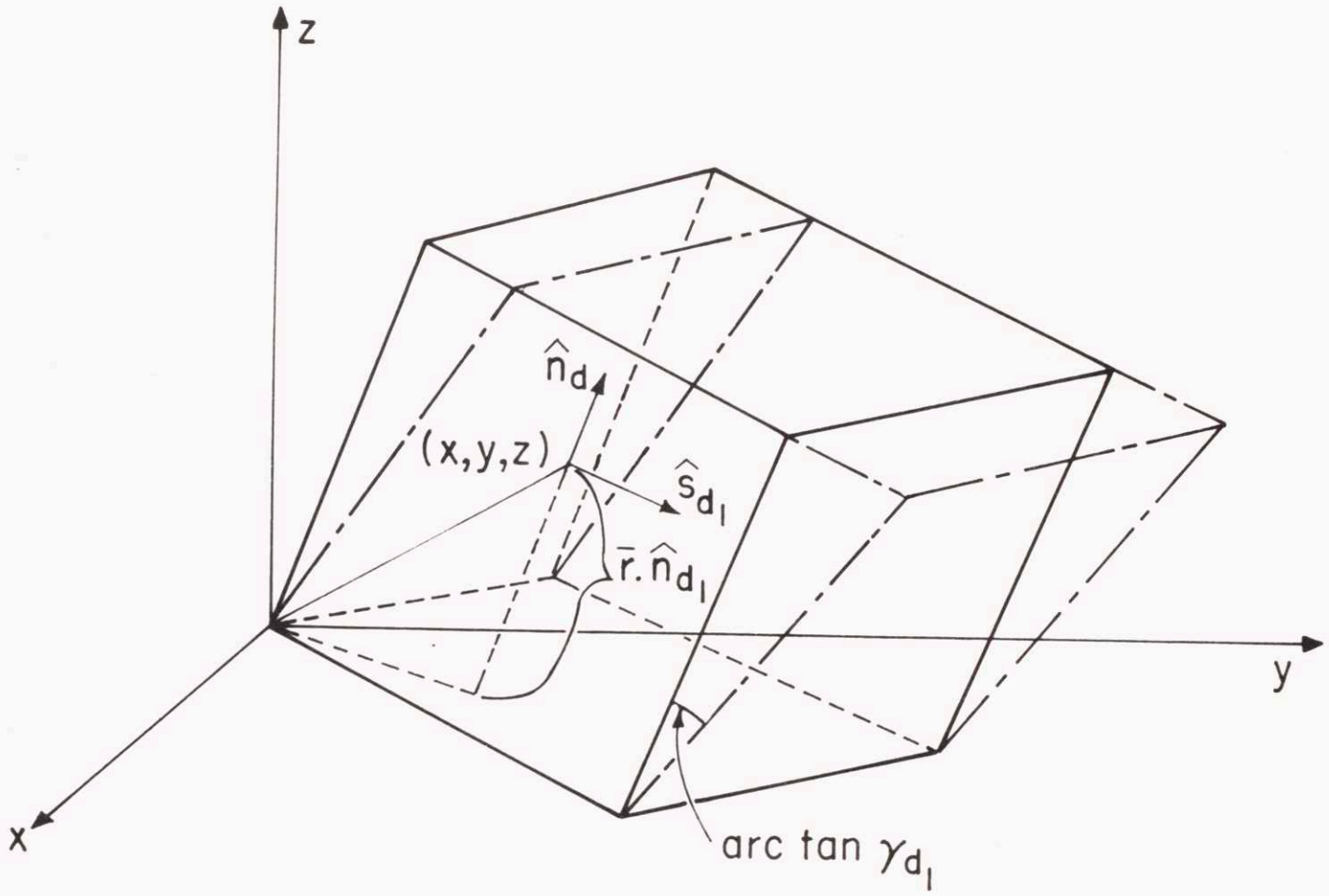

Fig. I-II. Geometrical representation of displacement vector $\bar{\mu} = \gamma_{d_1} (r \cdot \hat{n}_d) \hat{s}_{d_1}$.

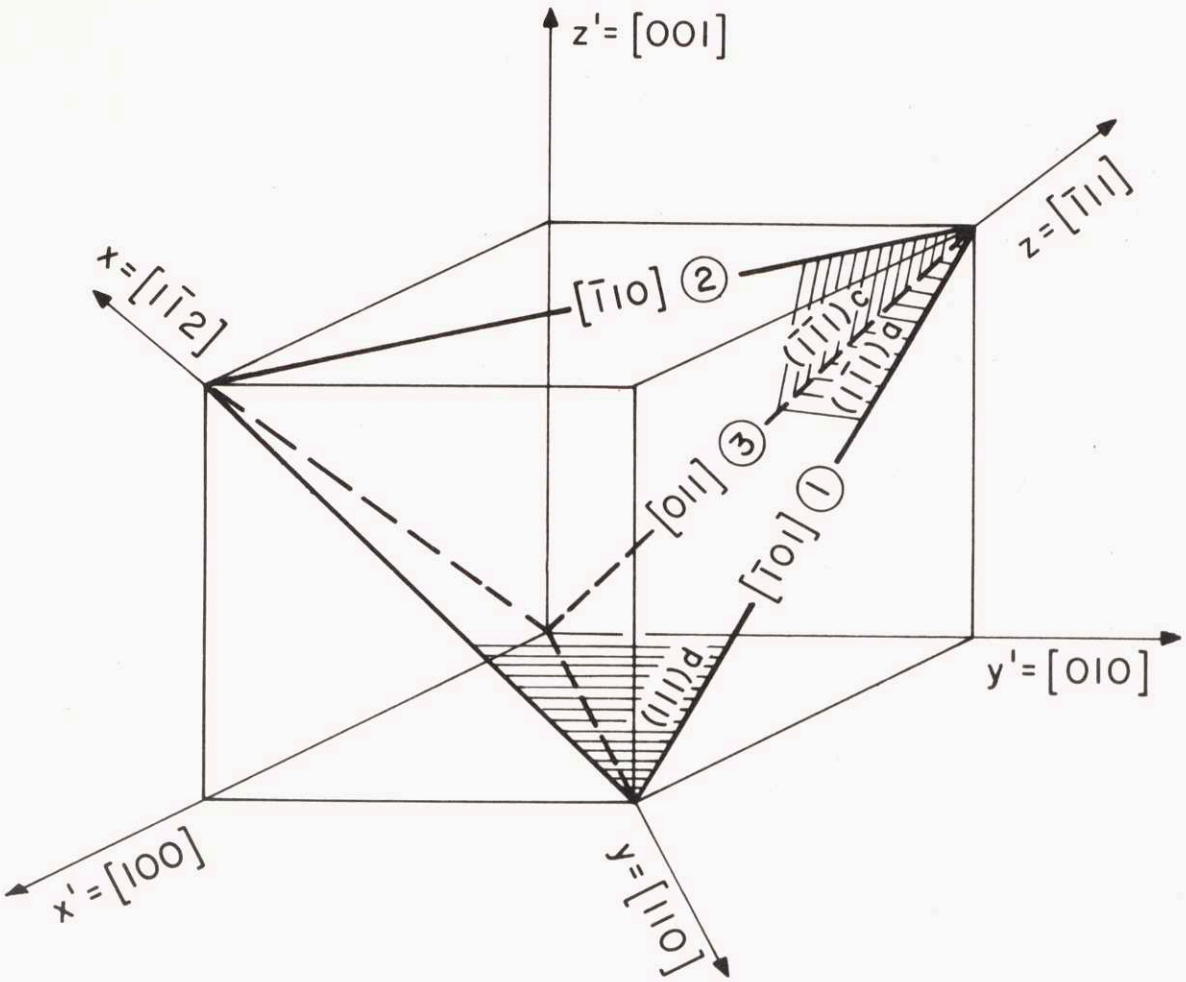

Fig. 2-II. Diagram designating the active slip systems under tension along [$\bar{1}$11]. The old coordinates are x', y', z' and the new coordinates, x, y, z.

Using this transformation matrix, the displacement caused by the shearing on $\{111\}\ \langle 110\rangle$ slip systems can be related to the new axes. For extension along $[\bar{1}11]$, the active slip systems and the amount of slip on each are:

$(111)\ [\bar{1}01],\ \gamma_{d_1}$ $\qquad$ $(111)\ [\bar{1}10],\ \gamma_{d_2}$

$(\bar{1}\bar{1}1)\ [011],\ \gamma_{c_3}$ $\qquad$ $(\bar{1}\bar{1}1)\ [\bar{1}10],\ \gamma_{c_2}$

$(1\bar{1}1)\ [\bar{1}01],\ \gamma_{a_1}$ $\qquad$ $(1\bar{1}1)\ [011],\ \gamma_{a_3}$

A sample calculation to determine $\bar{u}$ for slip on $(111)\ [\bar{1}01]$ with respect to the new coordinates follows: using the transformation coordination where $i_{1,2,3}$ are unit vectors referred to the old coordinates and $j_{1,2,3}$ to the new coordinates,

$$\hat{n}_{(111)} = \frac{1}{\sqrt{3}}(i_1 + i_2 + i_3)$$

$$= \frac{1}{\sqrt{3}}\left(\frac{2}{\sqrt{6}}\, j_1 + \frac{2}{\sqrt{2}}\, j + \frac{1}{\sqrt{3}}\, j_3\right)$$

$$\hat{s}_{[\bar{1}01]} = \frac{1}{\sqrt{2}}(-i_1 + i_3)$$

$$= \frac{1}{\sqrt{2}}\left(\frac{1}{\sqrt{6}}\, j_1 - \frac{1}{\sqrt{2}}\, j_2 + \frac{2}{\sqrt{3}}\, j_3\right);$$

Using $\bar{u} = d_1 \, (\bar{r} \cdot \hat{n}_d) \, \hat{s}_d$ where γ_{d_1} has been replaced by d_1,

$$\bar{u} = \frac{d_1}{\sqrt{6}} \left[\frac{2}{\sqrt{6}} x + \frac{2}{\sqrt{2}} y + \frac{1}{\sqrt{3}} z \right] \left[\frac{1}{\sqrt{6}} j_1 - \frac{1}{\sqrt{2}} j_2 + \frac{2}{\sqrt{3}} j_3 \right],$$

thus

$$u_x = \frac{d_1}{6} \left[\frac{2}{\sqrt{6}} x + \frac{2}{\sqrt{2}} y + \frac{1}{\sqrt{3}} z \right]$$

$$u_y = - \frac{d_1}{2\sqrt{3}} \left[\frac{2}{\sqrt{6}} x + \frac{2}{\sqrt{2}} y + \frac{1}{\sqrt{3}} z \right]$$

$$u_z = \frac{2d_1}{3\sqrt{2}} \left[\frac{2}{\sqrt{6}} x + \frac{2}{\sqrt{2}} y + \frac{1}{\sqrt{3}} z \right].$$

Similarly computing $\bar{u}$ for all six slip systems and differentiating it as shown in Eqs. (1), the components of strains and rotations are

$$3\sqrt{6} \; \epsilon_{xx} = d_1 - 2d_2 - 2a_1 - 2a_3 + c_3 - 2c_2 \tag{2}$$

$$\sqrt{6} \; \epsilon_{yy} = - d_1 - c_3 \tag{3}$$

$$\frac{3}{2}\sqrt{6} \; \epsilon_{zz} = d_1 + d_2 + a_1 + a_3 + c_3 + c_2 \tag{4}$$

$$\frac{1}{3\sqrt{2}}\ \epsilon_{xy} = -d_2 + a_1 - a_3 + c_2 \tag{5}$$

$$\frac{1}{12\sqrt{3}}\ \epsilon_{xz} = 5d_1 + 2d_2 - 7a_1 - 7a_3 + 5c_3 + 2c_2 \tag{6}$$

$$\frac{1}{12}\ \epsilon_{yz} = 3d_1 + 4d_2 - a_1 + a_3 - 3c_3 - 4c_2 \tag{7}$$

$$3\sqrt{2}\ w_x = -d_2 + d_1 + a_3 - a_1 - c_3 + c_2 \tag{8}$$

$$4\sqrt{3}\ w_y = -2c_2 - c_3 + 3a_3 + 3a_1 - 2d_2 - d_1 \tag{9}$$

$$\frac{1}{12}\ w_x = 4c_2 + 5c_3 - a_1 + a_3 - 4d_2 - 5d_1 \tag{10}$$

In the present work, during the tensile extension of $[\bar{1}11]$ crystals, the cross section of the crystals remained rectangular. This indicates that $\epsilon_{xy} = 0$. Since the ends of the crystals were firmly gripped, any shear strains parallel to the tensile axis would be minimized, as discussed by Hauser and Jackson.[3] Hence ϵ_{xz} and ϵ_{yz} can be assumed to be zero or near zero. From the conditions

$$\epsilon_{xy} = \epsilon_{xz} = \epsilon_{yz} = 0$$

and relations 5, 6, and 7, the three shear magnitudes can be expressed in terms of the other three. These are

$$d_1 = \frac{7}{5} a_3 - \frac{2}{5} c_2$$

$$d_2 = a_1 - a_3 + c_2 \qquad (11)$$

$$c_3 = a_1 + \frac{2}{5} a_3 - \frac{2}{5} c_2$$

From Eqs (2-4) and substituting (11), it follows that

$$\frac{\epsilon_{yy}}{\epsilon_{xx}} = \frac{(-9a_3 - 5a_1 + 4c_2)}{(3a_3 - 5a_1 - 8c_2)} \qquad (12)$$

and

$$\epsilon_{zz} = \frac{4}{15\sqrt{6}} (11a_1 + a_3 + 3c_2) \qquad (13)$$

Lateral strain measurements of $[\bar{1}11]$ crystals which were extended about 30 percent showed that $\frac{\epsilon_{yy}}{\epsilon_{xx}}$ for these crystals were less than 2. Hence using $\epsilon_{zz} = \frac{1}{\sqrt{6}} = 0.4$ for calculation convenience and $\frac{\epsilon_{yy}}{\epsilon_{xx}} = 2$, the rotations can be estimated only if another relation is found to determine uniquely the shear magnitudes; that is, there are only 5 relations relating 6 unknowns. A sixth relation of $\epsilon_{xx} + \epsilon_{yy} + \epsilon_{zz} = 0$ exists but this relation does not aid the computation since the shear magnitudes necessarily cancel each other. One reasonable assumption to make is that if the tensile axis should move away from the $[\bar{1}11]$ orientation, then Schmid factor considerations will show that the

amount of slip on one set of primary and conjugate systems should operate equal amounts. Letting $d_1 = c_3$ and using relations 11, 12, 13, the six shear magnitudes can be computed. Upon inserting these values into 8, 9, 10

$$w_x = 0,\ w_y = 3.6^{\circ} \text{ and } w_z = 0$$

It is important to note that this numerical computation was performed using relations derived for small plastic strains. However, even if the non-linear terms of the strain and rotation components are considered, the derived value would not be expected to change by more than a factor of two. This is borne out by the fact that Laue X-ray studies which could easily detect rotations larger than 4° did not do so. This exercise shows that under multiple slip conditions, axially asymmetric straining is possible without measurable change in the orientation of the crystal.

REFERENCES II

1. G. I. Taylor, Stephen Timoshenko 60th Anniversary Vol., p. 218, Macmillan Col, New York (1938).

2. J. F. Nye, Physical Properties of Crystals, Oxford Univ. Press (1957).

3. J. J. Hauser and K. A. Jackson, Acta Met. 9, 1 (1961).

APPENDIX III

Slip in Twinned Crystals

Since the time Blewitt, Coltman, and Redman[1] first reported deformation twinning in copper single crystals, other workers have also reported deformation twinning in other face-centered cubic metals.[2,3] However slip in twinned crystals, which is of interest in the study of ductile fracture in twinned crystals or in grains of polycrystalline metal with annealing twins, has not been considered. The purpose of this Appendix is to present a simple geometrical analysis of deformation in a twinned structure.

During the testing of crystals with the tensile axis parallel to $[\bar{1}11]$ bounded by faces parallel to (110) and $(1\bar{1}2)$, deformation twinning was observed at 78°, 20°, and 4.2°K.[4] Twinning does not convert the whole crystal to the twin orientation, rather a laminated structure of alternating twinned and untwinned matrix results.

Deformation after Lüders-band type propagation through the gauge section was observed to proceed by slip on systems which did not violate strain compatibility across the twin boundary. Figure 1-III shows two tetrahedra bounded by $\{111\}$ planes and $\langle 110 \rangle$ directions, one on the left corresponds to the original matrix with the tensile axis parallel to $[\bar{1}11]$ and one on the right, the twinned orientation. Twinning in the $(\bar{1}\bar{1}\bar{1})$ $[\bar{1}21]$ as indicated

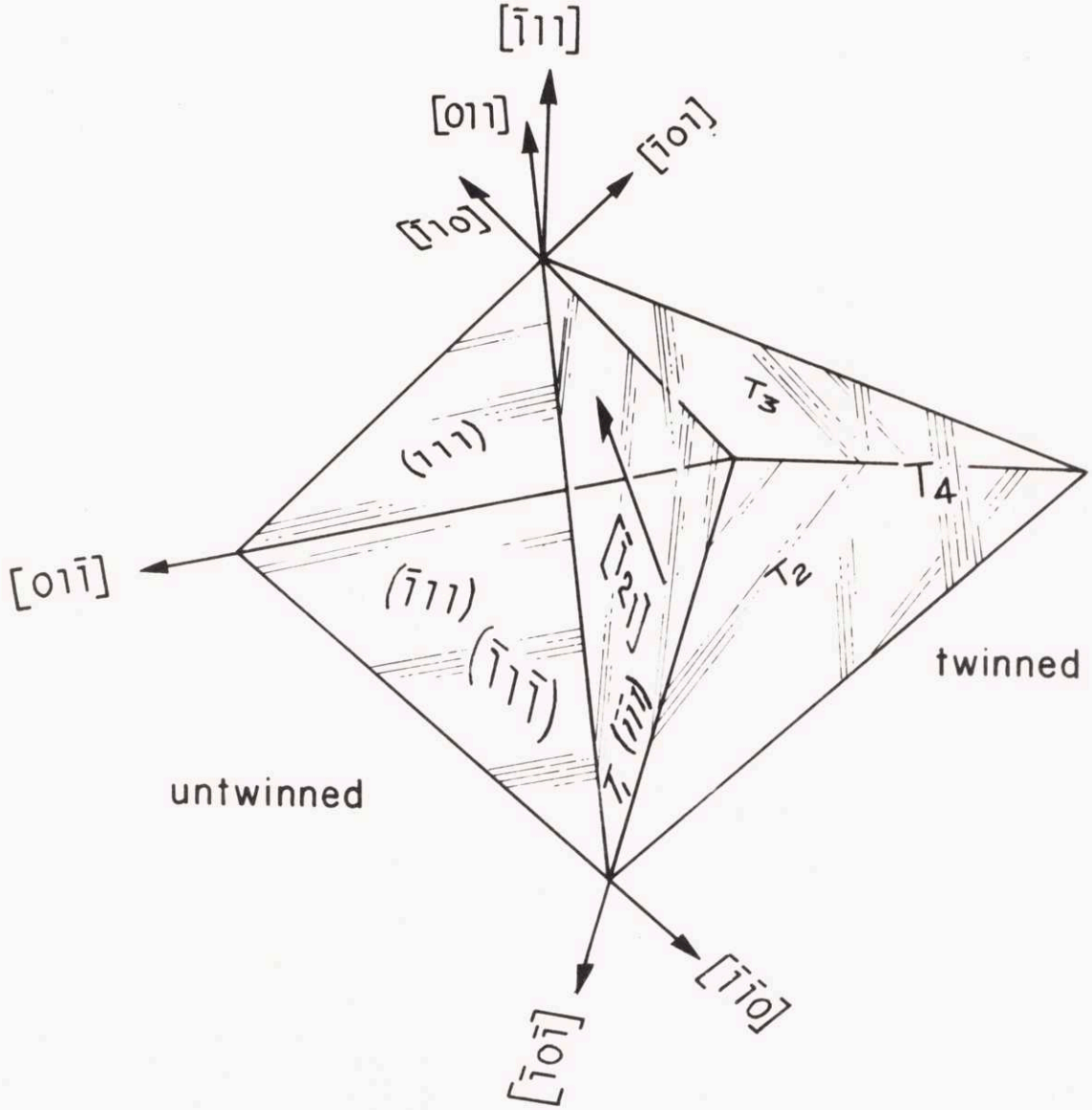

Fig. 1-III. Two tetrahedra with a common $\{111\}$ (twinning) plane; $(\bar{1}11)\,[\bar{1}21]$, the twinning system. That on the left represents the original, untwinned orientation, that on the right the twinned orientation. T_1, T_2, T_3 and T_4, the octahedral slip planes in the twinned orientation. Tensile axis parallel to $[\bar{1}11]$.

results in an orientation which has the tensile axis parallel to a $\{110\}$ 19° 28' toward $\langle 001 \rangle$ from $\langle \bar{1}12 \rangle$. The $\{111\}$ planes in the twinned orientation are labelled T_1, T_2, T_3 and T_4; the twinning plane is that plane common to both orientations and parallel to $(\bar{1}\bar{1}\bar{1})$ and T_1. From Fig. 1-III it is evident that slip can take place on T_4 $[011]$, T_3 $[\bar{1}10]$ and on T_1 in $[011]$ and $[\bar{1}10]$ without violating strain compatibility. Furthermore T_4 $[011]$ can cross-slip onto $(\bar{1}1\bar{1})$ and T_3 $[\bar{1}10]$ onto (111). It was possible to determine from the angular deflection as the slip trace crossed the twin boundary which $\{111\}$ planes were continuous.* In every case it was found to be either T_4-$(\bar{1}1\bar{1})$ or T_3-(111).

Figure 2a-III clearly shows the continuity of the slip traces as slip proceeds across a twinned region. Note the large amount of cross slip of the systems in T_4 (or T_3) onto T_1, the plane parallel to the twin plane. Figure 2b-III shows similar slip traces. Near the fracture the short cross traces join up and the slipping off occurs by localizing shear in a zone parallel to these traces.

The propensity to cross slip in the twinned orientation is due to the high resolved shear stress on T_4 $[011]$ and T_3 $[\bar{1}10]$, since the Schmid factor is 0.455 compared to 0.272 for all active slip systems

---

* This determination was facilitated by the fact that the lattice rotation in $[\bar{1}11]$ crystals was small making the surface analysis simple.

P. 88

Fig. 2a-III. Wide twinned band diagonally across the micro-photograph. Large clusters at low angles to tensile axis (horizontal) were formed prior to twinning; $(1\bar{1}2)$ surface, X250.

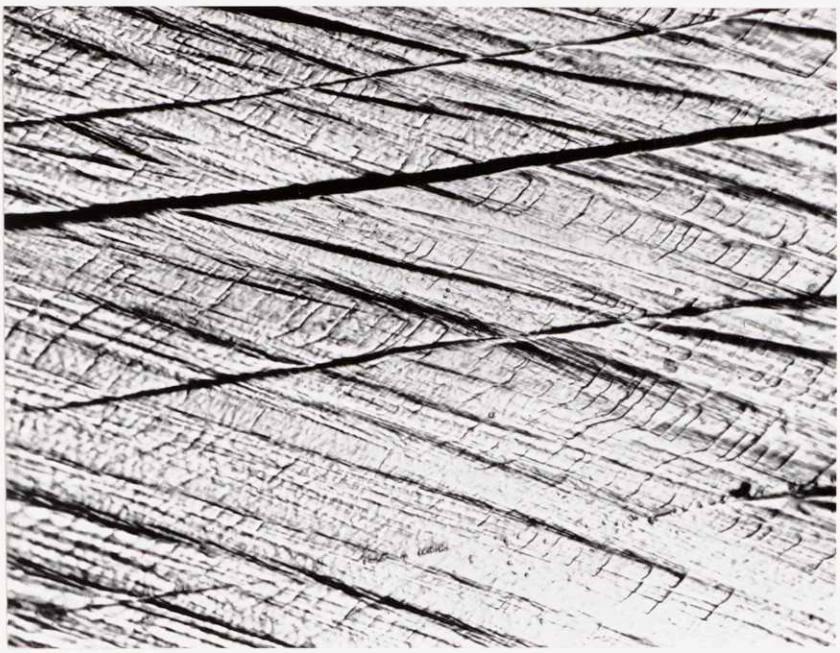

Fig. 2b-III. Laminated structure of twinned and non-twinned matrix. Traces of twin plane run diagonally down from left to right; tensile axis horizontal, (110) surface, X250.

in the original orientation. Owing to this geometrical softening upon twinning, should a shear stress concentration build up at the twin plane, Livingston and Chalmers' analysis[5] of computing resolved shear stresses on slip systems across a grain boundary shows that the most highly stressed systems in the original matrix are the $(\bar{1}1\bar{1})\ [011]$ and $(111)\ [\bar{1}10]$. These systems are precisely those which are favored from strain compatibility conditions.

From the symmetry of the orientation of $(\bar{1}1\bar{1})\ [011]\ -\ T_4\ [011]$ and $(111)\ [\bar{1}10]\ -\ T_3\ [011]$ combinations with respect to the tensile axis, for a crystal which upon twinning still remains geometrically uniform, double shear is expected. A crystal displaying just this is shown in Fig. 11-VI. For twinned crystals originally oriented for single slip, one of the above combinations has a larger resolved shear stresses and hence planar shear would be expected. The shear fracture in twinned crystals observed by Blewitt, Coltman, and Redman[6] could be explained in this way.

REFERENCES III

1. T. H. Blewitt, R. R. Coltman, and J. K. Redman, Defects in Crystalline Solids, p. 369, The Phys. Soc., London (1955).

2. H. Suzuki and C. S. Barrett, Acta Met. 6, 156 (1958).

3. P. R. Thornton and T. E. Mitchell, Phil. Mag. 7, 361 (1962).

4. S. Saimoto, Ph. D. Thesis, M.I.T. (1964).

5. J. D. Livingston and B. Chalmers, Acta Met. 5, 322 (1957).

6. T. H. Blewitt, R. R. Coltman, and J. K. Redman, J. Appl. Phys. 28, 651 (1957).

APPENDIX IV

Determination of Different Combinations of Slip-system Pairs in Face-centered Cubic Lattice

In the face-centered cubic lattice the slip plane in the $\{111\}$ plane, of which there are four; the slip directions are the $\langle 110 \rangle$ of which there are three on each $\{111\}$ plane. Hence, in all, there are 12 slip systems. On the reference sphere, on which the crystallographic planes intersect as great circles, there are 48 basic triangles bounded by $\{001\}$, $\{110\}$ and $\{0\bar{1}1\}$ type traces, 24 of these appear on the stereographic projection of Fig. 1-IV. Any arbitrary orientation of the tensile axis will appear in one of the triangles. Over each triangle the slip system with the largest Schmid factor will be one of the 12. Since there are 48 trinagles, the same slip system will appear four times, twice under tension and twice under compression.

In Fig. 1-IV, the four slip planes are designated P, U, K and Q after the notation of Diehl.[1,2] The slip system is denoted by two letters, the first refers to the slip plane while the second identifies another intersecting plane with the slip direction defined by the intersection. A bar over the two letters indicates slip in a direction opposite (or negative) to that when the bar is absent. The most highly stressed slip system in each of the triangles is labelled in Fig. 1-IV.

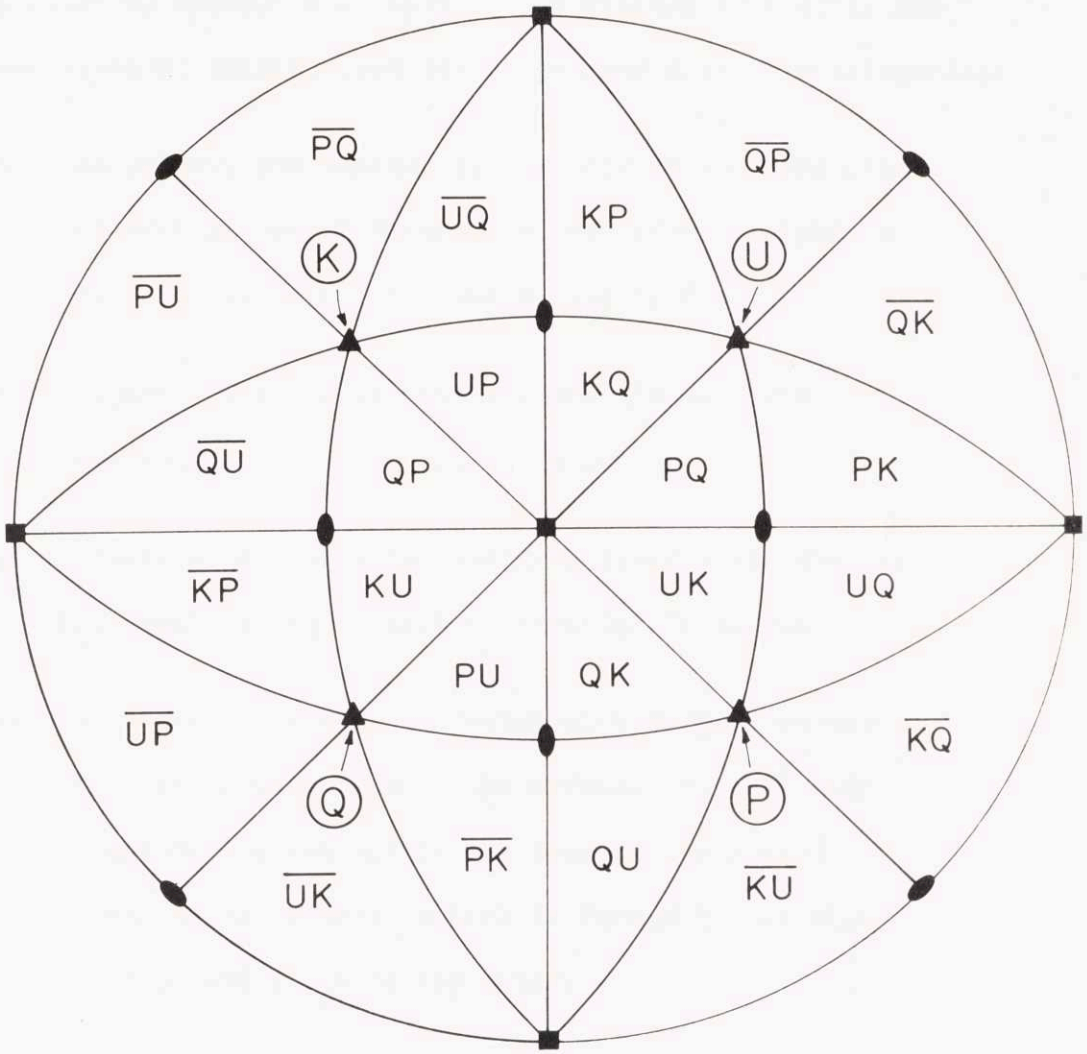

Fig. 1-IV. Standard stereographic projection showing Diehl's notation for slip systems.

As shown by Kocks,[3] when slip on two systems interacts, the different types of interactions can be grouped into five categories:

(a) The primary and another system sharing the same plane but with different Burgers vector (first letters of both are the same); no kink or jog is formed.

(b) primary - cross-slip combinations (letters are reversed); no kink or jog is formed.

(c) primary - conjugate combinations (second letters are the same); a jog in each dislocation is formed.

(d) the primary and another system with Burgers vector parallel to the plane of the primary (first letter in one of the systems is the same as the second letter in the other); a kink is formed in one dislocation and a jog in the other.

(e) primary - critical combinations (no letters appear twice); a jog in each dislocation is formed.

In the [001] orientation, eight systems are equally stressed: PQ, UK, QK, PU, KU, QP, UP and KQ. All possible combinations may be classified according to the above scheme, as follows:

(a) PQ - PU
QP - QK
KQ - KU
UK - UP

(b) PQ - QP
PU - UP
QK - KQ
KU - UK

(c) PQ - KQ
UK - QK
PU - KU
QP - UP

(d) PQ - UP KQ - UK
PU - QP UK - PU
QP - KQ UP - KU
KU - QK QK - PQ

(e) PQ - UK QP - UK
PU - KQ QP - KU
PQ - KU QK - PU
PU - QK QK - UP

In the $[\bar{1}11]$ orientation, the equally stressed (active) slip systems are PQ, KQ, KP, $\overline{QP}$, $\overline{QK}$ and PK. All possible combinations are:

(a) PQ - PK
$\overline{QP}$ - $\overline{QK}$
KP - KQ

(b) PQ - $\overline{QP}$
KQ - $\overline{QK}$
PK - KP

(c) PQ - KQ
PK - $\overline{QK}$
$\overline{QP}$ - KP

(d) $\overline{QK}$ - PQ KQ - PK
PK - KP PK - $\overline{QP}$
$\overline{QP}$ - KQ KP - $\overline{QK}$

(e) none

In the discussion of the present study of the deformation of copper crystals oriented for multiple slip, the different types of jogs possible in a face-centered cubic metal have been emphasized. A brief review on this topic with relation to the above classification of dislocation interactions seems to be in order.

A jog may be defined as a short segment* of dislocation connecting other portions of a dislocation lying on parallel but not the same plane. A dislocation kink connects a dislocation lying on the same plane and hence can easily be eliminated by glide of the dislocation. The glide plane of the jog is that in which the jog line and its Burgers vector lie. This means that the vector normal to the glide plane of a jog formed by any intersecting dislocations is defined by the cross product of the Burgers vectors of the two intersecting dislocations. In the face-centered cubic lattice cross products of $\langle 110 \rangle$ with 60° (or 120°) between them result in $\langle 111 \rangle$, whereas those with 90° result in $\langle 001 \rangle$. Therefore it follows that all 60° intersections produce jogs with $\{111\}$ glide planes and 90° intersections with $\{001\}$ glide planes, as pointed out by Stroh.[4] Hence in the preceding classification of dislocation interactions it is evident that type e (90° intersection)

---

* Length of a jog can vary from a segment about the magnitude of a Burgers vector (unit or elementary jog) to that of several hundred angstroms (long jogs).

produces jogs which are different from those of types c and d (60° intersection).

Seeger and Blank[5,6] have shown that for unit jogs in an unextended dislocation* the above specification of the glide plane is not valid. If the atomic configuration in the face-centered cubic lattice is considered, the glide planes for unit jogs formed by any type of intersection (either 60° or 90°) are either $\{010\}$ or $\{110\}$.[5,6] If an intersecting dislocation forms a $\{100\}$ - type jog on an intersected dislocation, the same dislocation but with antiparallel Burgers vector will produce a $\{110\}$ - type jog on the intersected dislocation. However, should the jog length become larger than a few Burgers vectors (greater than three) the glide plane would become the geometrically predicted $\{001\}$ for 90°-intersection jogs and $\{111\}$ for 60°-intersection jogs.

The first and simplest way to produce long jogs is by multiple intersection at the same place. Since Frank-Read source produce many dislocations on the same plane, formation of long jogs are not a rare event. A second means by which unit jogs can grow is by conservatively gliding along a pure screw[8] and coalescing with one another. However, this event is quite rare since the glide planes of the jogs must be identical. For the same reason, jogs in edge

---

* A detailed study of extended jogs has been presented by Hirsch.[7]

dislocations cannot coalesce or annihilate by conservative motion. A third process by which jogs can grow is by climb. By the aggregation of jogs in cusps formed on jogged screw dislocations as described by Louat and Johnson,[9] jogs can lengthen by climbing only short distances. Since annealing experiments indicate point-defect migration at reasonably low temperatures, climb at ambient temperatures cannot be totally discounted.

REFERENCES IV

1. J. Diehl, Thesis, T. H. Struttgart (1955).
2. J. J. Hauser and K. A. Jackson, Acta Met. 9, 1 (1961).
3. U. F. Kocks, Ph. D. Thesis, Harvard Univ. (1959).
4. A. N. Stroh, Proc. Phys. Soc. B67, 427 (1954).
5. A. Seeger and H. Blank, Z Natureforschg. 9a, 262 (1954).
6. A. Seeger, Defects in Crystalline Solids, p. 391, The Phys. Soc., London (1955).
7. P. B. Hirsch, Phil. Mag. 7, 67 (1962).
8. A. Seeger, Phil. Mag. 46, 1194 (1955).
9. N. Louat and C. A. Johnson, Phil. Mag. 7, 2051 (1962).

APPENDIX V

Deformation of [011] Crystals

In the program to study multiple-slip orientations, [011] oriented crystals were tested in tension. This orientation in which four slip systems are initially equally stressed was unstable, and the tensile axis rotated away from the [011] with strain. However, interesting deformation boundaries were observed and their formation was found to be temperature dependent. Since deformation boundaries are a result of dislocation interactions, the study of the temperature dependence of deformation-boundary formation could reveal the relative importance of different types of dislocation interaction with regard to strain hardening. The observations recorded below seem to indicate that at low temperatures forest hardening, especially by systems of primary-critical (90°-interaction) relationship, prevails.

Square crystals of [011] orientation (within 2°) approximately bounded by $(0\bar{1}1)$ and (100) faces were tested in tension at 295°, 78° and 4.2°K. The dimensions of the crystals directly after annealing were measured at three places with a micrometer, except for crystal L-5 which was measured using an optical comparator. After measurement, the crystals were electropolished and about 0.001 in. removed from each face. However, Bert-Barrett photographs[1,2] of the electropolished surface showed that the plastic strain caused by

micrometer had not been removed, thus forming new dislocation sources (as contrasted with grown-in sources) at such places.

The shear stress-strain curves are presented in Fig. 1-V together with the curves for inside-triangle (single-slip) crystals, the orientations of which are found in Fig. 2-V. The critical resolved shear stresses and θ_I values are listed in Table 1-V. The variation in the τ_o values is attributed to differences in purity from crystal to crystal and to handling effects.

295°K: Lattice rotation of an extended [011] crystal showed that although only a single set of slip traces was metallographically observed over most of the gauge length equal amounts of slip in two directions on the operative plane had taken place. This behavior would account for the higher θ_I value of this orientation compared to that for single slip (Table 1-V). Edwards, Washburn and Parker[3] have made similar observations in zinc crystals. Surface sources introduced by micrometer markings did not seem to inhibit primary slip during easy glide, since neither surface indications of slip traces nor Berg-Barrett photographs revealed extensive plastic strain due to slip on a second plane at their locations. However a short segment adjacent to the grip underwent slip on a plane other than that which was dominant throughout the remaining gauge length of the crystal. In a region on the $(0\bar{1}1)$ surface where the different traces met and became interpenetrating, the Berg-Barrett photographs revealed a definite boundary across the width of the

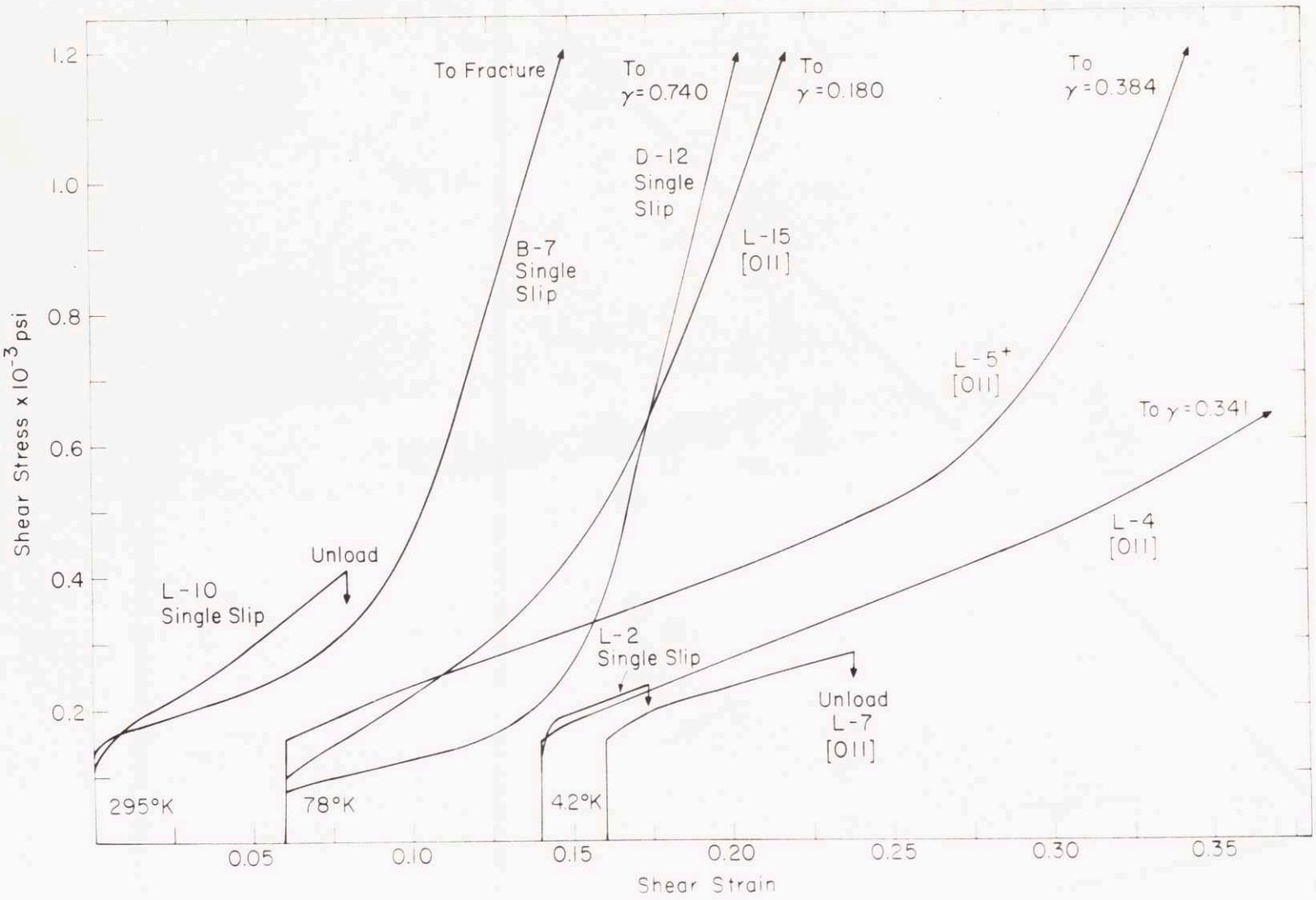

Fig. 1-V. Shear stress-strain curves of [001] and inside-triangle crystals tested at 295°, 78° and 4.2°K.
+ Free from micrometer-induced surface and sources.

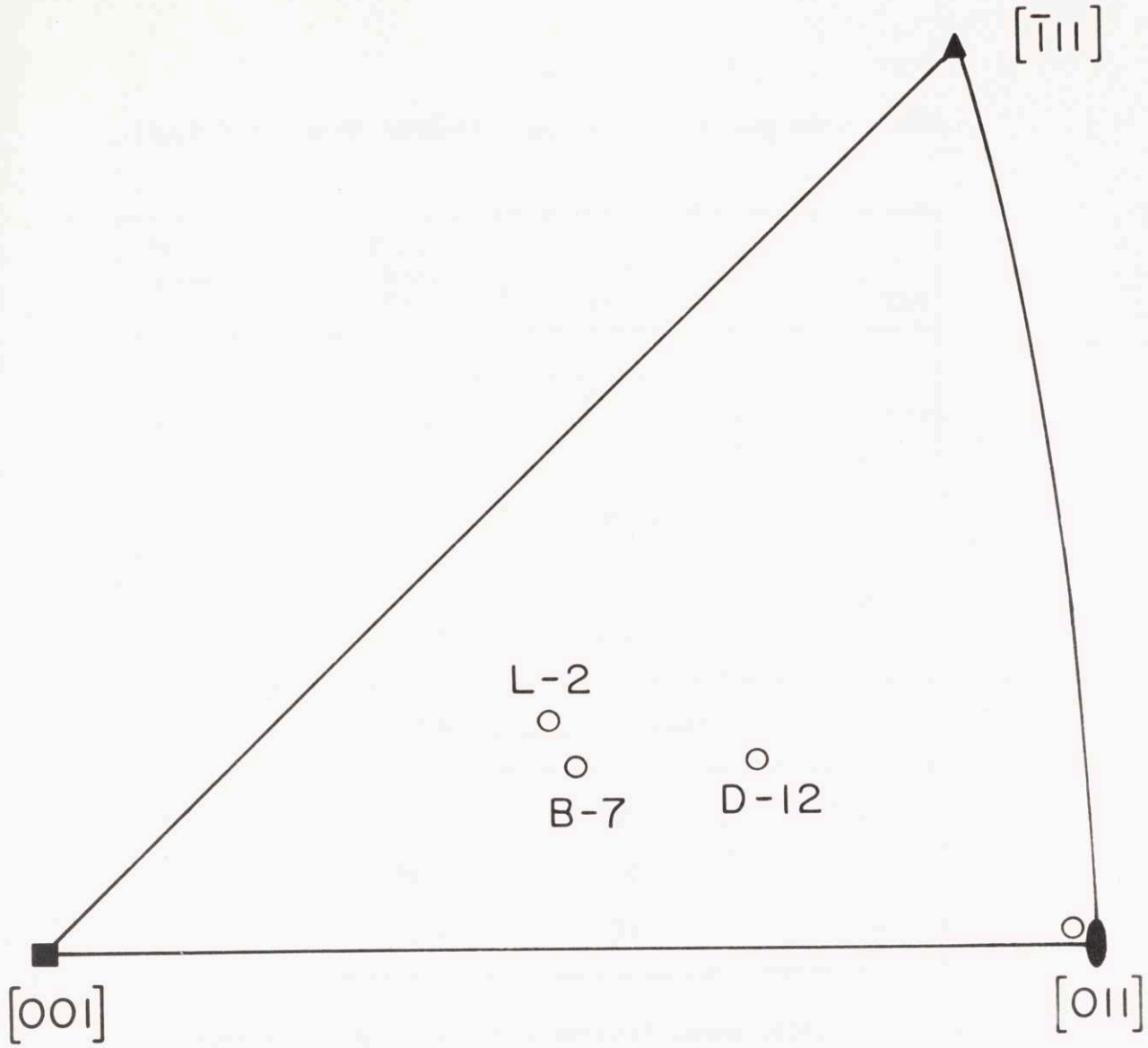

Fig. 2-V. Axial orientations of the crystals tested (open circles).

TABLE 1-V. Work hardening parameters during easy glide.

Code Number	Test Temp. ^{o}K	τ_o psi	θ_I $\times 10^{-3}$ psi
[011] Crystals			
L-10	295	113	3.7
L-15	78	98	3.1
L-5*	78	155	1.7
L-7	4.2	151	1.3
L-4	4.2	148	1.9
Single-slip Crystals			
B-7	295	135	1.6
D-12	78	75	1.1
L-2	4.2	133	1.65

* Dimensions measured with optical comparator, all others with micrometer.

crystal. The plane of the boundary appeared to be normal to the tensile axis. A determination of the combination of slip systems responsible for the formation of this boundary was not possible since the relative lattice rotation was too small.

78°K: On testing at this temperature, [011] crystals "broke up" into regions of different active slip systems as shown in Fig. 3-V, at the location of the surface sources introduced by the micrometer. However, the different systems formed deformation boundaries so that for low strains the thinning of the crystal was macroscopically uniform. In this case the slip systems responsible for the formation of one distinct deformation boundary were determined. In Fig. 4a-V, traces of two boundaries appear at right angles to each other, the vertical one being parallel to $(\bar{1}00)$ trace and the horizontal one, to (010) trace. In the regions removed from the boundaries where only a single set of slip traces is evident, one slip system is active and the lattice rotates in the manner described by Taylor and Elam.[4] The relationship of the slip systems across the deformation boundary, deduced from the lattice rotation on either side of it, is primary-critical. This combination can form "two-dislocation boundaries" as discussed by Kear[5] which are parallel to $(\bar{1}00)$ and (010). Hence the observed boundaries correspond to Kear's case vi and are schematically illustrated in Fig. 5b-V with $(111)\ [\bar{1}01]$ and $(\bar{1}11)\ [101]$, the primary and critical slip-systems,

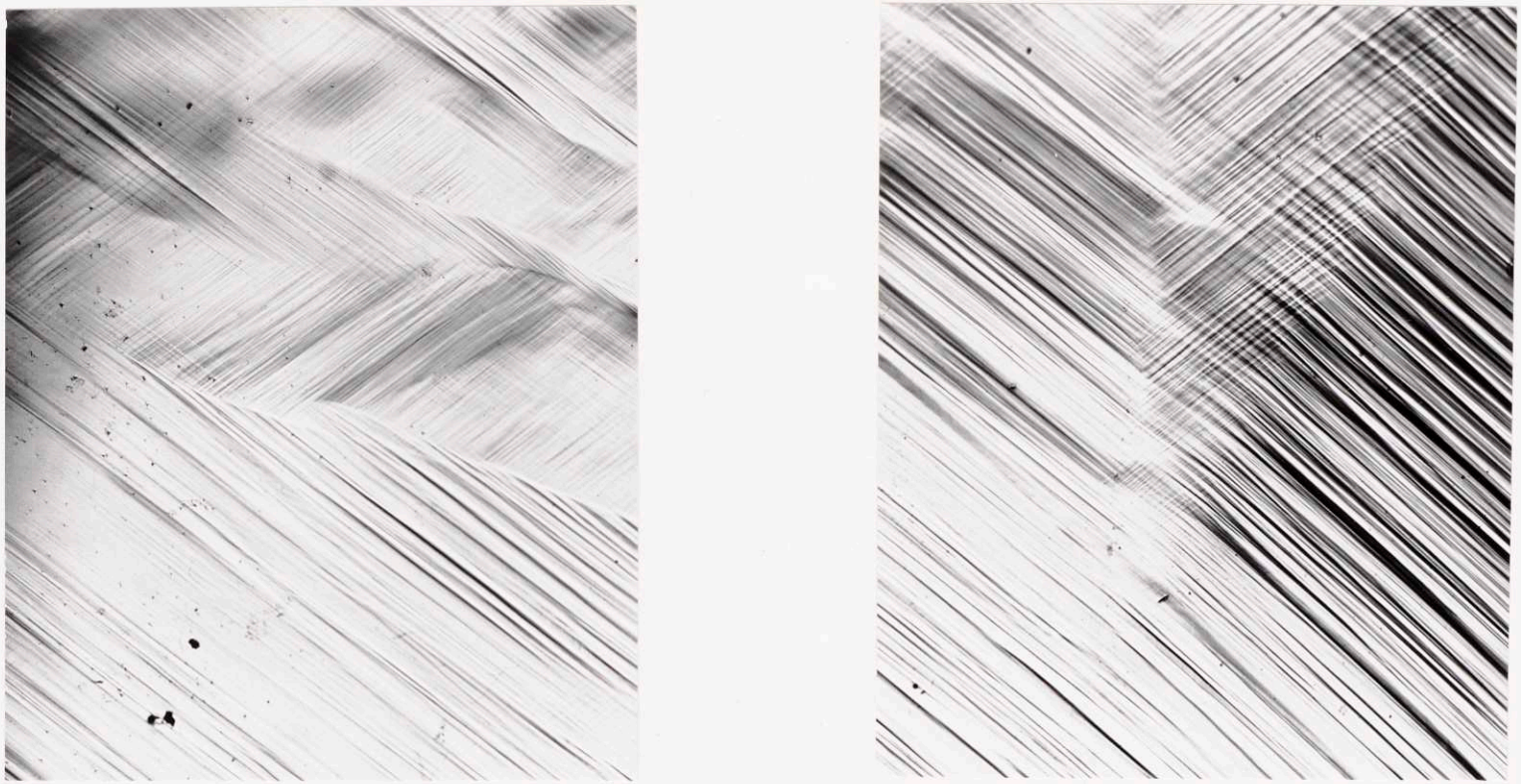

(a) (b)

Fig. 3-V. "Break-up" of [011] crystal tested at 78°K into regions of different slip systems at locations of micrometer-induced surface sources. Two examples, (a) and (b), at different places on (011) surface; tensile axis vertical, X100.

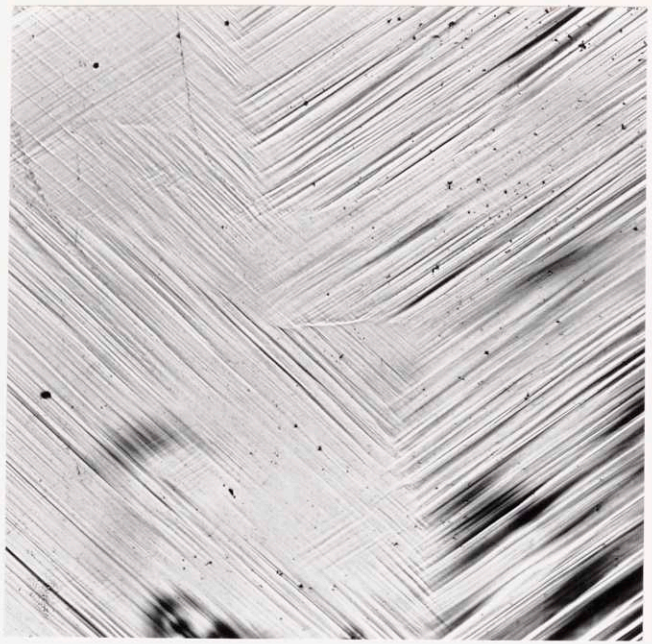

(a)

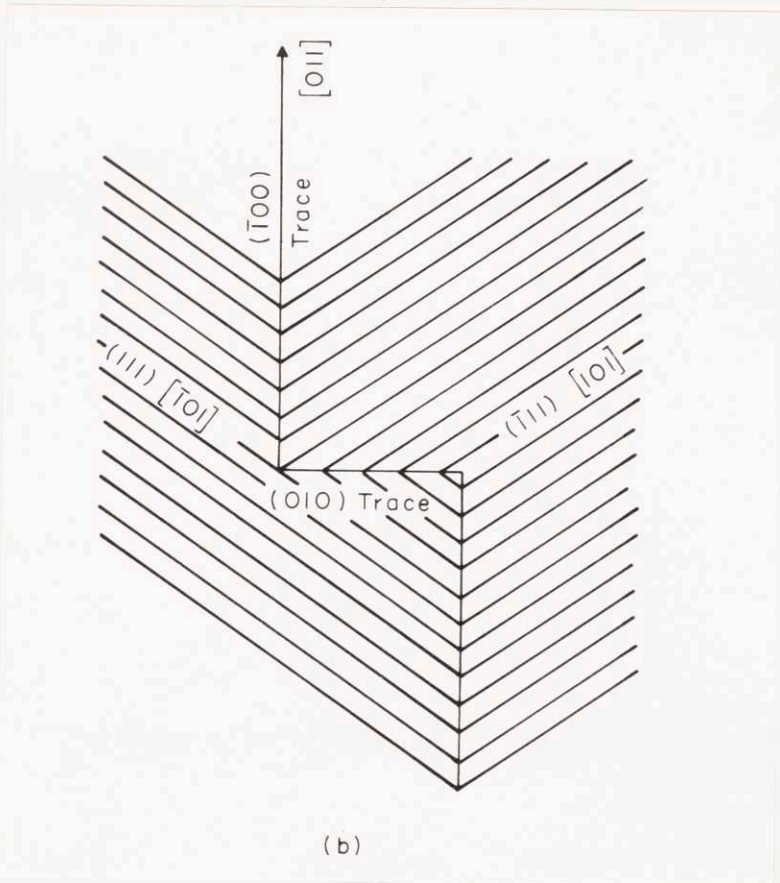

(b)

Fig. 4-V. (a) [011] crystal tested at 78°K showing "two-dislocation boundaries" as depicted in (b); tensile axis vertical (010) surface, X100. (b) Schematic representation of (100) and (010) "two-dislocation boundaries" formed by the slip systems indicated.

respectively. Not all deformation boundaries were as geometrically simple as the one described above. Complex configuration such as those in Fig. 3a-V and 3b-V were also observed.

One crystal, L-5, as mentioned earlier, did not have surface sources artificially introduced. When extended 18 percent into the Stage II region, it did not break-up but manifested large prominent kink bands and less distinct striae or bands of secondary slip similar to those observed by Cahn[6] and Calnan,[7] respectively. A few short cross-slip traces were also observed in bands roughly parallel to the primary slip trace. The absence of surface sources and slip on one active system determined from lattice rotation resulted in a θ_1 value smaller than that of L-15, upon which many deformation boundaries appeared, but similar to that of inside-triangle orientations (Table 1-V). Furthermore, the extent of Stage I was much larger than that of either L-15 or the inside-triangle crystal (Fig. 1-V).

4.2°K: The tendency to form deformation boundaries which makes uniform macroscopic thinning possible in the low strain region was less at 4.2°K than at 78°K. After 3.2 percent extension, the regions at the location of the micrometer-induced surface sources underwent less thinning than the remaining sections. In sections where a single set of traces was found, Laue X-ray studies confirmed that single slip had occurred, as was the case at 78°K. In the region

of the surface sources, the tensile axis rotated along the (100) trace towards [001] indicating equal operation of primary and critical systems. In this work, the crystal with the lower initial shear stress, which is assumed to be purer, formed boundaries more readily and over larger areas. However, the qualitative observation that the tendency towards formation of deformation boundaries is lower at 4.2° than at $78^{\circ}K$ seems reasonable since crystals with similar critical resolved shear stress also gave the same result.

REFERENCES V

1. W. Berg, Naturwissenschaften 19, 391 (1931); Z. Kristallographie 89, 286 (1934).

2. C. S. Barrett, Trans. Amer. Inst. Min. (Metall.) Engrs. 661, 15 (1945).

3. E. H. Edwards, J. Washburn, and E. R. Parker, Trans. Amer. Inst. Min. (Metall.) Engrs. 197, 1525 (1953).

4. G. I. Taylor and C. F. Elam, Proc. Roy. Soc. A102, 422 (1925).

5. B. H. Kear, Trans. Amer. Inst. Min. (Metall.) Engrs. 224, 675 (1962).

6. R. W. Cahn, Inst. Metals J. 79, 129 (1951).

7. F. A. Calnan, Acta Cryst. 5, 557 (1952).

APPENDIX VI

Ductile Fracture in Copper Single Crystals

INTRODUCTION

A single crystal of ductile metal generally fails under tensile load in one of two ways: either it necks and tapers down to a chisel edge, termed rupture in the case of 100 percent reduction of area, or it separates by shear in a localized zone.

It has been shown by Chin, Hosford, and Backofen[1] that rupture is usually associated with high purity and with high stiffness of the testing apparatus. On the other hand, shear fracture is more commonly found in stronger alloy crystals[2,3] or in pure metals at low temperatures.[1] Chin et al[1,4] further demonstrated that adiabatic heating is responsible for shear fracture at low temperatures, and that elastic softness in the loading device is an important factor contributing to adiabatic shearing. In principle at least, shear fracture at ambient temperatures could also be the result of adiabatic heating.

Rupture in the strict sense of necking down to a chisel edge may be prevented in crystals of lesser purity by voids being nucleated around extra-phase particles, such as inclusions,[5,6]

which lead to the "double wedge"* fracture observed in aluminum crystals by Elam,[2] and by Karnop and Sachs.[7] Further study of Elam's crystals by Puttick[8] has shown that the internal fracture did indeed originate at particles of an intermetallic phase. In a different vein, Rosi and Abrahams[9] and also Koppenaal[10] have suggested that voids may be formed by vacancy condensation in materials supposedly free from inclusions. However, the finding by Chin et al.[1] of rupture in every single-crystal and polycrystalline sample of high purity aluminum rules against the notion of a vacancy basis for void formation.

The shear-fracture surface, as usually observed, is characterized by a "dimpled" appearance growing out of voids developed around included particles. However, it is also possible to encounter what might be more appropriately called planar rupture, in that it results from a complete separation by plastic shear; hot deformation may supply an obvious example.[11] Elam[2] found that many crystals of high-zinc aluminum alloys sheared apart under tension along surfaces parallel to $\{111\}$. Similar behavior was noted in aluminum : 5 percent copper crystals by Karnop and Sachs.[3] Recently Beevers and Honeycombe,[12] studying the tensile fracture of aluminum : 5.5 percent copper crystals observed that for orientations away from $[\bar{1}11]$ the fracture surface was parallel to the active octahedral plane, but that for others near $[\bar{1}11]$ the fracture

---

* The counterpart to "double wedge" in polycrystalline metal is "double cup".

surface was parallel to a cube plane. In all cases, however, fracturing was identified with a nearly constant shear stress resolved on the most favored octahedral slip system.

Still more recently, tension tests were made on copper single crystals oriented for single and multiple slip.[13] The original purpose was to investigate hardening characteristics, but observations were also made on an orientation dependence of the fracturing process. Both metallographic and X-ray studies were carried out in the vicinity of the necks that formed. From results on the relation between operative slip systems and lattice rotations the geometrical understanding of ductile fracture in single crystals has been improved. That work is described below.

EXPERIMENTAL PROCEDURES

The methods of growing shaped crystals and of tensile testing in a "hard-type" machine are described elsewhere.[13] Testing speed was 0.013 in/min. Crystals after growth were annealed in helium for 36 hours at 1000°C, cooled at about 50°C/hr down to 600°C, and then finally cooled in the furnace simply by shutting off the power. Purity was sacrificed in the process, for Young[14] has shown that Cu_2O can be formed from the small amount of oxygen in tank helium. Therefore, the crystals in this study would be expected to be populated with small oxide inclusions.

For metallographic examination after pulling, the crystals were copper plated, mounted in an epoxy plastic setting at room temperature and sectioned by grinding on metallographic polishing paper. The mechanically abraded surface was further polished chemically by immersion in a solution of 1/3 acetic, 1/3 orthophosphoric and 1/3 nitric acid by volume, all in concentrated form. Etching was also practiced in a solution described by Young[15] as consisting of 0.53 gm of NH_4 Cl, 22.82 gm of $(NH_4)_2$ S_2O_8, 34.5 ml of NH_4 OH and 65.5 ml of H_2O.

RESULTS

Single-slip Orientation

An initially square single crystal was extended at room temperature until a neck had been formed (Fig. 1-VI). The final orientation of the tensile axis in regions well removed from the neck was in the (110) plane about 6° from $[\bar{1}12]$, approaching this stable end-orientation from the $[\bar{1}13]$ side (Fig. 2-VI). The result of sectioning nearly parallel to the $(1\bar{1}1)$ cross-slip plane (through A-A indicated in Fig. 1-VI), chemical polishing, and light etching is shown in Fig. 3a-VI; two distinctly dark-etching shear zones have been made apparent, one more prominent than the other. Firgure 3b-VI is a schematic representation of 3a-VI to identify the zones more clearly as well as the trace, S-S, of a symmetry plane parallel to (110) along which the zones intersected. One zone is associated

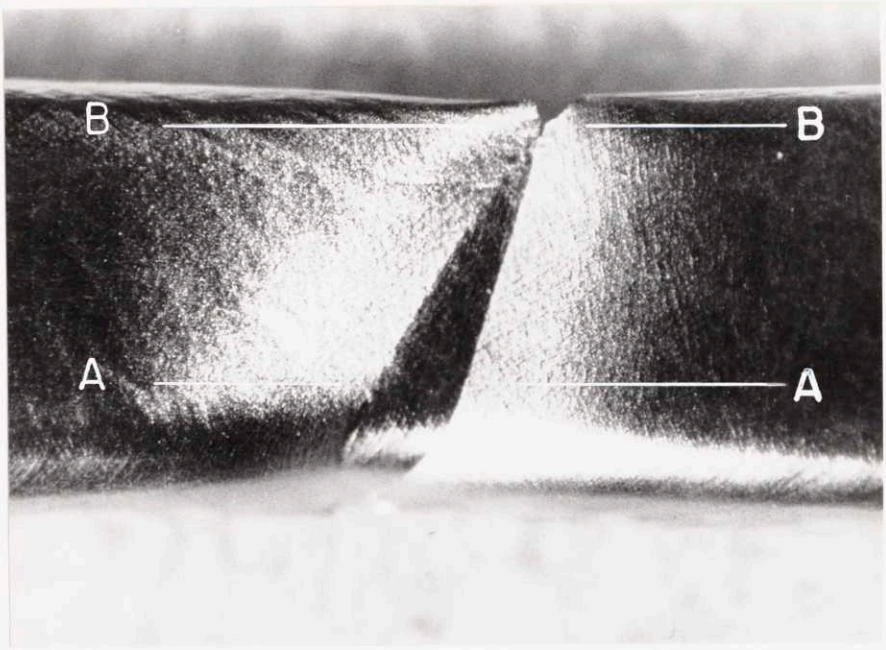

Fig. I-VI. Necking in a copper crystal initially oriented for single slip.

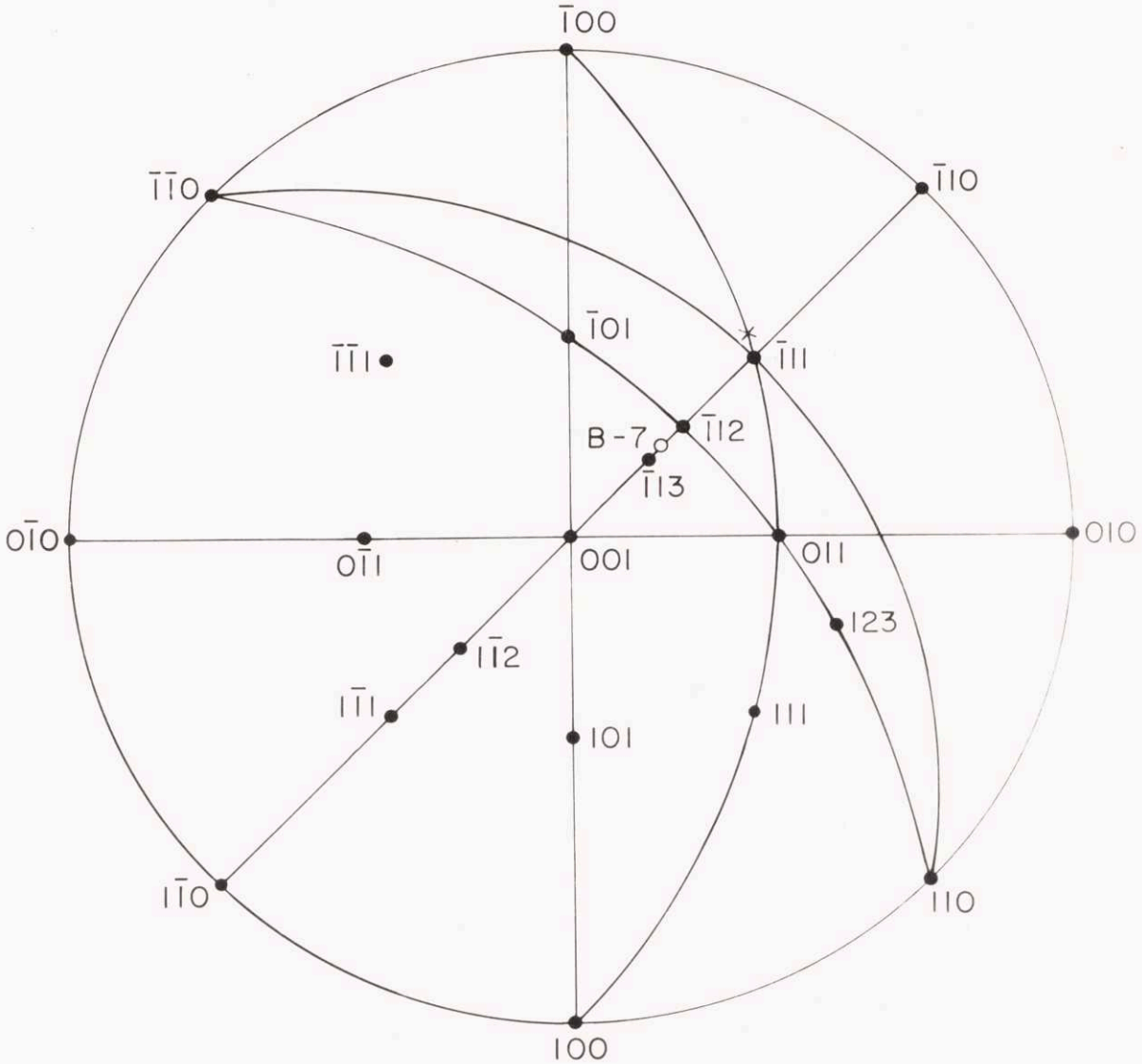

Fig. 2-VI. Standard stereographic diagram with poles of planes and directions mentioned in the text. Position X is the orientation of the tensile axis in the neck of the $[\bar{1}11]$ crystal (the X-ray beam was positioned about 0.10 in to the left of area shown in Fig. 10b).

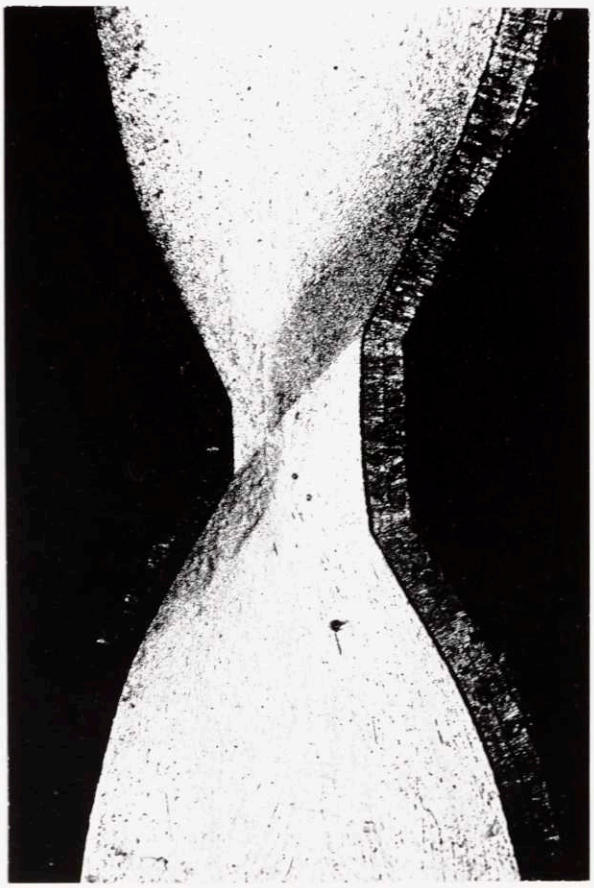

Fig. 3a-VI. Section parallel to $(1\bar{1}1)$ through A-A in Fig. 1-VI, etched to reveal shear zones. Crystal surface is copper plated; tensile axis vertical, X50.

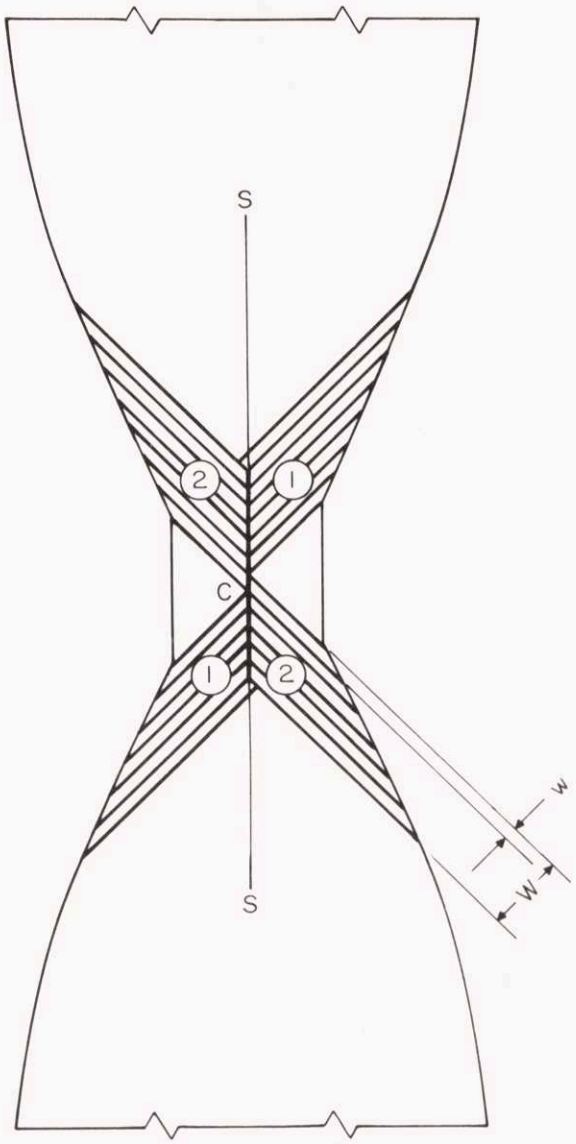

(b)

Fig. 3b-VI. Schematic diagram of (a) illustrating the two shear zones, 1 and 2, the width of the alternating shear lamellae, w, the width of the shear zone, W, and the trace, S-S, of the symmetry plane defined by the intersecting shear zones.

with the primary* slip system, (111) $[\bar{1}01]$, the other with the conjugate, $(\bar{1}\bar{1}1)$ $[011]$. The strong etching contrast between the shear zones and the triangular portions in the parallel section indicates a sharp discontinuity in shear strain along the boundaries. To account for the appearance of the shear-zone termination along the symmetry plane, formation of a zone must be viewed as a gradual development something like the step-wise process pictured schematically in Fig. 3b-VI; here, the intent is to suggest that shear in lamellae of width w occurs alternatively on primary and conjugate systems, and in this way acts to increase zone width W at the expense of the non-deforming triangular regions. If no voids opened up internally, the crystal should fail by a chisel-edge rupture.

A tear is evident at one edge in Fig. 1-VI. To observe its relation to the shear zones, another section was made along B-B. After brief chemical polishing, a quadrangular cavity with internal angles of $60^{\circ} \pm 5$ and $120^{\circ} \pm 5$ appeared (Fig. 4a-VI). Further polishing and etching revealed that the sides of the cavity were continuations of the boundaries of shear discontinuity and were parallel to (111) and $(\bar{1}\bar{1}1)$ traces. The preferential etching at the edges of the cavity has made it difficult to illustrate this

---

* Notation of slip systems after Rosi and Mathewson,[16] and Clarebrough and Hargreaves.[17]

(a)

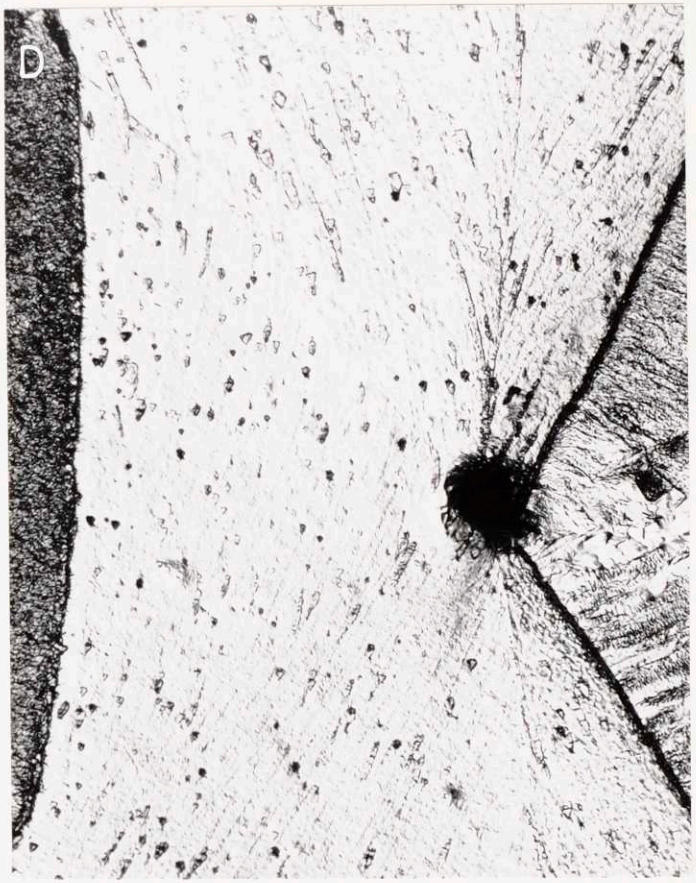

(b)

Fig. 4-VI. (a) Section parallel to $(1\bar{1}1)$ through B-B in Fig. 1-VI, chemically polished. The quadrangular cavity has not been completely filled by the copper plating. Tensile axis vertical, X1000. (b) Same section as (a) etched to reveal shear zone with distinct boundary of shear discontinuity; X250.

point with photomicrographs (Fig. 4b-VI). Upon continued extension this would result in "double wedge" fracture.

The orientations in various regions of the neck as determined from the etch pits, are summarized in Fig. 5-VI. X-ray photographs taken at points a and b (Fig. 5-VI) confirmed the reliability of orientation determinations by etch pits. Changes in orientation are such that in the neck on either side of the plane of symmetry the $[\bar{1}12]$ is rotated away from the tensile axis, the amount of rotation increasing with distance from the symmetry plane.

Figure 6-VI is a magnified view around point D in Figs. 4b-VI and 5-VI and shows that the lattice on one side of the shear discontinuity is misoriented by about 17° with respect to the other. Above, in the shear zone, the boundary is parallel to one edge of a triangular etch pit, while below it is not. The misorientation disappears, however, as the cavity is approached; here, the boundary of shear discontinuity makes an angle of 30° to the tensile axis, as it must if it represents either (111) or $(\bar{1}\bar{1}1)$ with tensile axis along $[\bar{1}12]$. In the region around Fig. 6-VI, the angle to the tensile axis is 47°, resulting from the 17° rotation in the shear zone near the surface of the neck. Recently Puttick[8] identified the boundary of the shear zone in Tipper's aluminum crystals as a $\{321\}$ slip plane. In the present work, the trace of (123) on the $(\bar{1}\bar{1}1)$ plane makes an angle of 41° with the tensile axis (Fig. 2-VI)

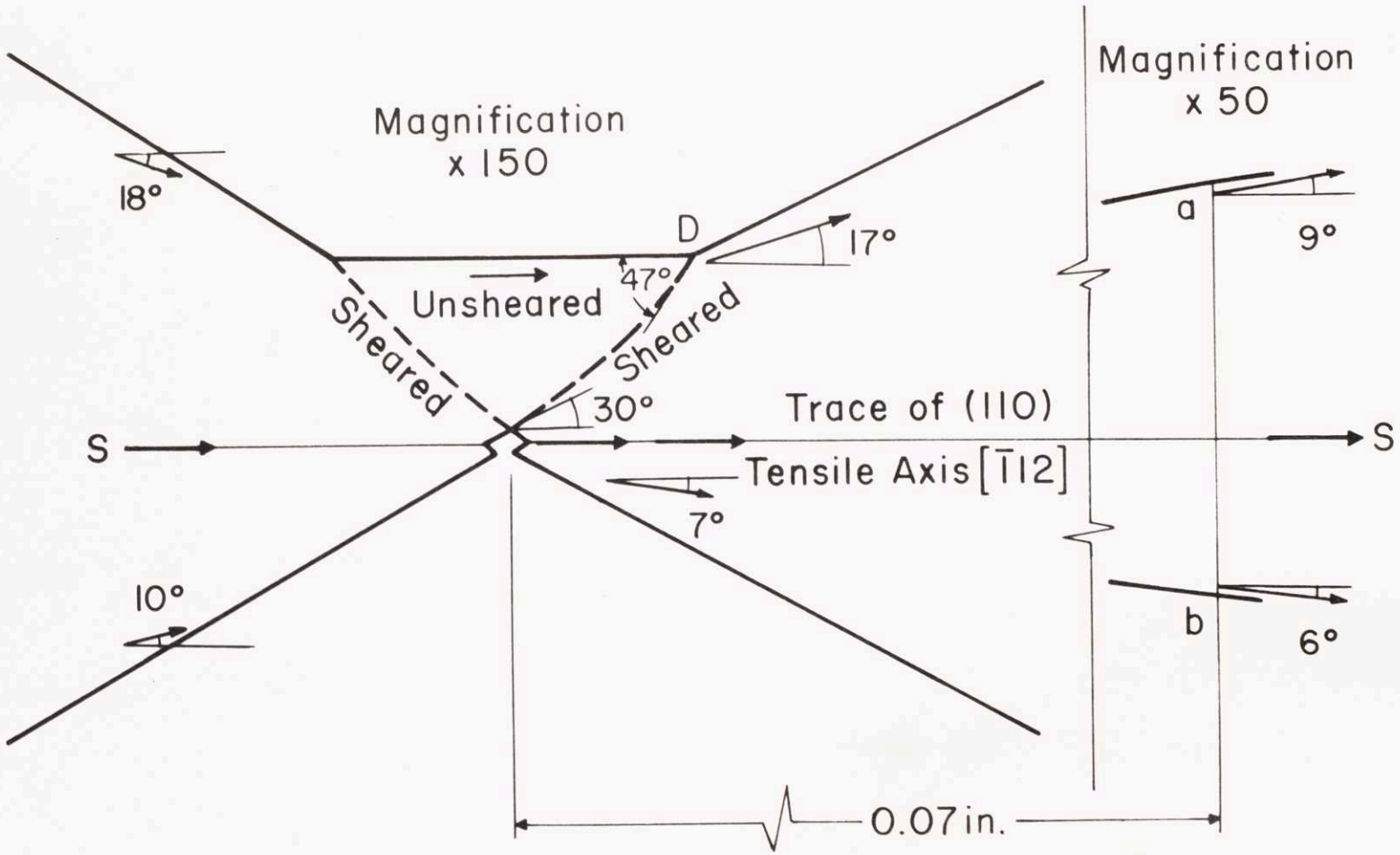

Fig. 5-VI. Schematic diagram of Fig. 4b-VI indicating the lattice orientation at various points in the neck. All arrow heads indicate [$\bar{1}$12], and the rotations indicated are in the plane of observation, ($1\bar{1}1$).

Fig. 6-VI. Magnified view of boundary of shear discontinuity showing crystallographic etch pits and a kink in the row of pits which straddles the boundary. Tensile axis vertical, X1000.

if it is assumed that the tensile axis is parallel to $[\bar{1}12]$ throughout the neck. Hence the $\{321\}$ is probably only an apparent slip plane.

A micro-hardness survey was made on the section of Fig. 4-VI with the results given in Fig. 7-VI. Maximum hardness was found in the shear zone with comparable hardness on either side -- in the triangular reservoir of material passing into the zone, at the one extreme, and in regions well removed from the neck, at the other.

$[\bar{1}11]$ Orientation

Crystals extended at 162°K and 273°K underwent no more than about 20% reduction of area after necking and before beginning to separate by shear along a single localized band. An arrested shear during testing at 273°K (after prestraining at 78°K) is shown in Fig. 8-VI. From the relative displacement of the edges of the crystal, the direction of shear (in Fig. 8-VI, at about 45° to the tensile axis) was determined to be $[011]$. The orientation of the crystal with respect to its surfaces is represented in Fig. 9-VI. Surface analysis* of the shear zone revealed that the normal to the plane of shear was coplanar with the tensile axis and the shear direction, and within 5° of $[\bar{1}00]$. This means that the slip systems operative in the shear zone were in primary-cross relationship, namely $(\bar{1}\bar{1}1)$ $[011]$ and $(\bar{1}11)$ $[011]$ (Fig. 9-VI). Hosford, Fleischer, and Backofen[18]

---

* Surface analysis was facilitated by the fact that during deformation of $[\bar{1}11]$ crystals lattice rotation was small.

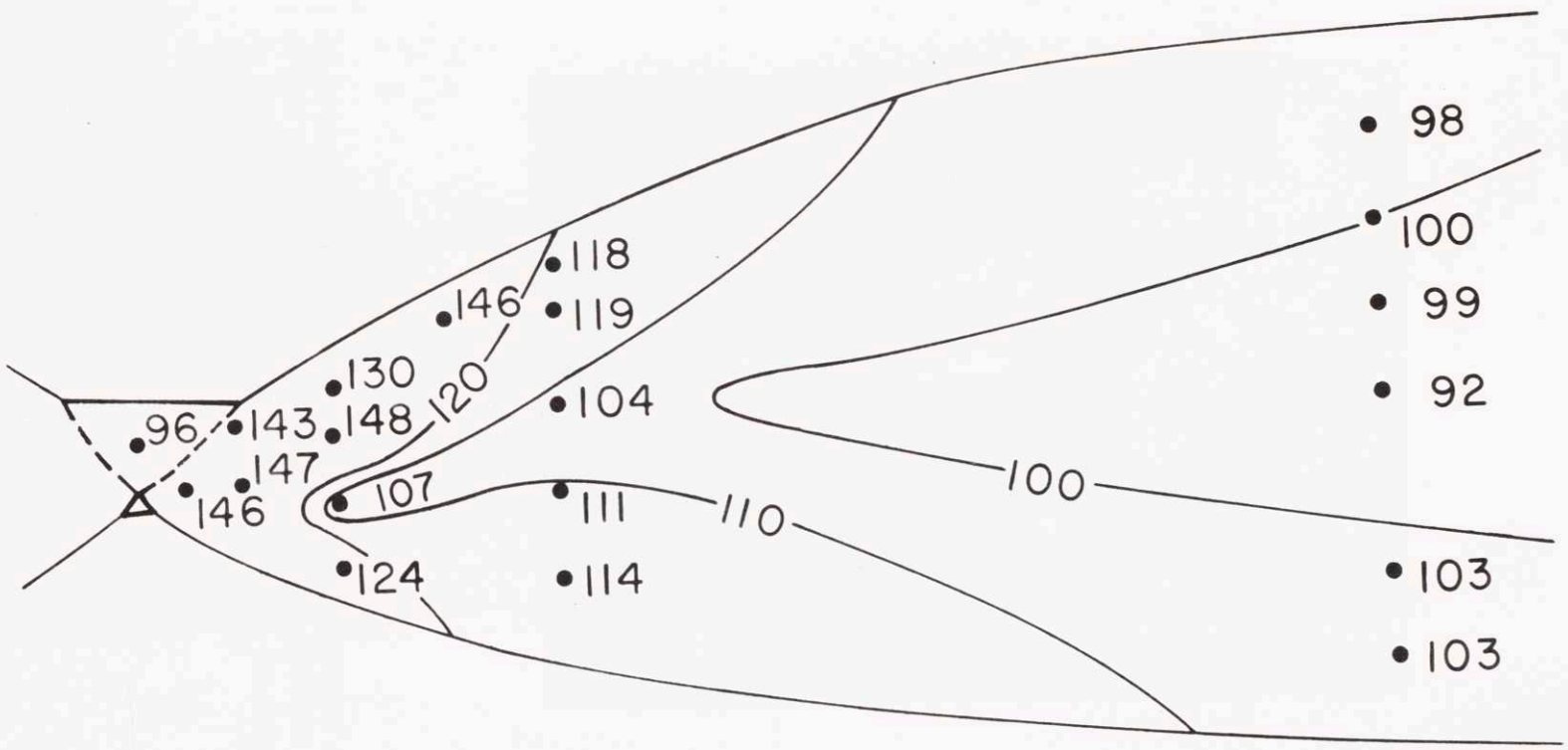

Fig. 7-VI. Micro-hardness values taken on the section of Fig. 4b-VI with Vickers indenter and 100-gm weight; X75.

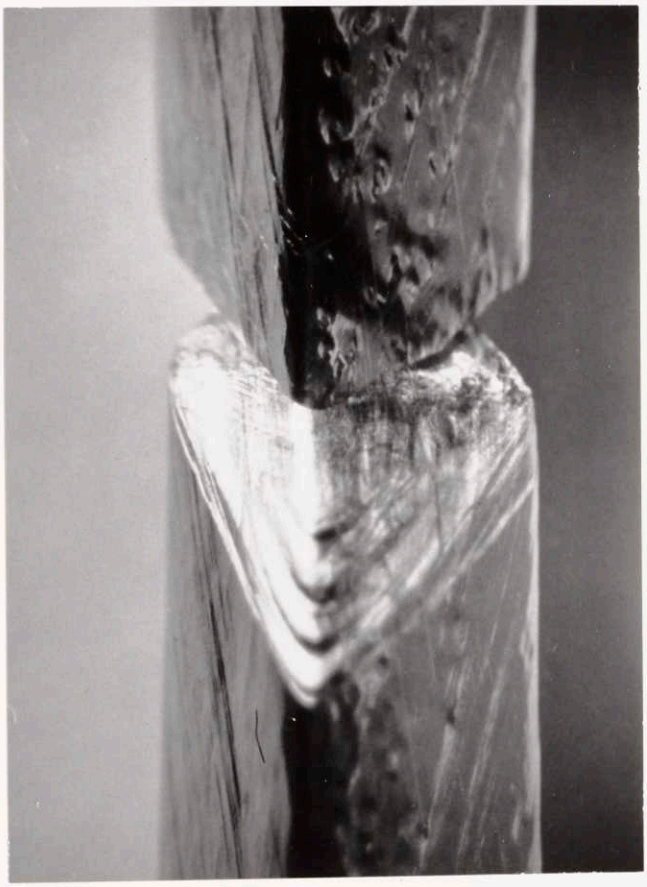

Fig. 8-VI. An arrested shear in a $[\bar{1}11]$ crystal tested at 273°K after prestraining at 78°K. Crystal surface on right is parallel to $(\bar{1}10)$ and that on left is parallel to $(\bar{1}12)$; X12.

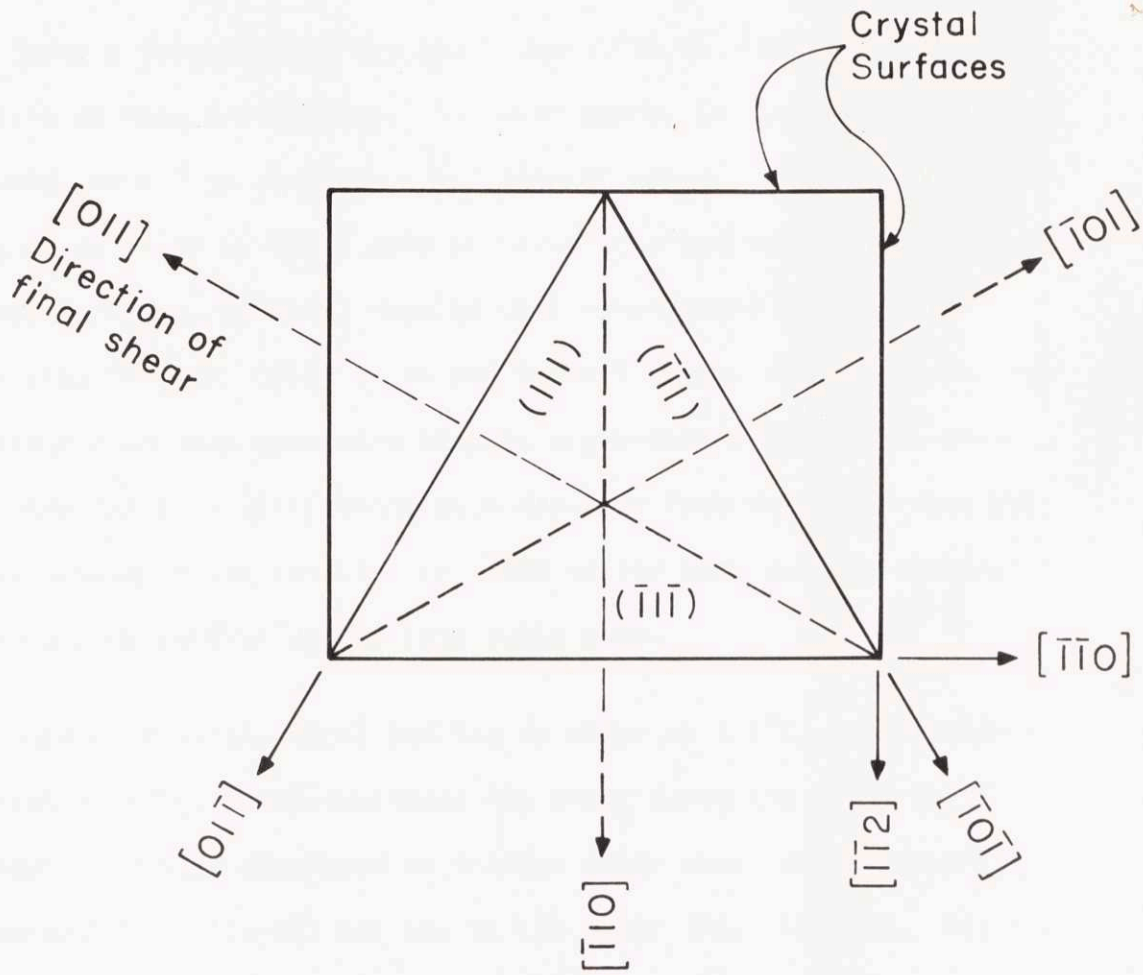

Fig. 9-VI. Tetrahedron bounded by $\langle 111 \rangle$ planes and $\langle 110 \rangle$ directions projected on the $(\bar{1}11)$ plane. Tensile axis is parallel to $[\bar{1}11]$ (perpendicular to the plane of view) and the projections of the stressed slip directions are shown as dashed lines.

also found a fracture surface nearly parallel to $(\bar{1}00)$ in aluminum crystals of this orientation. As noted above, in the work of Beevers and Honeycombe[12] on aluminum : 5.5 percent copper crystals, fracture surfaces parallel to (100) were observed in orientations near $[\bar{1}11]$; in that instance, however, results were interpreted in terms of cubic slip,[19] $\{001\}\langle 110\rangle$. In the present study, slip clusters near the shear zone were generally wavy in appearance (Fig. 8-VI); some were parallel to a $\{111\}$ trace at a distance from the shear zone but curved enough to lie parallel to $(\bar{1}00)$ as the zone was approached, indicating octahedral rather than cubic slip.

Another crystal, after failing by shear at 162°K, was sectioned parallel to $(01\bar{1})$ which contained the shear direction (Fig. 9-VI). Chemical polishing disclosed an intense shear zone, voids appearing at one end (Fig. 10a-VI) but not at the other (Fig. 10b-VI). Distinct crystallographic etch pits could not be produced on the surface shown in Fig. 10-VI, but it was found from X-ray studies that in the neck the tensile axis had rotated about 5° from $[\bar{1}11]$ towards $[\bar{1}00]$* (Fig. 2-VI).

---

* The measurement could only be approximate since the beam was 0.020-in. in diameter.

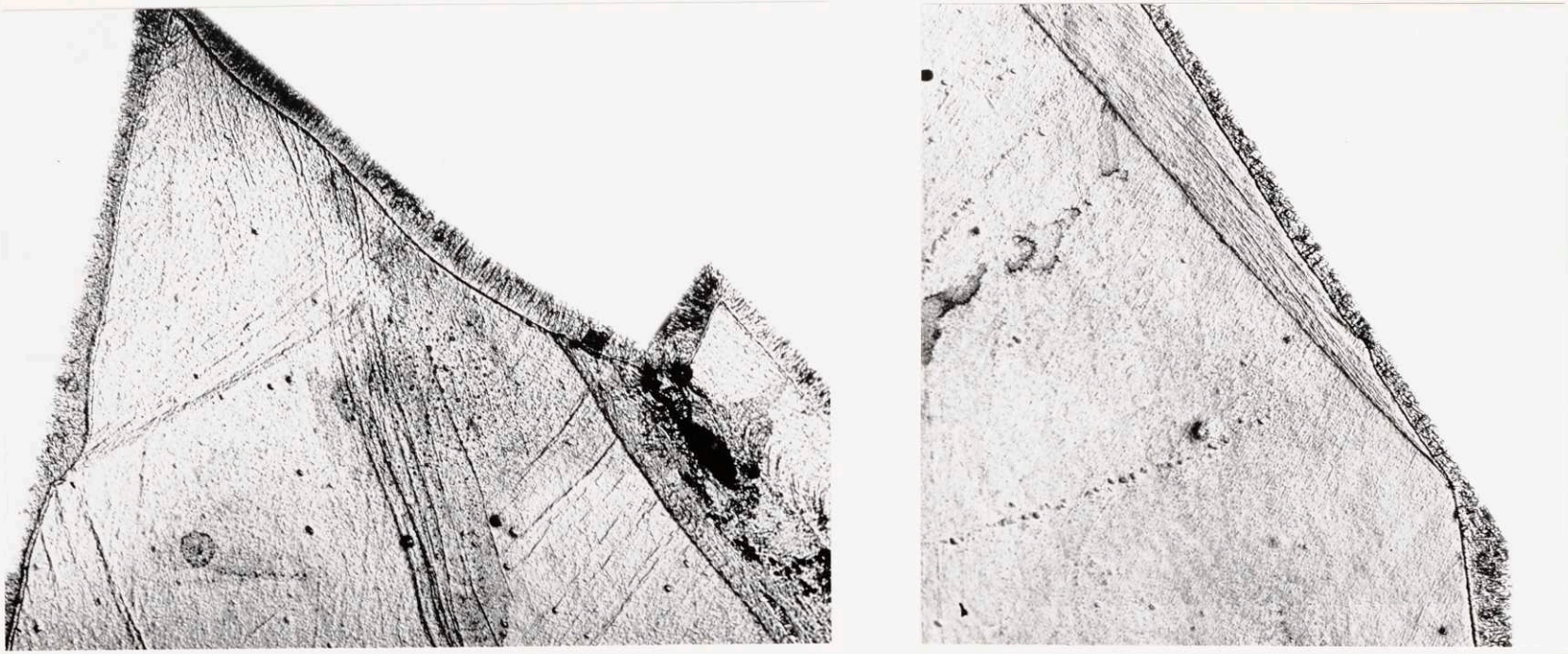

(a) (b)

Fig. 10-VI. Section parallel to $(01\bar{1})$ through a $[\bar{1}11]$ crystal after failing by shear at 162°K. (a) One end of the shear zone in which a large void is evident, towards the right. The many smaller dark spots are stain markings rather than voids. Crystal surface cooper plated; tensile axis vertical, X150. (b) The other end of the shear zone shown in (a). Tensile axis vertical, X150.

Twinned $[\bar{1}11]$ Crystals

Twinning occurred in $[\bar{1}11]$ crystals at 78°, 20° and $4.2^{\circ}K$, first locally and then generally with the propagation of a Lüders-band type of deformation. After this twinning front had travelled the full length of crystal and some further work hardening had taken place, fracture proceeded by slip in two intersecting zones. As in the case of the single-slip orientation, a cavity appeared at the intersection of the zones and grew into the quadrangular channel noted earlier (Fig. 11a-VI). The boundaries of shear-strain discontinuity were parallel, as before, to the sides of the channel (Fig. 11b-VI).

Slip at fracture was confined to the two zones for simple geometrical reasons. Twinning does not convert the whole crystal to the twin orientation; rather, a laminated structure of alternating twinned and untwinned matrix results. The relative orientation of twinned and untwinned regions is represented in Fig. 12-VI with two tetrahedra bounded by $\{111\}$ planes and $\langle 110\rangle$ directions; that on the left corresponds to the original orientation with tensile axis parallel to $[\bar{1}11]$, while that on the right gives the twinned orientation. The two most highly (and equally stressed) slip systems on the twinned tetrahedron are T_4 $[011]$ and T_3 $[\bar{1}10]$, and T_4 and T_3 representing $\{111\}$ planes. The slip systems in the untwinned matrix which will not disrupt strain compatibility across the twin boundary by their operation are $(\bar{1}1\bar{1})$ $[011]$ and (111) $[\bar{1}10]$ (also equally stressed). As each of the two pair, $(\bar{1}1\bar{1})$ $[011]$ and T_4 $[011]$,

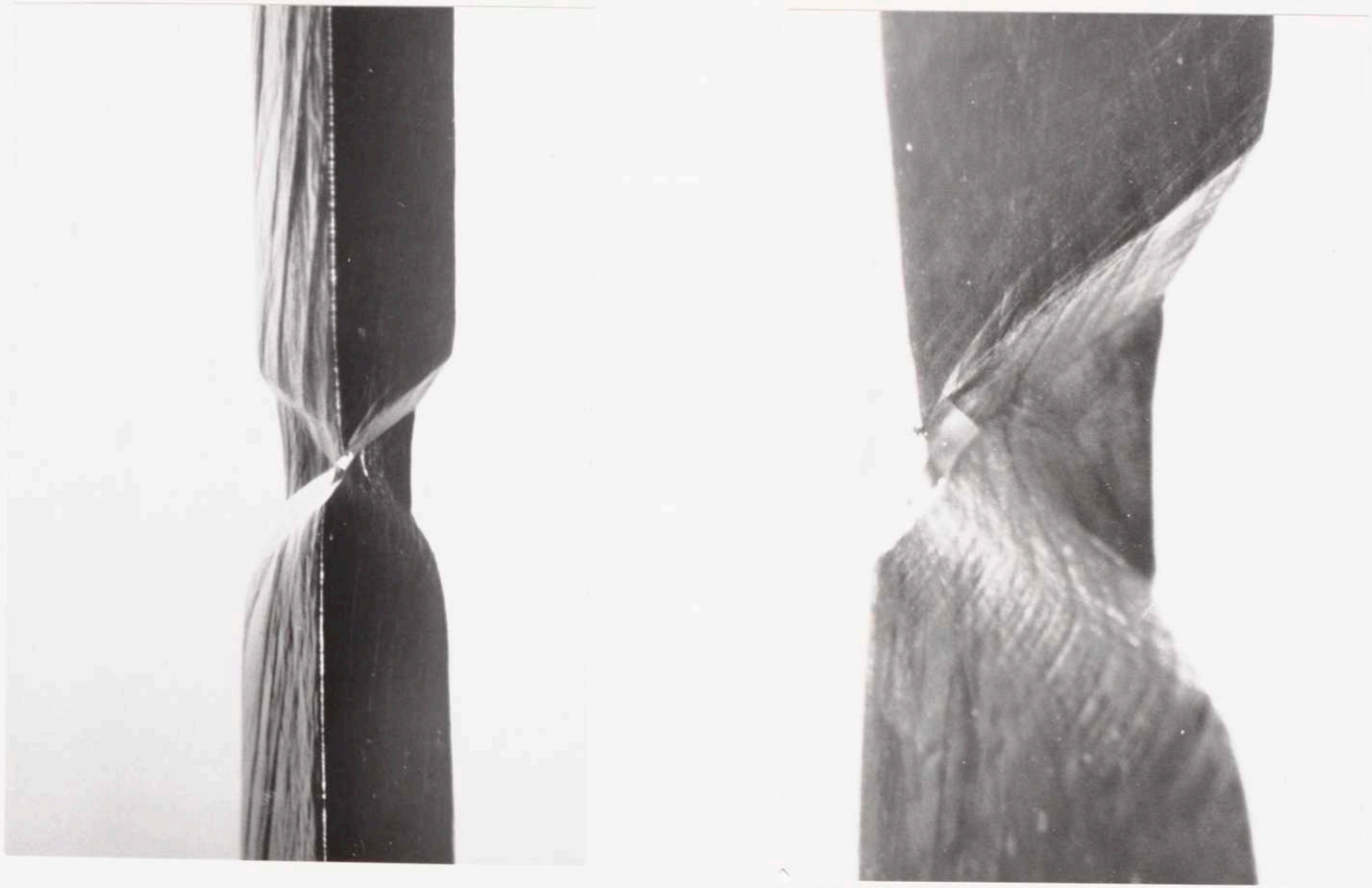

(a) (b)

Fig. 11-VI. (a) Twinned $[\bar{1}11]$ crystal tested at 78°K showing quadrangular channel formed by intersecting slip, X7. (b) Magnified view showing that the sides of the channel in (a) are coincident with the boundary of shear discontinuity, X20.

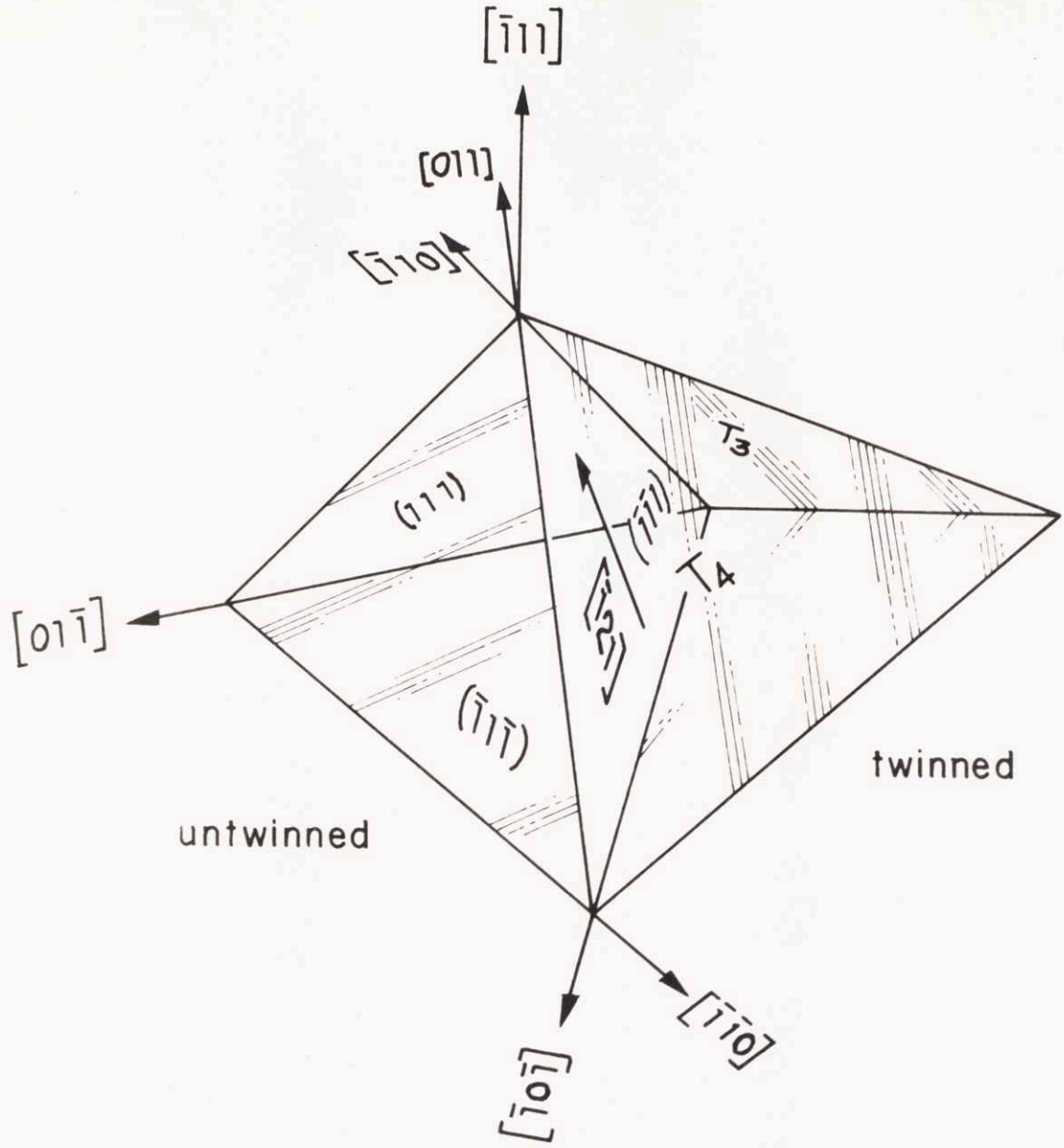

Fig. 12-VI. Two tetrahedra with a common $\langle 111 \rangle$ (twinning) plane. That on the left represents the original, untwinned orientation, that on the right the twinned orientation. T_3 and T_4, the active slip planes in the twinned orientation. Tensile axis parallel to $[\bar{1}11]$.

and (111) $[\bar{1}10]$ and T_3 $[\bar{1}10]$, has a slip direction in common, an essentially pencil-glide type of slip is possible. Thus slip occurs in two intersecting bands which were macroscopically parallel to planes about 50° to the tensile axis.

[001] Orientation

At 78°K and above, [001] crystals fractured either by rupture or by void formation after large reduction of area. Necking developed by practically equal amounts of slip either on four {111} planes (Fig. 13a-VI) or on two {111} planes (Fig. 13b-VI). The example in Fig. 13b-VI is another of the "double wedge" fracture associated with impure crystals. The difference in Fig. 13-VI is most probably a result of the tensile axis being parallel to [001] for (a), so that four planes were equally stressed, but not being so closely aligned for (b), resulting in only two planes equally stressed.

DISCUSSION

Void Formation by Slip Intersection

High strains would be expected at the intersections of shear lamellae, such as pictured at point C in Fig. 3b-VI. If voids were to form, e.g., because of oxide inclusions, this would be the logical site at which to expect them. A total strain estimate may be based on the shear strain, γ, at the boundary between the unsheared triangle and the shear zone; from the kink in the row of

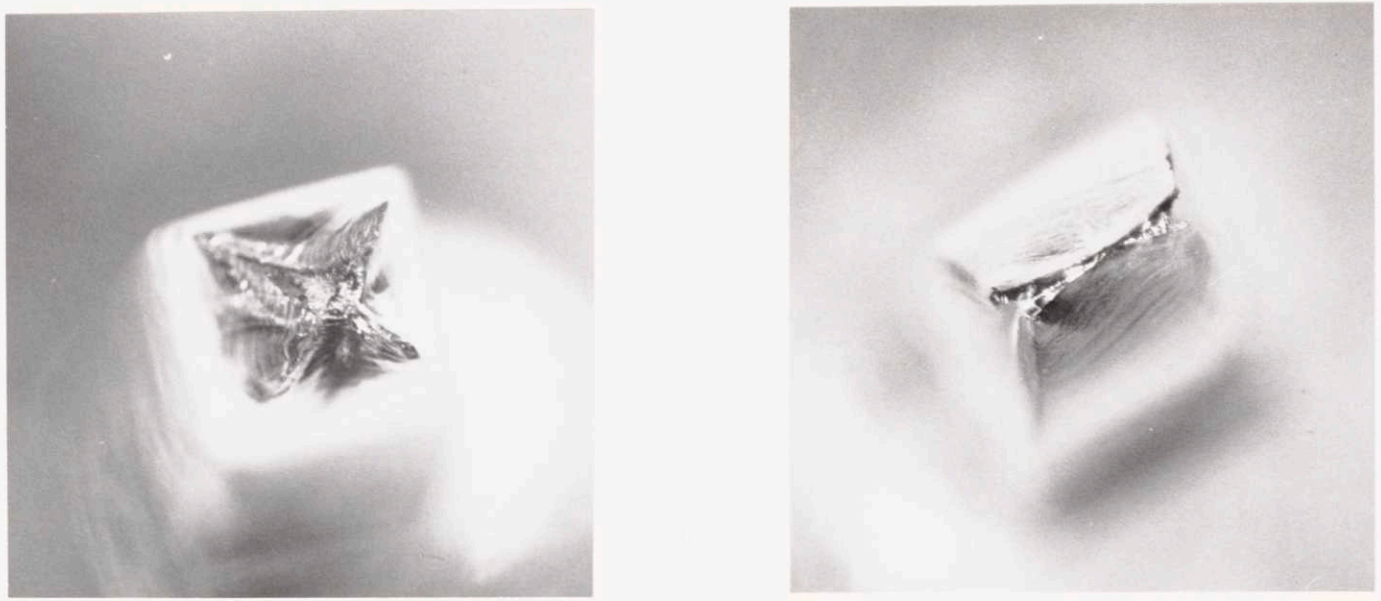

(a) (b)

Fig. 13-VI. (a) Appearance of fracture in an [001] crystal pulled at 78°K showing the symmetry from equal slip on four {111} planes; X13. (b) Appearance of fracture in an [001] crystal pulled at 273°K showing the two-fold symmetry from slip on only two {111} planes; X13.

etch pits straddling this boundary (Fig. 6-VI), γ is found to be about 0.8. The full width of the shear zone, W, can be measured in Fig. 3a-VI. For a value of w, the width of a shear lamella, the side-length of the quadrangular cavity (Fig. 4a-VI) might be taken. Then, assuming that the crystal elongated by alternating shear in zones 1 and 2, the total shear strain at point C is given by $\gamma_t = 2(W/w)\ 0.8$. Further multiplication by a factor of $\frac{1}{2}$ to obtain tensile strain yields a value of approximately 5. If the crystal could have been extended more, the tensile strain would, of course, have been even larger. It follows that along the symmetry plane S-S, the tensile strain decreases from a maximum value at C to that at which necking began in regions far removed from the neck. The voids observed by Rosi and Abrahams[9] occurred in a region about where the symmetry plane would be expected to lie, suggesting that the voids in that work resulted from intersection of slip.

Once a void has been formed, its growth can be explained with the alternating slip process suggested by Orowan.[20] Crystallographic boundaries on a cavity so formed would follow from that process.

Channel development in the twinned crystal (Fig. 11-VI) and the appearance of fracture in the $[\bar{0}01]$ crystal (Fig. 13b-VI) can be understood in the same way. In general, this agreement would seem to explain the "double-wedge" fracture in single crystals.

If shear is confined to a single zone, as in Fig. 10-VI, the rationale for void nucleation and growth does not have such a simple geometric basis. However, the combination of shear and tensile strain in the zone should be quite sufficient for void development (Fig. 10a-VI), even leading to the "void sheets" described by Rogers[21] in polycrystalline copper.

Lattice Rotation in the Vicinity of the Neck

The lattice rotation represented in Fig. 5-VI is a natural consequence of the strain gradient in a region of necking. The gradient is drawn schematically in Fig. 14a-VI. Extension is accomplished by slip on the two systems in primary-conjugate relationship. If the strain in a lamella (shaded) in Fig. 14b-VI is considered, it is evident that there must be a gradient of shear strain from a maximum at the center of the neck to some lesser amount near the ends of the lamella. Because of such differential straining, there is a rotation away from the tensile axis as shown in Fig. 14c-VI. A lamella identified with the second system is indicated by dashed lines as undergoing rotation in the opposite sense. If the neck is imagined to consist of lamellae, a lattice rotation reaching a maximum at the inflection point in the curvature of the crystal surface is predicted. Furthermore, rotation along the symmetry plane S-S ought to be zero because the effect of lamellae intersection here would be to cancel completely; at points approaching the crystal surface, the amount of cancellation must become less. Such predictions are consistent with the findings.

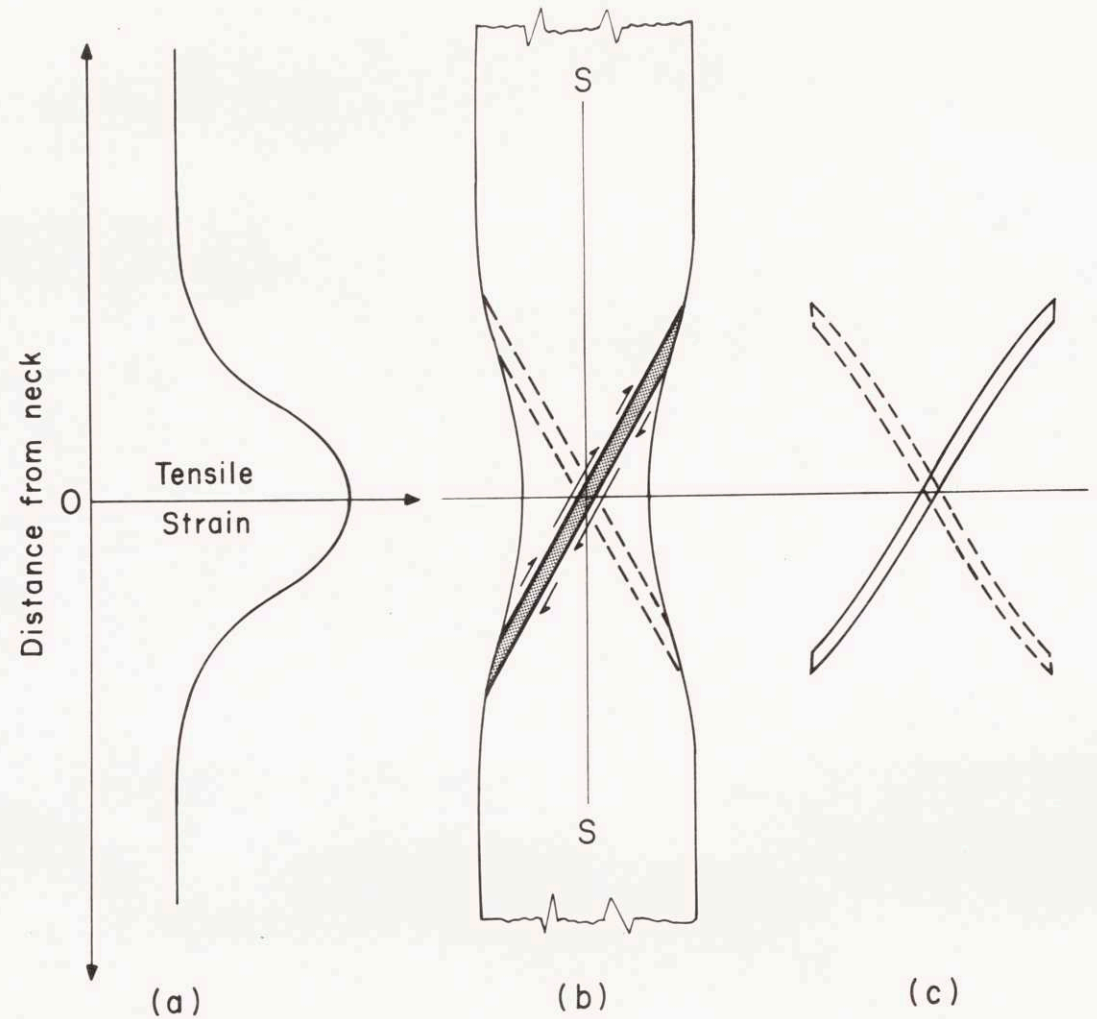

Fig. 14-VI. (a) Schematic representation of the gradient of tensile strain in the neck of a crystal. (b) Schematic diagram of a necked crystal illustrating a lamella undergoing differential shearing. (c) Schematic diagram of the lamella in (b) which has undergone a differential strain resulting in a bending away from the tensile axis.

There is some problem attached to explaining why deformation in the necked region becomes localized in the form of shear lamellae (Fig. 3b-VI). However, the reason may be found in one consequence of the tensile axis rotating away from the $[\bar{1}12]$ and the active slip direction; this is an increase in Schmid factor of the active system[22] or, equivalently, a geometrical softening, which could outweigh the strain hardening and thus allow a localized shear to develop. Beyond this, it can be argued that the rotation in a lamella acts to sustain its flow because dislocations are accumulated within it as a result of the bending, and these serve to harden the latent (intersecting) system relatively more.

The lattice rotation in the neck of a $[\bar{1}11]$ crystal is shown in Fig. 2-VI by the placement of the tensile axis some distance from $[\bar{1}11]$. Again, the idea of a differential shear strain or the operative $(\bar{1}\bar{1}1)$ $[011]$ and $(\bar{1}1\bar{1})$ $[011]$ slip systems (in primary-cross relationship, Fig. 9-VI) can be used in explanation. However, a problem is posed by the continued operation of the observed systems during the rotation. Considering only changes in Schmid factor, the systems in primary-conjugate relationship, $(\bar{1}\bar{1}1)$ $[\bar{1}10]$ and $(\bar{1}1\bar{1})$ $[\bar{1}01]$, become the most highly and equally stressed. The primary-cross combination can, nevertheless, be expected to continue in operation for two reasons: (1) The primary-cross Schmid factor also increases,[22] although not as rapidly as that for the primary-conjugate combination. (2) Hardening on the primary-cross combination ought to be less.

Thus with geometrical softening from lattice rotation and a more rapid drop in hardening rate, it seems reasonable for plastic instability to develop as observed. The localization of flow is facilitated by the fact that equal operation on these systems can be confined to a single zone bounded by $(\bar{1}00)$ without violating strain compatibility. On this basis, the observation of single-shear (Fig. 8-VI) rather than double or even triple-shear zones can be understood.

The principal difference between $[\bar{1}11]$ crystals (with tendency to shear fracture) and crystals initially oriented for single slip (with tendency to rupture) is that a stable orientation is reached in the latter (namely $[\bar{1}12]$) and duplex (intersecting) slip persists during necking; in $[\bar{1}11]$ crystals, however, some single primary-cross combination is favored at necking, and its operation acts to rotate the tensile axis away from $[\bar{1}11]$ and thus to insure its continued operation for reasons just discussed.

CONCLUSIONS

The tensile fracture of copper single crystals occurs in either of two general modes, depending upon orientation. In crystals of $[\bar{1}12]$ and $[001]$ orientation, and in partially twinned crystals of $[\bar{1}11]$ orientation, a symmetrical positioning of slip systems about the stress axis permits the crystals to neck and to undergo large reductions of area, approaching rupture along a chisel-edge in the

extreme. Because of impurities (presumably oxide inclusions) voids are nucleated at the intersection of shear zones and grow into quadrangular channels penetrating the crystal. Large strains may be required for the nucleation; a tensile strain estimate of more than 500 percent was made in these experiments.

Lattice rotations in the necked region are a natural consequence of the gradient of strain over the length of the neck. As a result, slip planes may become curved and give the appearance of other than octahedral planes; this was most apparent in crystals of the end-orientation $[\bar{1}12]$.

In crystals of $[\bar{1}11]$ orientation, the active systems when necking begins are in primary-cross relationship and non-symmetrically disposed. For that reason, such crystals fractured by shear in a narrow zone parallel to $(\bar{1}00)$. Voids appeared within the zone.

REFERENCES VI

1. G. Y. Chin, W. F. Hosford, Jr., and W. A. Backofen, Trans. Amer. Inst. Min. (Metall.) Engrs. to be published.

2. C. F. Elam, Proc. Roy. Soc. A115, 133 (1927).

3. R. Karnop and G. Sachs, Z. Physik 41, 480 (1928).

4. G. Y. Chin, W. F. Hosford, Jr., and W. A. Backofen, to be published; G. Y. Chin, Sc. D. Thesis, M.I.T. (1963).

5. C. F. Tipper, Metallurgia, 39, 133 (1949).

6. K. E. Puttick, Phil. Mag. 4, 464 (1959).

7. R. Karnop and G. Sachs, Z. Physik 41, 116 (1927).

8. K. E. Puttick, Acta Met. 11, 986 (1963).

9. F. D. Rosi and M. S. Abrahams, Acta Met. 8, 807 (1960).

10. J. J. Koppenaal, Acta Met. 9, 1078 (1961).

11. I. S. Servi and N. J. Grant, Trans. Amer. Inst. Min. (Metall.) Engrs. 191, 917 (1951).

12. C. J. Beevers and R. W. K. Honeycombe, Fracture, p. 474, Eds. B. L. Averbach, D. K. Felbeck, G. T. Hahn, and D. A. Thomas, Wiley, New York (1959).

13. S. Saimoto, Ph. D. Thesis, M.I.T. (1964).

14. F. W. Young, Jr., Direct Observations of Imperfections in Crystals, p. 103, Interscience Pub. (1962).

15. F. W. Young, Jr., J. Appl. Phys. 32, 192 (1961).

16. F. D. Rosi and C. H. Mathewson, Trans. Amer. Inst. Min. (Metall.) Engrs. 188, 1159 (1950).

17. L. M. Clarebrough and M. E. Hargreaves, Prog. in Metal Phys. 8, (1959).

18. W. F. Hosford, Jr., R. L. Fleischer, and W. A. Backofen, Acta Met. 8, 187 (1960).

19. C. J. Beevers and R. W. K. Honeycombe, Acta Met. 9, 513 (1961).

20. E. Orowan, Reports on Progress in Physics 12, p. 185, The Phys. Soc., London (1948-49).

21. H. C. Rogers, Trans. Amer. Inst. Min. (Metall.) Engrs. 218, 498 (1960).

22 J. Diehl, M. Krause, W. Offenhauser, and W. Staubwasser, Z. Metallk. 45, 489 (1954).

SUGGESTIONS FOR FUTURE WORK

The present study on crystals oriented for multiple slip strongly suggests that obstruction to dislocation motion is greater with forest dislocations of 90° intersection than those of 60° intersection. It was suggested that such a behavior may be due to the lower mobility of the jogs of the former case. To investigate this process further two experiments can be performed.

(1) Etch pit studies of $[00\bar{1}]$ crystals: The determination of the relationship between the flow stress and etch pit density is expected to result in a $\tau \propto \rho^{n}$ relationship with n larger than $\frac{1}{2}$. However, diligent experimentation would have to be done on different low index planes since debris density may be large, resulting in a large scatter.

(2) Strain-rate studies on crystals involving only two specific interactions at temperatures below $78^{\circ}K$: It was shown in Appendix V that tensile deformation of $[0\bar{1}1]$ crystals with new dislocation sources introduced at the surfaces operated only primary and critical systems in equal amounts at $4.2^{\circ}K$. Similar introduction of surface sources in $[\bar{1}\bar{1}2]$ crystals should operate only primary and conjugate systems, eliminating extensive easy glide.

Strain-rate dependence of flow stress of these crystals should manifest differences in the thermally aided intersection of forest dislocations from which further elucidation of the intersecting process can be derived.

The study of hardening in polycrystalline material has indicated that the relative higher hardening owing to the presence of 90°-intersection forest dislocations may dictate the choice of slip systems which are required by the imposed strain. Such behavior may give a clue towards understanding the difference in the deformation texture of different face-centered cubic metals. A theoretical calculation similar to Bishop and Hill, and Lin and Lieb using only those slip systems which minimize the 90° intersection could lead to accounting for the higher $[001]$ component in the fibre texture of lower stacking-fault energy metals.

BIOGRAPHICAL NOTE

Shigeo was born to Kunimatsu and Kiku Saimoto on April 3, 1935 in Steveston, B. C., Canada. After completion of high school in 1953, he attended the University of British Columbia where he received a B.A.Sc. (Engineering Physics) in 1958 and a M.A.Sc. (Metallurgical Engineering) in 1960. He enrolled at the Massachusetts Institute of Technology in 1960.